UNIVERSIDAD ADOLFO IBÁÑEZ

MASTER OF SCIENCE THESIS

IMPROVEMENT AND EVALUATION OF A 3D PRINTABLE BIOREACTOR CHAMBER FOR *EX VIVO* TRABECULAR BOVINE BONE CORE TESTING WITH MECHANICAL STIMULATION

Author:

Alejandra Victoria
Correa Belloso

Supervisors:

Dr. Juan F. Vivanco
Dr. Heidi-Lynn Ploeg

A thesis submitted in conformity with the requirements for the degree of Master of Science in Bioengineering and Professional Degree in Bioengineering from the

Faculty of Engineering and Sciences

January 2024

FACULTAD DE INGENIERÍA Y CIENCIAS

UNIVERSIDAD ADOLFO IBÁÑEZ

SMITH ENGINEERING
Queen's University

Dedication

A Mamá y Papá.
Gracias por apoyarme en cada uno de mis pasos.

Abstract

IMPROVEMENT AND EVALUATION OF A 3D PRINTABLE BIOREACTOR CHAMBER FOR *EX VIVO* TRABECULAR BOVINE CORE TESTING WITH MECHANICAL STIMULATION

by ALEJANDRA VICTORIA CORREA BELLOSO

Better understanding of bone tissue mechanics is key in the development of more effective strategies to prevent bone fracture, regenerate, and repair bone pathologies like osteoporosis. Functioning as a bridge model between two-dimensional *in vitro* and *in vivo* studies, the *ex vivo* bioreactor and loading systems allow the study of trabecular bone explants in a closed system that can be mechanically stimulated. Polycarbonate bioreactor chambers have been successfully used to study trabecular bone tissue mechanics in bone cores *ex vivo.* However, polycarbonate bioreactor chambers are difficult and expensive to fabricate, and the height-diameter ratio for bone cores is below the standard for mechanical compression tests.

Three-dimensional (3D) printing, in contrast to subtractive fabrication methods, enables the fabrication of complex structures with high resolution and processing accuracy for diverse biomedical applications. Because of its adaptability and cost-effectiveness, a new bioreactor and loading system inspired by previous system like Zetos was developed using polyjet 3D printing and MED610™ as printing material. The first version of the *ex vivo* bioreactor chamber showed leakage and concerns regarding the material biological viability. Therefore, the overall aim of the current thesis research was to correct and improve the first version design limitations, by proposing and verifying a second design iteration. Biological viability of MED610™ for complex constructs (like a bioreactor chamber) was evaluated. The findings support continuing developments of MED610™ 3D printed bioreactor chambers for organ culture and other complex 3D-printed structures for *in vitro* or *ex vivo* studies in biomedical applications.

Finally, an *ex vivo* bovine trabecular bone core study with the second version of the 3D printable bioreactor chamber confirmed that previous system issues were addressed: neither system leakage nor loss of samples occurred throughout the study; and bone cores remained visibly viable during the 21-day period. Although contrasting bone behavior trends were observed when compared to previous similar studies, where mean apparent elastic modulus (E_{app}) decreased in the loading treatment group by 14.7%, these results give valuable insights for the 3D printable bioreactor chamber and loading system's continuing process validation.

Keywords: *ex vivo***,** bioreactor, trabecular bone, mechanical stimulation, biological viability, 3D printing, MED610™.

Statement of Co-Authorship

Chapter 1: Alejandra V. Correa B. – manuscript composition
Juan F. Vivanco – manuscript review
Heidi-Lynn Ploeg – manuscript review

Chapter 2: Alejandra V. Correa B. – literature review, manuscript composition
Juan F. Vivanco – manuscript review
Heidi-Lynn Ploeg – manuscript review

Chapter 3: Alejandra V. Correa B. – manuscript composition
Juan F. Vivanco – manuscript review
Heidi-Lynn Ploeg – manuscript review

Chapter 4: Alejandra V. Correa B. – study design, data collection and analysis, manuscript composition
Mahsa Zojaji – data collection and analysis
Juan F. Vivanco – manuscript review
Heidi-Lynn Ploeg – study design, manuscript review

Chapter 5: Alejandra V. Correa B. – study design, data collection and analysis, manuscript composition
Brian A. Kunath – study design
Juan F. Vivanco – manuscript review
Heidi-Lynn Ploeg – manuscript review
Roshni Rainbow – study design, manuscript review

Chapter 6: Alejandra V. Correa B. – study design, data collection and analysis, manuscript composition
Mahsa Zojaji – data collection and analysis
Roshni Rainbow – study design
Juan F. Vivanco – manuscript review
Heidi-Lynn Ploeg – study design, manuscript review

Chapter 7: Alejandra V. Correa B. – manuscript composition
Juan F. Vivanco – manuscript review
Heidi-Lynn Ploeg – manuscript review

Acknowledgments

This thesis became a possibility thanks to the guidance and help of several individuals and institutions who, in one way or another, contributed and extended their valuable assistance in the preparation and completion of this project. It is my pleasure to extend my gratitude towards those who made this possible.

Firstly, I would like to acknowledge funding from the *Emerging Leaders in the Americas Program* (ELAP) Scholarship, awarded by Global Affairs Canada. Without this support, this research and international collaboration between our institutions would not have taken place, and I am deeply thankful for the opportunity I was given.

I would like to wholeheartedly thank my supervisors, Dr. Juan Francisco Vivanco and Dr. Heidi-Lynn Ploeg, for seeing what I could not see in myself and inspiring me to take on this wonderful and challenging project. Your guidance, expertise, and constant support were crucial in helping me finish this dissertation. I have said this an infinite number of times, but words will never suffice to express how grateful I feel for all the opportunities and lessons both of you have given me over the course of the last three years. A huge thank you is extended to Dr. Roshni Rainbow; this research wouldn't have been possible without your help. Thank you so much for teaching me how to work around the tissue culture lab and for your valuable insights during the planning of this study. I am incredibly thankful for your support, guidance, and willingness to be a part of this project.

I must also express my gratitude towards the Faculty for Engineering and Sciences, and the Research Direction from Universidad Adolfo Ibáñez (UAI). Thank you for your financial support for my travels and conference attendances to share our research. I will forever be grateful for all the opportunities UAI gave me as an undergraduate and graduate student. Thanks to Leone Ploeg and the Center for Health Innovation (CHI) as well, for all your help and patience with 3D printing and materials acquisition.

Pursuing a master's degree made me understand the importance of being surrounded by caring and supporting peers during research, which is why I must thank my friends and peers of the Biological, Bioinspired and Biomaterials (B3MAT), Queen's Bone and Joint Biomechanics (QBJBL), and Regenerative Engineering (ReL) labs. Especially, I would like to extend my gratitude towards Mahsa Zojaji

and Andrew Parkhill, who kindly helped with the experimental setup and data collection during mechanical testing and the *ex vivo* trabecular bone core study.

The most significant acknowledgement is reserved for my parents. Their endless love, effort, and support enabled me to be where I am and who I am today. Thank you, mom and dad, for putting yourselves out there by moving to a new country and leaving everything behind so that I could make my academic and professional dreams and goals come true. This is also your achievement, and I am deeply grateful and happy I get to share this with you. *Gracias, por todo.*

Table of Contents

List of Figures

List of Tables

List of Abbreviations

$\%\Delta E_{app}$	Percent change in apparent elastic modulus between two timepoints
α	Level of significance
δ (mm)	Displacement
Ɛ	Mechanical strain
μCT	Micro-computed tomography
μƐ	Microstrain
2D	Two-dimensional
3D	Three-dimensional
A	Cross-sectional area
AA	Antibiotic-antimycotic solution
aBMD	Areal bone mineral density
ALP	Alkaline phosphatase
AM	Additive manufacturing
ANOVA	Analysis of variance
AP	Autoclave protocol for MED610™ cleaning & sterilization
ARD	Age-related disease
ATDC5	Murine chondrogenic cell line
BMD	Bone mineral density
BM-MSC	Bone-marrow derived mesenchymal stem cells
BMU	Basic multicellular unit
BTE	Bone tissue engineering
CO_2	Carbon dioxide
DBM	Decalcified bone matrix
DMEM	Dulbecco's modified eagle medium
DXA	Dual-energy x-ray absorptiometry
E_{app} (MPa)	Apparent elastic modulus
ET1	Endothelin-1
F (N)	Force
FBS	Fetal bovine serum

FEA	Finite element analysis
H (mm)	Height
HA	Hydroxyapatite
HUVEC	Primary endothelial cells from umbilical cord vein
ID (mm)	Inner diameter
IPA	Analytical grade isopropanol
iPSC	Induced pluripotent stem cells
iPSC-CM	Cardiomyocytes-derived induced pluripotent stem cells
K_{app} (N/mm)	Apparent stiffness
$K_{app,res}$ (N/mm)	Apparent residual stiffness
L929	Murine cell line
MC3T3	*Mus musculus* calvaria cell line
MES	Minimal effective strain
MESm	Minimal effective strain for bone modeling
MESp	Minimal effective strain for bone microdamage and fracture
MESr	Minimal effective strain for bone resorption
MP	Manufacturer's protocol for MED610™ cleaning & sterilization
MSC	Mesenchymal stem cells
Na_2SiO_3	Sodium metasilicate
NaOH	Sodium hydroxide
No	Number
O1	Option 1 (second version of the 3D printable bioreactor chamber design)
O2	Option 2 (second version of the 3D printable bioreactor chamber design)
OD (mm)	Outer diameter
PBS	Phosphate buffer saline
PC	Polycarbonate
PTFE	Polytetrafluoroethylene
PZA	Piezoelectric actuator
R^2	Coefficient of determination
RFUs	Relative fluorescence units
RR	Resazurin reduction
RT-PCR	Real-time polymerase chain reaction

Saos-2	Human osteosarcoma cell line
SD	Standard deviation
SEM	Standard error of the mean
SP	Sonication protocol for MED610™ cleaning & sterilization
SP+A	Sonication and autoclave protocol for MED610™ cleaning & sterilization
TE	Tissue engineering
UV	Ultraviolet
vBMD	Volumetric bone mineral density
WHO	World Health Organization

Chapter 1

INTRODUCTION

1.1. Background and Motivation

Tissue damage and organ function loss can be found within the most expensive and serious problems of current human health conditions [1]. Although there has been a great increase of human life expectancy [2] due to technological progress since the nineteenth century within the biomedical field, longevity does not necessarily reflect the state of health of those individuals that live longer [3].

Osteoporosis -a systemic skeletal disease- is a chronic condition characterized by "low bone mass and microarchitectural deterioration of bone tissue" [4]. It is considered an age-related disease (ARD), because of the increasing loss of equilibrium in the natural bone remodeling process due to skeletal senescence [5]. Osteoporosis, then, can cause the increase of bone fragility and susceptibility to fracture [6], which is considered one of the major complications of this skeletal disease [7]. Its prevalence has risen significantly over the last decades, accounting for 18.3% of the world's population being diagnosed with osteoporosis in 2021 [8]. In Latin America, a study conducted in Brazil, Mexico, Colombia and Argentina concluded that over 840,000 osteoporosis-related fractures were predicted to occur in 2018, amounting to a total annual cost of approximately USD $1.17 billion [9].

Typical fractures caused by osteoporosis occur in the bones of vertebral columns, ribs, hips, and wrists. In the case of long bones and hip bones fractures, surgical treatments are often required. In Chile, local experts estimated in 2012 that 90% of hip fractures related to osteoporosis are treated surgically [10]. However, there are major limitations related to surgical treatments: the bone healing capacities post-surgery are relatively poor in patients with osteoporosis [7], and is correlated with a far higher (~50%) failure rate of implant fixation compared to non-osteoporotic patients [5]. Even so, in severe bone defects caused by osteoporosis, autologous or allogenic bone grafts could still be considered [11].

Osteocytes, a specific type of bone cell, are known to be the main sensors for mechanical loading of bone [12], and play a crucial role in bone (re)modeling and even bone (re)generation. They translate the mechanical stress and strain from mechanical loading into the production of biochemical signaling molecules that regulate bone resorption (by osteoclasts) and bone formation (by osteoblasts) [13]. This shows the importance of osteocytes, along with osteoclasts and osteoblasts [14], in bone healing after

fracture. Osteocytes are located in both the cortical and the spongy or trabecular bone. Trabecular bone is the heterogeneous, anisotropic and highly porous part of bone that can be found at the extremity parts (epiphysis) of long bones and in the core of short bones [15]. However, compared to healthy bone, in an osteoporotic bone the osteocyte number per unit of bone area declines as the disease progresses. This translates in lower trabecular thickness and higher intracortical porosity, which deteriorates bone quality and lowers the bone natural healing capacity, making it less resistant to mechanical loading [5].

1.2. Research Opportunity

During the last two decades, a research area focusing on the development of new methods to regenerate tissue and damaged organs has emerged [16]. Bone Tissue Engineering (TE), then, makes use of different types of biomaterials, living cell lines and growth factors to address bone defects by implants and other biomedical devices [17], [18], taking into consideration relevant factors such as sex, age, type of tissue damage/trauma, overall health profile, among others [19], [20]. To address the challenges and consequences of osteoporosis, bone tissue engineering researchers have been working with different strategies to study the potential of bone tissue regeneration, these include *in vitro, ex vivo* and *in vivo* methods [21]. However, it is still a major challenge to overcome the osseointegration of implants and weakened regeneration potential of the host bone in the healing process of osteoporotic fractures and surgeries [5]. Moreover, it has been reported that most studies about osteoporosis focus on preventing the fracture rather than looking for better treatment alternatives and healing strategies [7], [22]. Hence, better understanding the cellular dynamics and, along with bone tissue mechanics knowledge, the mechanical factors of the natural trabecular bone tissue under mechanical loading, are crucial to develop effective strategies for osteoporotic bone regeneration and repair.

To address the difficulties and limitations associated with either *in vivo* or two-dimensional (2D) cell cultures *in vitro* studies on the biophysical response of trabecular bone, ex *vivo* dynamic tissue cultures in bioreactors have proven to mimic *in vivo* metabolic conditions and three-dimensional (3D) conditions [23]. *Ex vivo* testing makes it possible to control and monitor relevant factors such as the pH value, O_2 saturation, flow rate, and temperature [24], while also convectively transporting the required nutrients to maintain the tissue or cells under study alive [25]. Bioreactor systems like Zetos currently allow *ex vivo* bone culture methods through cyclic mechanical load and medium perfusion, making it possible to study bone explants in their natural 3D environment, while also keeping both cell-cell and cell-matrix interactions [26], [27]. This method of testing is becoming widely used to study bone biology, bone diseases and pathologies like

osteoporosis [14], [28], since it is possible to apply both physiological and mechanical signals to the bone, making it possible to keep the explant alive for up to 28 days [29].

Although Zetos and similar systems have the above discussed advantages, these bioreactors are difficult and expensive to fabricate or purchase. To address this problem, interdisciplinary research involving design engineering can provide novel, precise, and reliable alternatives. Therefore, the *Bone, Joints and Biomechanics* laboratory at Queen's University, Ontario, Canada, developed a novel 3D printable bioreactor system inspired by the Zetos *ex vivo* organ culture system [30]. However, the first design evaluation iteration showed some limitations related to the material biocompatibility and leakage during the experiment, causing a significant loss of samples during a 21-days study due to dehydration. Hence, there is an opportunity to improve and optimize the bioreactor system design, addressing the previously identified limitations in a second version of the bioreactor design for *ex vivo* bone core experiments. Moreover, thanks to 3D-printing versatility, a system like the one proposed could be adapted for dynamic *in vitro* culture of 3D bone tissue engineering scaffolds. As a result, a widely known and used *ex vivo* organ culture system like Zetos could be adapted for its application in different biological tissue models (e.g., scaffolds), while also considering important tissue maintenance criteria.

Chapter 2

LITERATURE REVIEW

2.1 Bone Biology and Physiology

Bone is a metabolically active connective tissue [31] that forms most of the adult skeleton. The skeletal system, composed by bones and cartilage, then, mechanically supports the body, facilitates movement, protects vital structures, produces blood cells (hematopoiesis) and stores/releases minerals and fat (homeostasis) [32], [33].

2.1.1 Bone Anatomy and Structure

At an organ level, there are two main structural types of bone: cortical and cancellous bone [31]; both are anisotropic [34] and have the same overall matrix composition. The bone matrix, hence, is composed by the organic matrix (~25%), which is mostly type I collagen, and has the function to give bone its form and provide resistance to tensile forces; inorganic mineral (~65%), consisting mainly in hydroxyapatite (HA), which provides most of the bone strength, stiffness, and resistance to compressive forces; and water and lipids (<15%) [31], [33].

Although their matrix is composed similarly, cortical and cancellous -or trabecular- bone differ significantly in their density or porosity, 3D structures (as seen in Figure 2-1) and metabolic activity. These factors, combined, have a strong influence over the function and physiology of each type of bone [31].

The cortical bone, which makes up to 80% of the adult skeleton by weight, has a porosity of 5-10%, and provides maximum resistance to torsion, bending, and compressive forces, as well as protection for bone marrow [31], [33]. On the other hand, trabecular or cancellous bone has a porosity of 50-90% [31], and can be found at the ends of long bones (epiphysis) and in the core of short bones [15]. Moreover, trabecular bone tissue is a hierarchical, spongy, and porous material

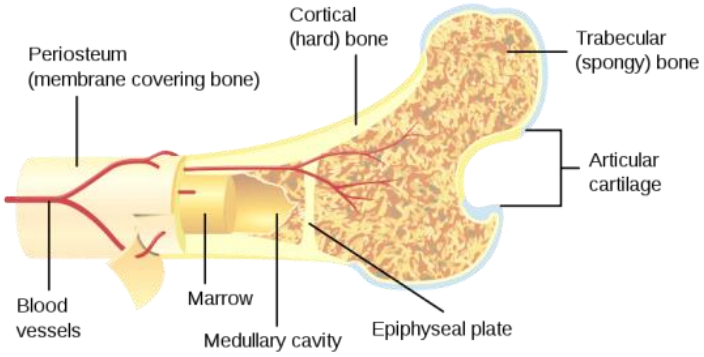

Figure 2-1. Visualization of cortical and trabecular bone in a long bone. The cortical bone is the "outer-layer" of the bone, whereas the trabecular part is at the epiphysis (end) of the long bone.

with a lattice-like architectural appearance with higher metabolic activity and remodeling rates [35]. As a result, it has a lower calcium content by weight [36] and more water than cortical bone [15]. Its primary function is the allowance of deformation and absorption of loads, which is possible thanks to its primary bone cells lying on the surface and being closer in proximity to growth factors and cytokines. Therefore, trabecular bone has a faster adaptation response to mechanical stimuli than cortical bone [31].

In the adult skeleton and from a histological point of view, lamellar or secondary bone has completely replaced woven or primary bone, and is a highly organized structure, with collagen fibrils packed tightly and uniformly in sheets of osteocytes and bone matrix [31]. A form of lamellar bone called *osteon* forms the major structural unit of cortical bone, and is organized in a tubular arrangement (*lamellae*) with the Harversian canal in the central part of the tube, which contains blood vessels, lymphatics, and nerves [31], [37]. The longitudinal distribution of these *"tubes"*, along with the cement lines -thin layers of organic matrix- as boundaries explain why the cortex is more resistant to fracture when loaded in parallel than perpendicular to its long axis. Moreover, this prevents fatigue cracks in osteons when a fracture occurs in healthy bone, since it follows the cement line instead of crossing the osteons [38].

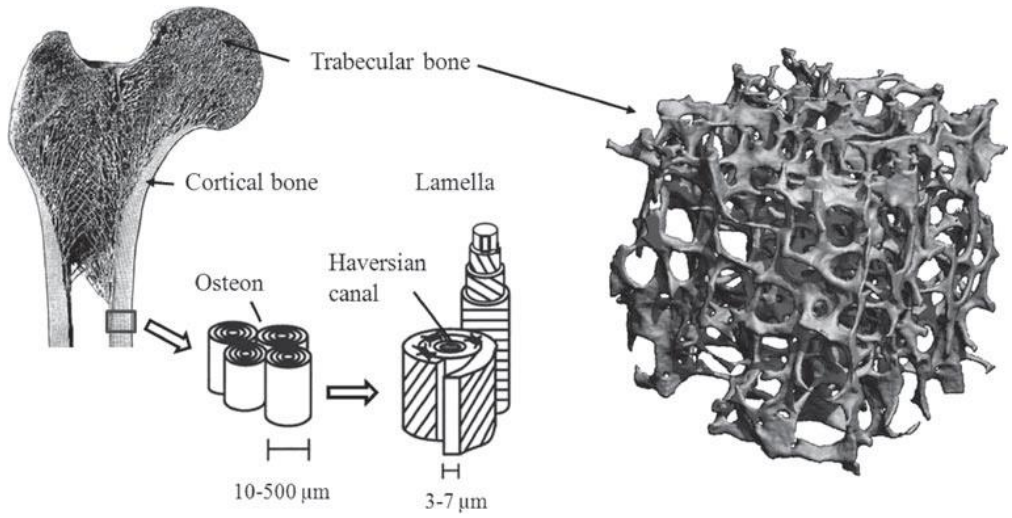

Figure 2-2. Differences in the lamellae structure between cortical and trabecular bone [37].

Trabecular bone also contains lamellar bone, however, it has a different structure to that in cortical bone; the cancellous lamellae are arranged in semicircular shapes that form the trabeculae (as seen in Figure 2-2) [31]. The architecture of the trabecular bone, then, consists in a highly heterogeneous network and individual trabecular struts that are organized to optimize mechanical load transfer [15], [33], [35]. Individual trabecula in humans can vary in shape, from flattened plates to cylindrical rods, the latter being

more common as individuals lose bone mass. However, rather than the size of the individual trabecula, the number of trabeculae has a greater effect on connectivity. This results in a greater effect on structure weakening (around 2-3 times compared to thinning) when trabeculae are lost through resorption [33].

2.1.2 Bone Cell Types and Lineages

There are three main cell types that participate in the formation and removal of bone tissue, and they make up about 10% of total bone volume [31], [33]. Two of them, osteoblasts and osteocytes, differentiate from mesenchymal stem cells (MSC). The *osteoprogenitor cells*, that differentiate from MSC before turning into osteoblasts, are considered the "stem cells" of the bone, and can be found in the bone canals, endosteum -membranous structure on the inner surfaces of bone-, periosteum -membrane that covers outer layer of the bone-, and bone marrow. They differentiate into osteoblasts only when signals to migrate and proliferate are received [31]. The last cell type, osteoclasts, are of hematopoietic origin [37]. Their morphology and primary functions are shown in Figure 2-3.

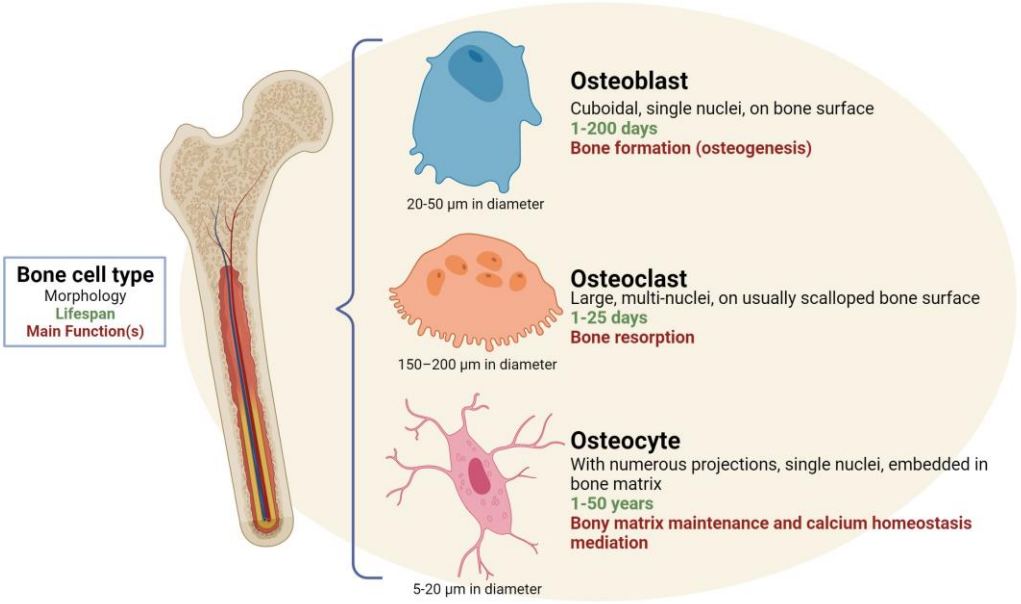

Figure 2-3. Main cell types in bone biology. Below the cell name, its morphology and primary function(s) are described. Image created with BioRender.com

Osteoblasts are responsible of osteogenesis -forming new bone-, more specifically, these cells synthesize organic bone matrix as type I collagen scaffolding and proteoglycans, forming the basis of mineralized tissue [31]–[33], [37]. They are characterized for being packed tightly against each other on the bone surface at active sites of bone formation, like bone development or fracture repair [37]. Most osteoblasts undergo

apoptosis once new bone was formed, although some of them remain embedded in the secreted bone matrix, and even a smaller number of them can become quiescent, remaining in the bone surface and prone to be rapidly reactivated to form new bone [33].

Osteoclasts are considered the functional interactive partners of osteoblasts since they are responsible for bone resorption [32]. This means that osteoclasts break down old, injured, or unnecessary bone while osteoblasts are continuously forming new bone. These interactions between the two cell types create an ongoing balance for bone remodeling. Osteoclasts, then, break down bone by attaching to the bone matrix through a rough border and solubilizing it via acidification, which then causes matrix phagocytosis [31]. As mentioned before, osteoclasts are of hematopoietic origin, more specifically, they arise from monocytes and macrophages [37]. Osteoclasts can contain 3-25 nuclei per cell and can be found at sites where resorption is taking place or within cavities where an active resorption has already occurred [31], [37].

Osteocytes are the most abundant cell type in bone tissue (90-95% of all bone cells) [12], [13]. When the secreted bone matrix calcifies, the osteoblasts that remained embedded in it differentiate into osteocytes and locate within vacuoles called lacunae that are surrounded by bone tissue [31], [32]. Once differentiated and surrounded by bone matrix, they develop cytoplastic projections -dendritic processes- that connect with other osteocytes, cells at the bone surface, and nearby blood vessels through a network of canaliculi -channels withing the bone matrix- [12], [37]. This allowance of direct communication between them and with other bone cells makes them responsible for maintaining the bony matrix and mediating calcium homeostasis, while also creating a network of cells that has the ability to respond with adaptation to external bone stimuli [12], [31].

However, the relevance of osteocytes in the regulation of the dynamic nature of bone started to be studied a little more than a decade ago [12]. Nowadays, they are considered the *master orchestrator* of bone homeostasis [39]. They can sense mechanical stimuli and stress changes, and transduce them into biochemical signals through their network to regulate bone remodeling both directly and indirectly, by either regulating matrix remodeling or orchestrating the osteoclasts/osteoblasts activity [13]. This knowledge implies that the study and use of osteocytes can potentially be useful for bone regeneration [40].

2.1.3 Bone Adaptation: Modeling and Remodeling Processes

Throughout an individual's lifetime, bone tissue remains highly active and responsive. During childhood growth, bone modeling takes place in order to form the shape of the bones, increasing the diameters of the

diaphysis and medullary cavity [32]. Therefore, this process often leads to an increase in bone mass, and it occurs on trabecular, endocortical, and periosteal bone surfaces [33]. Although this process occurs primarily during childhood, the bone tissue remains highly responsive to environmental and physiological conditions throughout an individual's lifetime, thus adapting itself [41].

In bone modeling, osteoblasts and osteoclasts work independently at an active site, with no coordinated action between formation and resorption on the same surface at the same time [33]. However, osteoclasts and osteoblasts do act temporarily coordinated - through an effect called coupling- on the same bone surface in bone remodeling, a lifelong process of renewing or replacing of bone tissue to repair microdamage and maintain overall bone health, mineralization and plasticity [31], [33], [37], [42]–[44]. Therefore, the importance of coupling in bone remodeling lays on preserving bone mass, which requires the adequate synchronization of both removal and repair [43]. This process can take over several weeks depending on the bone type, and can occur on any bone surface and envelopes [33], [42]. It has been reported that bone remodeling is responsible for the renewal of around 10% of the skeleton per year [45].

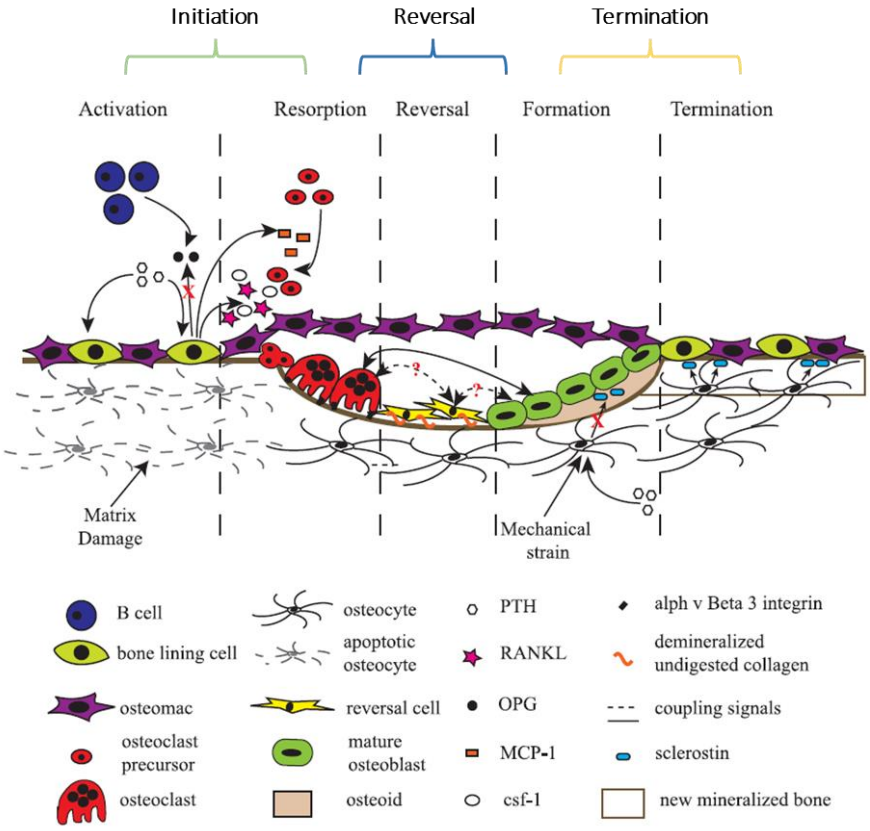

Figure 2-4. Schematic representation of a BMU and the associated bone remodeling process. Adapted from [42].

If the cycle of bone remodeling is not tightly regulated and coordinated by local and systemic factors, significant deviations result in the acceleration and unbalanced bone gain or bone loss, with potentially dangerous consequences in terms of increased fracture risks or compression syndromes [42]. Thus, regulation is crucial in this process, and different types of cells lineages are involved, such as osteoclasts,

osteoblasts, osteocytes, immune cells (T- and B-cells), megakaryocytes, and osteomacs (resident tissue macrophages) [43]. Hormones (e.g. growth factors) also play a role, as well as different pathways involved in bone metabolism [43], [44], [46]. Moreover, it has been reported that bone remodeling is also regulated epigenetically by DNA methylation and non-coding RNAs [44].

On the process itself, bone remodeling occurs in what is known as Basic Multicellular Unit (BMU), which is a combination of osteoclasts, osteocytes and osteoblasts within the bone remodeling cavity; there, some sequential steps are followed: initiation, reversal, and termination phases [33], [42]. However, the process of bone remodeling is also be split by some of the literature into activation, resorption, reversal, formation and termination [43]. An illustrated representation of this process is shown in Figure 2-4.

The remodeling process starts with an activation signal that triggers bone resorption. This signal could be either systemic -disruption in mineral homeostasis or hormonal-, or local -microdamage or osteocyte apoptosis- [33]. Once activated, osteoclast precursors are recruited and osteoclastogenesis takes place with M-SCF and RANKL as key mediators, forming mature osteoclasts that initiate resorption [43], [44]. During resorption, MSCs are recruited by different factors that also lead their differentiation to enable bone formation [44]. Then, the reversal stage follows, making a transition from bone resorption to bone formation, where different and not completely known factors get involved in the coupling resorption to formation [33]. Finally, during the termination phase, an equal amount of the bone resorbed is replaced, where osteoblasts produce protein matrix that, progressively, becomes embedded with mineral crystals [33], [43], [44]. Some of these osteoblasts, as mentioned before, become buried within the matrix, and differentiate into osteocytes in the mineralized tissue. It is important to note, however, that complete mineralization can take up to one year [33].

2.1.3.1 Mechanical and Time-Dependent Properties of Trabecular Bone

From an engineering perspective, trabecular bone consists of a porous composite solid material, and thus highly heterogeneous. The mechanical and cellular properties of trabecular bone are highly dependent on its microstructure, as well as on its age, overall health, sex and anatomical site [35], [47].

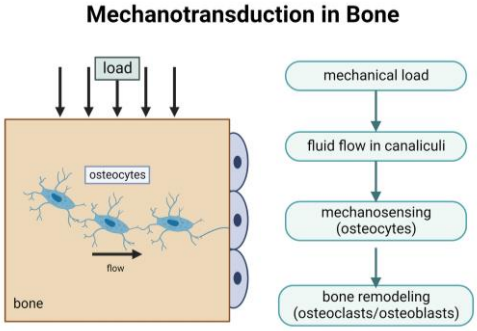

Figure 2-5. Mechanotransduction process in trabecular bone. Adapted from Oftadeh et al. (2015) [14]. Figure created with BioRender.com

Mechanical loads can also stimulate bone modeling, which is considered mechanically induced adaptation (historically referred to as Wolff's Law) [31], [43]. There is an empirical relationship between the internal architecture of bone and load trajectories [41], thus it is observed that mechanical loads influence the remodeling process and help bone tissue adapt to its mechanical environment. Hence, it is hypothesized that osteocytes in the trabecular bone sense the mechanical loads and orchestrate adaptive alterations to bone mass (mechanosensation), and then "translate" the physical stimuli into biochemical factors (mechanotransduction), activating osteoblasts and/or osteoclasts [15]. An illustrated representation of this process is shown in Figure 2-5.

Frost's Mechanostat Theory [48] further described the role of mechanical stimuli in the bone remodeling process, identifying mechanical strain as the key parameter that determines bone remodeling. Frost introduced the concept of four different strain zones separated by three boundary levels; these determine the strain ranges during loading that can be considered below or above appropriate physiological levels, where osteoclasts and osteoblasts are functionally in balance [41]. The four main strain zones and boundary layers are shown in Figure 2-6, along with the fracture window, in which strains centred near 25,000 με (Fx) can fracture a healthy young adult bone.

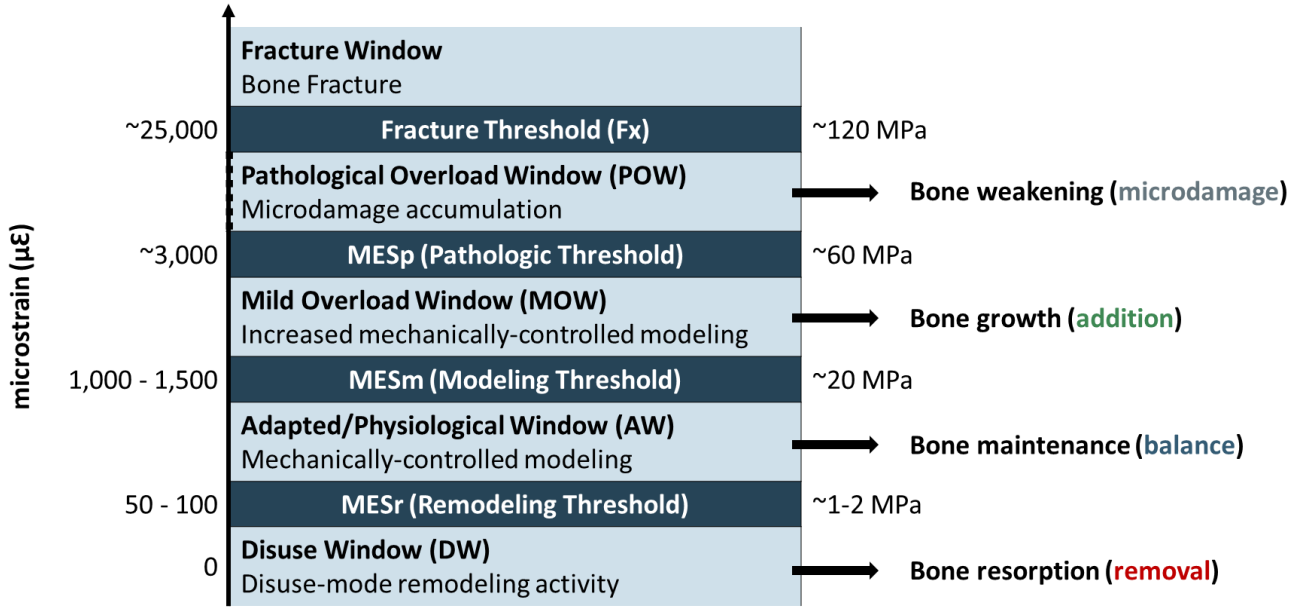

Figure 2-6. Mechanical strain usage window defined by Frost's Mechanostat Theory for bone remodeling (adapted from [41], [48], [49]). The vertical arrow on the left-hand side shows the typical minimum effective strain (MES) levels and the set point values for bone's threshold microstrain (με). Bone's ultimate strength values for stress (MPa) are shown on the right-hand side. Black horizontal arrows denote the bone tissue response to each microstrain window of loading.

Moreover, bone's response to mechanical loadings has been recognized to also be time dependent [47], [49]–[52]. In particular, trabecular bone has been reported to develop a substantial amount of creep even at small load levels [47], and that its time-dependent response is non-linear, thus varying with different levels of applied stress and strain [47], [53]. Macroscopically, trabecular bone yields below 0.8% strain in compression [54], and reports have shown that strain always comprises of recoverable and irrecoverable components, even when small strain/stresses levels are applied [47]. Regarding bone tissue health, researchers have found that low-amplitude high-frequency postular strains (muscular contractions) could be just as or even more effective for the maintenance of bone mass than locomotive strain (high-amplitude, low-frequency) [49].

Additionally, the viscoelastic properties of trabecular bone enable the dissipation of energy when mechanical loads are applied, helping bone to resist fractures under dynamic or impact loading [50]. Not only viscoelastic (fluid-flow independent), but also, thanks to the (micro) porous structure of bone, it has also been described as "poroelastic" (fluid-flow dependent properties) [55]–[57]. However, it has been reported that viscoelasticity plays a significantly greater role in the mechanical response of bone tissue than poroelasticity [55].

2.1.4 Bone Healing and Regeneration

Thanks to the incorporation of bone development, modeling and remodeling, bone tissue has the capacity of scarless healing [58]. In the appendicular skeleton, which includes the shoulder girdle, upper and lower limbs and the pelvic girdle, both endochondral ossification and intramembranous ossification processes can be involved in bone healing [33], [58]. Mechanical load is among the most influential factors to determine the type of healing [59], but most clinical-level bone injuries -where there has been significant vascular damage- heal through endochondral ossification, also known as the secondary process [58]. However, in most long bone injuries, a combination of endochondral and intramembranous ossification is responsible for the healing of the bone [33].

In intramembranous ossification for bone healing, a direct transition of MSC to bone forming osteoblasts takes place [58]. For endochondral ossification, the bone healing process consists of three main phases: the inflammatory, repair (or fibrovascular) and late remodeling stages [58], [60]. It is important to note that, although these are three temporarily differentiated stages, they also overlap with associated cell-types coexisting [33], [58], [60]. A timeframe of the whole process and its phases are shown in Figure 2-7.

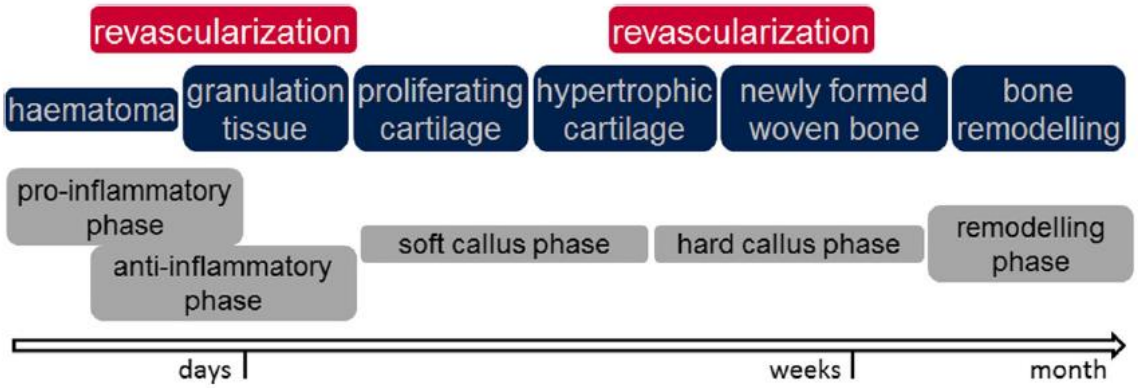

Figure 2-7. Bone healing phases and tissues involved in the process within the time it takes to completely heal an injured bone are shown. Obtained from [61].

Thus, the secondary healing process starts with a haematoma formation, which marks the beginning of the inflammatory phase. Inflammatory cells form the haematoma as a response to the loss of mechanical stability, the decrease of tissue oxygenation and nutrients supply, and the release of bioactive factors after the bone and vascular supply disruption [58], [61]. It has been reported that this clot prevents bleeding and provides provisional stability [33]. Within about 48 hours, the fibrovascular phase starts, where vascular remodeling and MSCs recruitment that will later differentiate into chondrocytes and osteoblasts occur [58]. Then, an internal callus is created between the two ends of the broken bone by chondrocytes from the endosteum in the healing phase [32]. On the other side, osteoblasts and chondrocytes from the periosteum -which is known for playing an essential role in bone healing [62]- create an external callus of hyaline cartilage and bone, which stabilizes the fracture, thus forming woven bone [61]. Lastly, the late bone remodeling stage takes place, in which the injured bone undergoes remodeling to re-establish its normal structure and function, including its material and mechanical properties [33].

The bone healing process is highly coordinated and involves both cellular and molecular factors to properly coordinate the callus formation and resolution, which makes it a highly sensitive process. For instance, both hypoxia and mechanical loading have shown to play a role in the extension of both primary and secondary healing; a decrease in oxygen, then, causes less extension of endochondral bone formation in the callus, while an increase in mechanical stability translates in more endochondral bone formation [33].

2.2 Osteoporosis Physiopathology and Current Treatments

2.2.1 Metabolic Bone Diseases: Osteoporosis

As it has been previously explained, bone is a metabolically active tissue [31]. Hence, an alteration in skeletal homeostasis, bone cell activity or bone matrix proteins cause what are known as metabolic bone diseases [44], [63]. Usually, these diseases are associated with atypical levels of calcium, phosphate, and/or vitamin D metabolites [63].

Osteoporosis is the most common metabolic bone disease, affecting around 200 million people worldwide [64]. It is characterized by the reduction of bone mineral density due to resorption exceeding formation [13], which causes the deterioration of bone tissue, its strength and its microarchitecture [11], [44], [65]. Aging, menopause, and other diseases can affect the balance of remodeling, favoring resorption and leading to net loss of bone mass over time [33]. Interestingly, osteoporosis is more common in females than males. About 1 in 3 females exhibit low bone mass and/or osteoporotic fractures in their lifetime; whereas, the occurrence in males is about 1 in 5 [64]. Moreover, genetic factors can also have a significant influence over the development of osteoporosis [44].

In osteoporosis, a pathologic fracture is one of the major complications [7], especially in the elderly population [6]. The deterioration of overall bone tissue increases the risk of fragility fractures, especially to the wrists, spine, proximal humerus, pelvis, and/or hip [44], [65], [66]. These fractures can severely impact the individual's health and involve a high number of complications. In the case of hip fractures, the mortality rate associated can be up to 12-24% in females and 25% in males, within the first year of fracture [67]. Unfortunately, osteoporosis often remains undiagnosed until it manifests as a fracture [65].

Most fragility fractures due to age-related osteoporosis occur in regions of the trabecular bone [15], [65]. This region shows trabecular resorption cavities due to unbalanced bone remodeling [33], in which osteoblasts are unable to refill the resorption lacuna [42]. As a result, the bone apparent density, architecture and mechanical properties of cancellous bone are significantly affected [15]. In females, the decrease of estrogen levels causes alterations in bone tissue homeostasis [32], which then translates into bone loss and osteoporosis. This hormone inhibits osteoblast and osteocyte apoptosis, as well as supresses osteoclasts formation and activity, preventing excessive bone resorption [13].

For osteoporosis diagnosis, most organizations -including the World Health Organization (WHO)- around the world suggest that all individuals of 50 years old or older with a history of fracture should get a bone mineral density (BMD) screening. Different studies have shown that BMD, expressed in $grams/cm^3$

for volumetric BMD (vBMD) or in $grams/cm^2$ for areal BMD (aBMD) [68], can predict future fracture risk and is correlated to bone strength [6], [69].

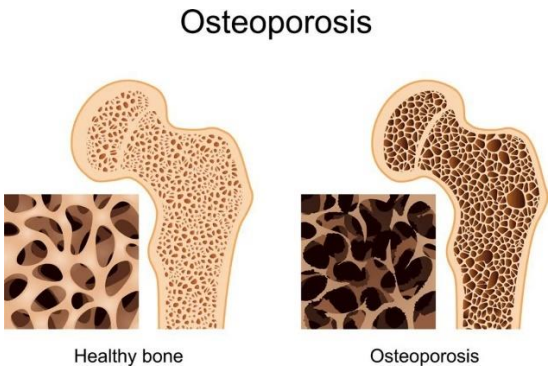

Table 1 T-Scores and WHO Diagnostic Criteria for Osteoporosis[4,14]

Interpretation	T-Score*
Normal	–1.0 and higher
Osteopenia	–1.0 to –2.5
Osteoporosis	–2.5 and lower
Severe osteoporosis	–2.5 and lower with one or more fragility fractures

* Reference values vary by geographical location.
WHO = World Health Organization.

Figure 2-8. A visual representation of healthy versus osteoporotic bone is shown (left). It can be seen how the osteoporotic bone has higher porosity, which translates in less bone strength and higher fragility. The table for the interpretation of BMD screening study is also shown (right) [65]. This test is made using dual-energy X-ray absorptiometry (DXA) scanning to measure BMD. Imaged obtained from [70].

To interpret BMD, the T-Score is used following the screening study. This T-Score represents the number of standard deviations above or below the average bone density for a healthy adult of the same sex and age; when compared, the fracture risk as a correlated result can be obtained. According to WHO, results of -2.5 and lower meet the criteria to diagnose osteoporosis [65]. Figure 2-8 shows the visual difference between an osteoporotic and a normal bone, as well as the before-mentioned table to interpret BMD screening.

2.2.2 Current Treatments for Osteoporosis and Osteoporotic Fractures

Most studies to date on osteoporosis treatments focus on preventing fragility fracture, rather than looking for better and more effective options for post-traumatic recovery therapies and options [7], [22], [65]. Thus, current treatments commonly used consist of anti-resorptive therapies, which aim to prevent the net loss of bone mass -and potential fracture- by decreasing or inhibiting osteoclasts activity and suppressing bone remodeling [6], [33]. Among the medications used are bisphosphonates -to help strengthen the bone-, calcitonin, and estrogen -females only- [32]. Denosumab, a monoclonal antibody to RANKL, decreases development of osteoclasts and bone resorption [71]. Another type of pharmacological treatment is anabolic medication, like teriparatide, which promotes bone formation by stimulating osteoblastic activity [72]. Romosozumab, a monoclonal antibody to sclerostin (an osteocyte-derived inhibitor of osteoblast activity), has also been proposed for post-menopausal females to increase bone formation and BMD, showing promising results [73], [74]. However, although small, a significant increase

of serious cardiovascular events was observed in females treated with romosozumab; additionally, its effectiveness decreases after the first year of treatment [74]. Non-pharmacological treatments and recommendations for osteoporotic patients include calcium and vitamin D intake, weight-bearing exercise, smoking cessation, limitation of alcohol/caffeine consumption, and fall-preventing techniques [65].

Although most treatments focus on preventing osteoporotic fractures, this disease still causes more than 8.9 million fractures per year, and this being a number expected to increase as the global population ages [65], [75]. Hence, when the fracture occurs, a surgical procedure is often required, depending on the severity of the fracture [22], [76]. However, the outcomes of given surgical procedures and implants are still negative or unideal in more than one case. In the case of hip fractures, 20-30% patients die within a year, another 40% end up being unable to walk independently [76]. Moreover, once a fragility fracture occurs, there is a clinically significant implication for subsequent fractures [77].

Fracture healing and recovery possibilities also decrease in individuals with osteoporosis. A study conducted by Nikolau *et al.* (2009) on femoral fractures concluded that there is a slower fracture healing response in elderly individuals with osteoporosis, where mechanical stability -given by the bone strength- is one of the most important factors that play a role in the healing process. The weakened osteoporotic bone affects the initial fracture osteosynthesis and lead to various future complications [78]. As a result, most surgical treatments involve limitations in achieving firm and stable fixation, as well as require re-surgery due to mal- or non-union from failed fixation in cases of severe osteoporosis. The latter happening because of reduced BMD and poor bone quality that do not allow the fixation of metal plates and screws [76]. Thus, studies conclude that there is currently no optimal bone substitute for osteoporotic fracture care [79].

2.3 Bone Behavior and Regeneration Studies: Bone Tissue Mechanics & Engineering

2.3.1 Bone Tissue Mechanics

Tissue Mechanics consists of the study of mechanics as an important cell and tissue regulator, and its importance relies on the increasing literature proving that there are key relationships between changes in mechanics and disruptions in tissue homeostasis and disease progression [80]. Bone Tissue Mechanics, also known as Bone Biomechanics, then, study bone as an important load-carrying tissue that is optimized for this mechanical function when healthy [81].

More specifically, the scientific knowledge of the biomechanics of trabecular bone enables important insights into skeletal problems (e.g., osteoporosis and bone fracture) and processes (e.g., bone remodeling) so that designs and/or analyses can be done to treat diseases, for instance, using bone-implant systems. Research has been ongoing in this field for about 50 years, and the main interests are focused on understanding the role of trabecular bone damage in the weakening of whole bones and stimulating biological bone remodeling [35], [52].

2.3.2 Bone Tissue Engineering

Tissue Engineering (TE) is a multidisciplinary research field that aims to fabricate functional tissue substitutes for regenerative and pharmaceutical medicine applications [24]. Using both engineering and biomedical emerging technologies, TE makes use of different types of biomaterials, living cell lines and growth factors to address different types of tissue defects [17], [18]. Thus, Bone Tissue Engineering (BTE), biomechanics and biomedical researchers work together to address bone defects, where bone grafting is among the most common topics of interest for research.

Bone grafting, then, is commonly used to improve bone regeneration in orthopedic surgery. When there is a considerable net bone mass loss, bone grafts play a crucial role in helping bone self-heal, because otherwise the process would be slow or fail entirely [5]. Around 2,000,000 bone grafts procedures are carried out every year [82], proving that it is a promising line of research where new, better and more cost-effective strategies and techniques are constantly needed.

Moreover, and thanks to advances in additive manufacturing (AM) technologies such as 3D (bio)printing [83], bone tissue engineering has focused on the development, design and fabrication of scaffolds – porous tridimensional structures that aim to mimic bone architecture and functionality –, which are made of different biomaterials, loaded with human cells and studied their potential to replace and regenerate damaged tissue [84]. This explains why scaffolds must be biocompatible and biodegradable, as well as have adequate structural, biological, and mechanical properties to provide appropriate structural control and induce tissue regeneration simultaneously [85], [86].

For bone tissue engineering, specifically, scaffolds or any other bone graft alternative must meet and consider three important criteria: osteoconductivity, osteoinductive stimuli and the use of osteogenic stem/progenitor cells [40], [87]. Hence, when a bone graft or scaffold is developed, the first approach would

be to seed and grow cells in it and in the presence of regulating factors that promote cell survival, differentiation, and mineralized bone formation *in vitro* for further and more complex studies [87].

2.3.3 Bone Tissue Mechanics' and Bone Tissue Engineering's Advances for Osteoporosis

Due to osteoporotic bones having low BMD, low capacity of bone regeneration and an increased osteoclastic activity previously discussed, bone microarchitecture changes. As a result, there is a reduction in interconnectivity and mechanical stress tolerance [5]. Considering this and addressing the lack of novel fracture treatment alternatives [22], bone tissue mechanics and engineering researchers have been working on studying the trabecular bone -the most affected by osteoporosis- and its mechanisms to develop not only more accurate drug delivery systems, but also on functionalized therapies and scaffolds that have the ability to improve osteointegration and fast fracture healing [5].

Wang *et al.* (2015) reported that they were able to repair critical-sized radius bone defects using an allogenic fetal graft based on decalcified bone matrix (DBM) and bone-marrow derived MSCs (BM-MSC) -harvested *in vitro*- in a rabbit osteoporosis model [7]. Mai *et al.* (2021) also reported the successful development of a tridimensional microporous (150–300 μm) scaffold made from reduced a graphene oxide/polypyrrole composite and modified by strontium (Sr) (3D rGO/PPY/Sr) for the repair of bone defects caused by osteoporosis [88]. Their scaffold showed promising biocompatibility, osteoconduction, and osteoinduction abilities.

Nevertheless, despite the advances and potential showed in animal and *in vitro* studies, more clinical evidence is required to prove that the outcomes of these approaches can be better compared to conventional techniques [40]. Thus, the use of more accurate and realistic models to study and mimic the mechano-biology of the bone is imperative [17].

2.4 Models of Study for Bone Tissue Mechanics and Engineering

Different methods have been used to evaluate and study different aspects of bone - its biology, cellular mechanisms, biomechanics and/or regeneration/remodeling processes for bone grafting applications. Such methods are *in vitro*, *in vivo* and *ex vivo* experimentations, where each of them has its own characteristics and limitations [15], [17], [24], [87], [89]. **Non-viable bone testing methods**, that commonly use cadaveric bone samples, have been also used to study trabecular bone biomechanics [35], [47], [50], [52], [54], however, most of these studies involve the embedding, drying or artificially hydrating of the tissue for

testing, which can alter the bone's natural mechanical properties [50]. Table 2-1 shows a detailed description of the characteristics, benefits, and limitations of each of these models of study that have been used historically to understand the mechanics and biological processes of bone tissue, as well as to develop new treatment strategies.

Table 2-1. Description and Characteristics, Benefits, and Limitations of the different models to study bone tissue: in vivo, in vitro, ex vivo. In vitro models have been separated into bidimensional (static culture) and tridimensional (dynamic culture) for better representation [49], [51].

Model of Study	Description and Characteristics	Benefits	Limitations
In Vivo	Consists of the use of an animal model. It remains the gold standard to study bone metabolism, systemic bone diseases or fracture healing due to the nature of the model. For orthopaedic implants or biomaterials, larger animals are preferably used.	- Only model that adequately represents the interplay between all the different cell types in bone tissue. - There exists a great variety of inbred stains with specific gene over-expression or knock-out that can be used to study specific mechanisms. - Bone of smaller animal models can be broken with a defined force, which is a relatively reproducible fracture to represent the pathology of a trauma.	- No specific species fulfills the requirement of an ideal animal model. Moreover, there are important species-dependent differences in bone metabolism. - Ethical implications are often implied. - Expensive. - Leads to animal sacrifice. - Large degree of systemic complexity. - Often not considered satisfactory for the investigation of the mechanisms that underlie cellular processes in bone. - Data for the mechanical properties values obtained must be considered as approximations of real values because the effect of muscle fatigue on the bone strain/strain rates cannot be excluded in all studies. - Small anatomy of some animal models limits the possibilities to fix fracture bones. Animals are not exposed to the same environmental influences as patients.
***In Vitro* (2D)**	Consists mostly of the use of cell culture techniques, where cells are harvested from tissue and proliferate in a suspension or attached to a surface in a monolayer. Tissue fragments are maintained in culture conditions (not necessarily maintaining architecture).	- The local environment can be tightly controlled. - Molecular and biochemical tools can ensure that experimental replicated are almost identical. - Cellular loss is not a major concern due to fluid shear stress, compared to dynamic cell cultures.	- Considered too simple to study the osteocyte physiological response to mechanical loading. - The organic and inorganic matrix characteristics are missing. - Hardly representative of the complex bone environment. - Cell proliferation in scaffolds is limited by diffusion. - Co-cultures with different cell lines are time-consuming and not representative of *in vivo* situations.
***In Vitro* (3D)**	3D cell growth environments (commonly referred to as bioreactors) to overcome cell culture disadvantages, mimic the physiological complexity	- The use of flow perfusion bioreactors for scaffolds culture enable to pump culture medium through the scaffold's interconnected pores.	- Risk of cellular loss due to shear stress. The levels of shear stress required to induce cellular detachment are significantly greater than those expected to cause osteogenesis *in vivo*.

	of real tissue, and avoid the use of organ cultures.	- Bioreactors enable the close monitoring and precise control of key environmental conditions. - High degree of reproducibility and automation. - There is great advance in reproducing the formation of bone-like matrix and cell-mediated substrate degradation.	- If a cell adapts a bridging morphology type, it will show greater levels of cytoskeletal deformation than a flat cell. - Limitations have been reported depending on the aim of different studies. - Risk of diluting important factors secreted by cells, thus lowering the sensitivity of established analytical methods.
Ex Vivo	A whole organ/tissue or parts of it are maintained and grown in culture conditions. It is used to bridge the gap between cell culture and *in vivo* models. Trabecular core cultures utilize bone of larger animals and even humans. These are used to study bone metabolism and biocompatibility of materials.	- It is more similar to the *in vivo* situation compared to *in vitro* studies. - This system respects the bone's natural 3D structure and retains the extracellular matrix. - The conservation of the tissue architectural organization has greater chances in simulating the physiological distinct mechanical consequence of loading. - Not as complex as the whole animal. - Local effects (like mediators and mechanical stress) can be isolated from the systemic ones. - Best option to observe stem cell behaviour during linear bone growth and hypertrophic ossification.	- Loss of a vascular system, limiting the organ sample size that can be harvested. - Explants, unless maintained in culture system, cannot be used for experiments longer than 24h. - The artificial environment created requires higher attention from the researcher to the extrapolation of the results obtained to an *in vivo* situation.

2.5 Bioreactors in Bone Tissue Mechanics & Engineering

Regardless of the experimentation method used in a specific study -either *in vitro*, *in vivo* or *ex vivo*-, bioreactors have proven to be useful in the emulation of physiological conditions of natural bone, including not only chemical but also biomechanical stimuli for the dynamic culture of a biological model [24]. Moreover, parameters like pH values, O_2 saturation, flow rate, temperature and mechanical stimulation can be controlled with a dynamic bioreactor system [90]. Hence, they have proven to hold a clinical significance in providing testing platforms that is more similar to that of a whole tissue response, which facilitates the screening of treatments before the initiation of clinical trials, as well as helps reduce the use of animals for *in vivo* studies [91].

For *in vitro* cultures of scaffolds, for instance, bioreactor systems for dynamic culture are used to address some of the limitations of static culture of scaffolds. Scaffolds cultured statically are seeded with cells, and covered with media; then, this media is exchanged manually throughout the duration of the experiment [83]. However, mass-transfer limitations of nutrients and oxygen or waste removal are among the disadvantages of static culture, which can affect the cell viability within the scaffold [24].

In *ex vivo* studies of bone explants (including human), bioreactors play a crucial role in maintaining the bone viability for a certain period of time [91], while also offering the possibility to study cellular interactions, biomechanical cues, extracellular matrices and intercellular communication in the local bone microenvironment in a controlled experimental setting [92]. As a result, it is possible to maintain the natural diversity of bone cells and their spatial distribution [26]. Additionally, the use of bioreactors also helps the comprehension of bone mechanisms that otherwise would be too difficult to study in *in vivo* conditions [15].

Nowadays, different bioreactor models for various functional tissues can be found in the literature. Among the most common bioreactors, there are the spinner flask, rotating-wall vessel and perfusion [24], [91], [92], which are shown in Figure 2-9. Spinner flask bioreactors, then, consist of a dual-side cylindrical flask in which scaffolds are threaded into needles connected to the cover and submerged in the culture medium. A magnetic bar or shaft is used for cell culture media convection, providing a homogeneous distribution of oxygen and nutrients [93]. However, reports have shown that magnitude of shear stresses can vary greatly between different locations, not exposing all cells to the same shear stress [24].

On the other hand, rotating-wall vessel bioreactors comprise two concentric cylinders where the cell culture medium are contained in the annular space. The outer cylinder, then, rotates causing centrifugal forces that result in cells falling gently through the medium [24]. This configuration allows CO_2 gas exchange and oxygen supply, although it is an optimized suspension culture system, the transport of nutrients to the center of the scaffold has been reported to still be limited. Hence, convective forces could not extend to the interior of large constructs [94]. Lastly, perfusion bioreactors consist of flow perfusion - usually with a peristaltic pump [89], [95]–[97]- through the scaffold, bone graft or bone construct. Perfusion generates shear stress on cells and improves the transport of nutrients and oxygen to the constructs since the culture medium is continually recirculated [24]. These systems allow more precise control of the culturing environment, but the adequate incorporation of perfusion flow and mechanical loadings for long-term cultures still remain a challenge in bone tissue engineering [89]. Moreover, perfusion bioreactors also allow specimen-specific culture medium supply and storage, making it easier to control and monitor the specific conditions of each sample during the study.

Finally, although these systems have proven to address previous limitations and represent advances in tissue engineering, more work needs to be done in their optimization, scalability and cost-effectiveness [92], so they can be widely used in several regions for both bone tissue mechanics and engineering applications.

This way, possibilities of clinical translational research in the field may increase significantly, widening the horizons of clinical applications.

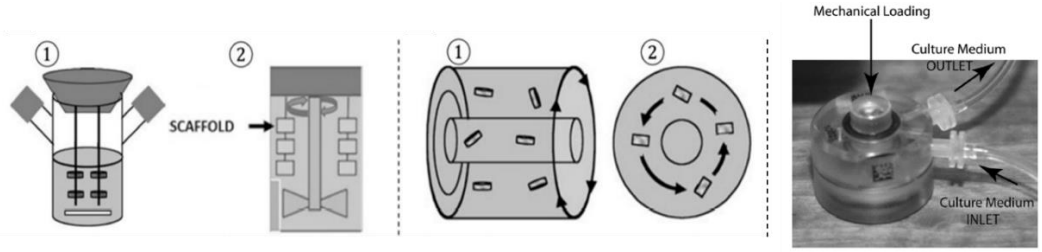

Figure 2-9. Most used bioreactor systems in the literature for dynamic culture of tissue models -in vitro and ex vivo-. On the left side is a spinner-flask bioreactor, on the center is a rotating-wall vessel, and to the right side of the image a perfusion bioreactor is shown. Image adapted from [14], [24].

2.6 Bioreactors with Mechanical Loading in Bone Tissue Mechanics & Engineering

Bioreactor systems have been widely used in literature because they provide 3D environments with mechanical stimulation, that can be provided with fluid flow [25] or with the use of a micro-mechanical testing machine. Osteogenic grafts for bone repair and bone itself can be studied under this type of dynamic stimulation [98], hence feasible for both *in vitro* and *ex vivo* studies [24], [89], [91], [92], [95]. Moreover, in the case of perfusion culture, it has been proven to promote homogeneous cell distribution [99], and efficient transport of critical nutrients by forcing media through the pores of the construct [98].

2.6.1 *In vitro* studies using perfusion bioreactors

When conducting *in vitro* studies with tissue engineered scaffolds, perfusion bioreactors can be used for both seeding and culture of scaffolds. Several studies [95], [96], [98], [100]–[103] have reported that for both seeding and culture scaffolds and the appropriate control of different process parameters, better outcomes in terms of viability, cell differentiation or proliferation are found in the dynamic conditions. Growth and mineralized matrix deposition enhancement by bone cells, and the expression of specific tissue markers are other good outcomes observed with the use of direct perfusion bioreactors in tissue engineering [90]. However, it is important to note that although these perfusion bioreactors follow the same functionality principle, specific designs vary between studies – some of them being designed by the research group. Moreover, static preculture has been reported to be crucial before perfusion, otherwise samples would get no benefit of the dynamic culture [102]. The reader is referred to Appendix B for a summary of the dynamic seeding/culture parameters controlled in the before-mentioned studies, as well as the experiments done to test viability, metabolic activity, differentiation, or proliferation of cells in *in vitro* dynamic culture studies.

2.6.2 *Ex vivo* studies using mechanically loaded bioreactors - Zetos system

For *ex vivo* studies of the viability maintenance of bone explants and their study, *ex vivo* organ culture systems have been developed to provide the biochemical and mechanical environment necessary to maintain the viability of bone samples for up to 4 weeks [14], [29], [89], [104]. These systems have been also employed to study mechanical loading, interactions between different bone cell types, and the molecular steps involved in bone resorption and formation [26], [97]. The integration of mechanical stimuli in these systems has been able to extend the lifespan of explants and induce bone formation [105]. Dua *et al.* (2021), for example, developed an *ex vivo* culture system [106] and characterized the process of mineralization on an implant surface using their *ex vivo* bone bioreactor. Their results showed that the bioreactor was able to sustain bone life and mineralization for up to 7 weeks under dynamic loading conditions [89], proving the potential of systems like these to study and develop orthopedic devices that require fixation through bone ingrowth.

In 2003, Jones *et al.* (2003) developed an *ex vivo* mechanically loading culture system of bone explant called Zetos, where force and/or compression can be applied and measured in real time to trabecular bone explants, and the physiochemical environment can be monitored and controlled [27], [28]. Therefore, physiological and mechanical signals can be applied to the bone core explants during the experiment, which can last up to 28 days [29]. Another important characteristic of the Zetos system is that it allows the maintenance of intact bone marrow within the trabecular bone core. Hence, both bone cores and marrow retain the stem cells necessary for bone (re)modeling during the perfusion of culture medium [14]. These explants consist of cylinder-shaped bone cores with a diameter of 10 mm and 5 mm of height obtained from trabecular bone [14], [27], [29], [104].

The Zetos system, like most bioreactors, can be used for studies that cannot be conducted in *in vivo* conditions. For example, the function of calcium channels in the osteoblast/osteocyte response to parathyroid hormone, since these channels cannot be blocked in live animals and keep bone metabolism active simultaneously [28]. Thus, this model makes the isolation of specific stimuli possible, in combination with mechanical stimuli, to understand phenomena like bone metabolic pathways [14]. It has been reported that the cyclic loading using Zetos for human, bovine and ovine trabecular bone explants reduced osteocyte apoptosis, enhanced osteoblastic activity, and promoted thicker and plate-like trabeculae with higher mechanical resistance, when compared to control groups that were unloaded [91].

The Zetos system for trabecular bone cores is shown in Figure 2-10, where both system and chambers are kept at 37°C throughout the study [28], [29]. The way this system works is that by using different wave forms and frequencies, force and/or compression can be applied to the trabecular bone with high precision (+/- 3%) [28], mimicking *in vivo* conditions. A frequency range of 0.1 to 50 Hz can be obtained to stimulate the samples dynamically -via uniaxial compressive displacement- with a piezoelectric (PZA) actuator, and compression that can be measured real-time with a precision of ±0.5 to ±1.5 με [29]. Thus, a quasi-static loading regimen can also be applied via the PZA, which allows the determination of the bone samples apparent stiffness [14], [29]. Bone cores are kept in the bioreactor chambers (polycarbonate) that are perfused with a peristaltic pump connected to culture medium reservoirs [104], where the effects of direct perfusion depend significantly on the medium flow-rate and the overall state of the constructs [90]. Additionally, dynamic loading is used to stimulate bone cells, where various oscillation patterns such as standard sinusoidal-, triangular-, square-signals and complex waveforms can be applied on a bone sample [14], [27].

Regarding the maximum force that has been applied for bone loading with the Zetos system, it is limited by the control software and load cell. It has been reported to be 1500 N and 4500 N [14], [27], [29], although calibration protocols usually establish the maximum force to be 1500 N. The maximum displacement is around 70 mm and is limited by the maximum expansion of the unloaded PZA, in which the nominal maximum expansion under no load conditions is typically 60 μm, although this also depends on the load application [14], [27]. Thus, process parameters depend on the specific load conditions and research question but can be controlled during the system configuration. Figure 2-11 shows a summary of different reported process parameters in the literature. To date, only Zetos has shown the potential for screening factors and biomaterials under physiologically relevant loading; whereas, other bioreactor systems have been developed to be used for specific research questions and only allow the use of specific bone explant shape and sizes [105].

Most bioreactor chambers used in the literature for Zetos are made of polycarbonate (PC). However, some limitations include its high price, with the whole system costing approximately USD $22,000 [107]. It is also difficult to fabricate [14], [28], and the size limit for the bone core of 10 mm x 5 mm (diameter x height) is below the recommended height-diameter ratio for adequate bone mechanical properties characterization [108].

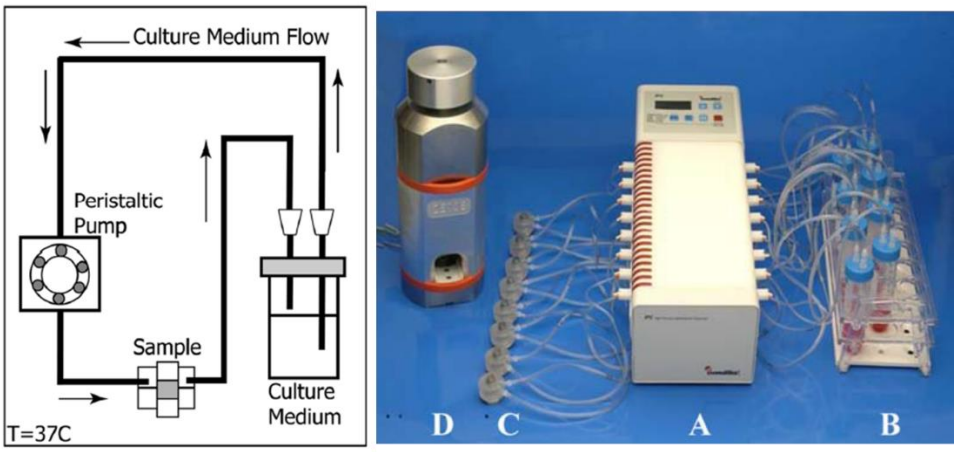

Figure 2-10. Schematic diagram of the Zetos system for ex vivo organ culture of trabecular bone on the left. On the right, the real-life photos of the system are shown: (A) is a peristaltic pump that allows the diffusion of fresh media stored in (B). The culture media, hence, is diffused through the bone cores within the chambers (C). (D) is a controlled mechanical loading device that serves to stimulate the bone cores daily. Diagram and photo adapted from [14], [28].

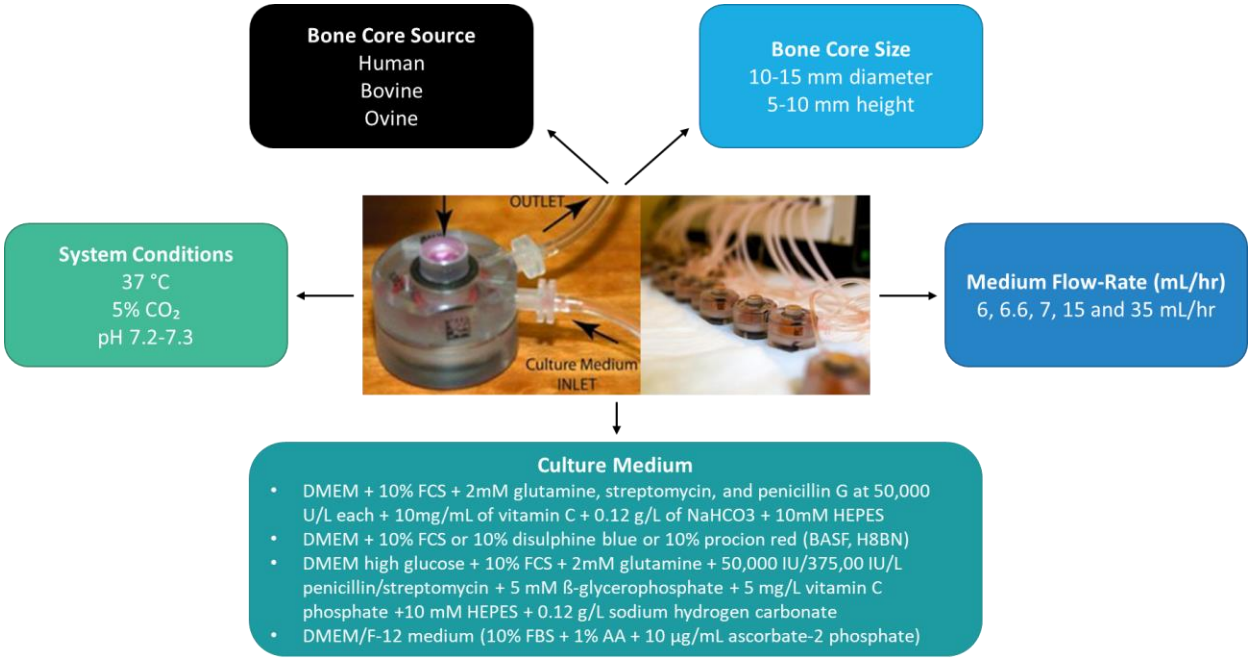

Figure 2-11. Controllable Zetos system configuration parameters. Oscillation patterns and waveforms for cyclic loading are not included. Information obtained from [14], [29], [30], [104], [106].

Advances achieved with Additive Manufacturing (AM) technologies allow the creation of complex 3D structures of varying sizes [20], [84], and the possibility to control both internal and external microarchitectures of fabricated structures [83]. A 3D printable bioreactor system, then, could address the before-mentioned limitations while also keeping the same principles established in Zetos – being more cost-effective, easier to implement and optimize with flexible designs and specific requirement considerations.

This is what Kunath *et al.* (2022) did using a polyjet 3D printer and MED610™ as a biomaterial for the bone chambers. Although it was demonstrated that the system can be used for the long-term culture of *ex vivo* bovine trabecular bone cores, further studies are required to assess cell viability and metabolic activity, as well as address leakages observed in some bioreactors and define a mechanical stimulation waveform to test the effects of strain rate and magnitude independently [30].

In conclusion, although significant advances on bone explant culture systems have been achieved, more research is needed to make it easily reproducible and more reliable, in order to tackle the gap between *in vitro* and *in vivo* research in preclinical testing [105]. A cost-effective bioreactor system, then, could have the potential to address these limitations by allowing the study of cellular dynamics for both bone tissue mechanics and bone tissue engineering applications. If properly designed and manufactured, a bioreactor system would allow the isolation of desired effects (e.g., mechanical loading) on the bone response behavior, and more specific studies could be conducted.

Chapter 3
OBJECTIVES AND OUTLINE

3.1 Overall Objective

The overall objective of this research is to improve and evaluate the current design of QBJB's open-source 3D printed bioreactor system for *ex vivo* and *in vitro* dynamic long-term culture of different biological tissue models for bone tissue mechanics and engineering applications.

3.2 Specific Objectives

3.2.1 Address previous design limitations to improve the QBJB's MED610™ bioreactor functionality and biological viability.

3.2.2 Evaluate the biological viability of MED610™ as a biomaterial for the bioreactor fabrication using additive manufacturing technologies.

3.2.3 Evaluate the new MED610™ 3D printable bioreactor system in an *ex vivo* bovine trabecular bone core study using a different stimulation load profile to previous study.

3.3 Thesis Organization

This thesis document is composed of seven chapters, comprising the work done thanks to the collaborative effort between Queen's University (Kingston, ON, Canada) and Universidad Adolfo Ibáñez (Viña del Mar, Chile). Chapters 1, 2 and 3, provide the primary background and motivations, literature review and objectives of this thesis project to improve an open-source 3D printable bioreactor and loading system design, respectively. Chapter 4 proposes the design changes of the previously evaluated open-source 3D printable bioreactor design for *ex vivo* bone organ culture, addressing the identified limitations. In Chapter 5, an evaluation using cell culture of the cleaning and sterilization protocol for the 3D printable photopolymer MED610™ is done, along with an update of said protocol, to reduce the cytotoxic properties of the manufacturing procedure. This work was presented as a podium presentation at the *XXI Congreso Internacional de Metalurgia y Materiales 2023* conference in Viña del Mar, Chile and has been prepared for journal paper submission. Chapter 6 provides the results from an *ex vivo* study performed with bovine trabecular bone cores using 3D printed bioreactors to test the efficacy of the MED610™ bioreactor design

changes for long-term trabecular bone organ culture. The work from this chapter was presented as a podium presentation in the 2023 version of the European Society of Biomechanics Congress in Maastricht, Netherlands. Finally, Chapter 7 comprises the final conclusions, and an insight into future applications for both bone tissue mechanics and engineering. Additional figures, tables and information are provided in the appendices.

Chapter 4

BIOREACTOR CHAMBER RE-DESIGN AND EVALUATION

4.1 Abstract

Polycarbonate bioreactors allow *ex vivo* studies of trabecular bone cores and have been used during the last twenty years to study the dynamics and/or the mechanical behavior of trabecular bone tissue in response to stimulation. Single-sample bioreactor chambers like those of the Zetos bioreactor and loading system address several limitations of both *in vitro* and *in vivo* studies, thus working as a bridge between both models. However, limitations with polycarbonate bioreactors, such as high fabrication costs and not meeting bone tissue mechanical testing standards, inspired researchers to design an open-source 3D printable bioreactor system that is more cost effective and easier to adapt, so that specific study requirements can be met with slight designs modifications. The first version of the 3D printable bioreactor chamber was fabricated using MED610™ as printing material, however, a significant number of samples were lost during the first evaluation iteration due to system leakage. Therefore, the aim of this work was to investigate and address the source of leakage and propose a second version of the 3D printable bioreactor chamber design. The problems with the first version design were addressed and an updated second version of the 3D printable bioreactor chamber was proposed and evaluated in terms of leakage, thus allowing the next steps in the bioreactor chambers and loading system's validation process.

4.2 Introduction

Bone biomechanical behavior studies have shown that better understanding of bone tissue mechanics is key in the development of more effective strategies to prevent bone fracture, regenerate, and repair bone defects such as osteoporosis [49]. Although polycarbonate (PC) bioreactor chambers have been successfully used to study tissue mechanics in trabecular bone cores *ex vivo* [14], [28], [104], [109], they are difficult and expensive to fabricate, and the height-diameter ratio for bone cores (½) is below the standard for mechanical compression tests [108]. A bioreactor chamber was developed using polyjet 3D printing and photopolymer MED610™ as printing material that has been suggested as suitable for long-term culture [110], [111]. This bioreactor chamber design was inspired by the Zetos bioreactor and loading system [28], where each bone core sample is contained in a closed system with an individual culture medium reservoir,

and can be mechanically stimulated without opening the system, so that sample contamination risks are minimized.

The first version of the 3D printable bioreactor chamber had been evaluated in a previous study [30], however, leakage and loss of samples (about 26% of the specimens) were observed due to key aspects that were not considered in the design of the original bioreactor chambers. Leakages in bioreactor chambers are critical, since constant nutrient-enriched culture medium circulation from the reservoir to the bone core sample (situated inside the bioreactor chamber) is required for the *ex vivo* tissue maintenance during long-term studies, typically 21 to 28 days [109], [112], [113]. Thus, the objective of this work was to identify the source of the current design malfunctions, propose, and evaluate an updated (second version) 3D printable bioreactor chamber design for trabecular bone core culture with compressive load application.

4.3 First Version Design Analysis & Limitations

4.3.1 First Version 3D Printable Bioreactor Chamber Design Description

Kunath *et al.* (2022) reported the first 3D printable bioreactor chamber design [30], based on the Zetos PC bioreactor chambers [14], [28], [29], [109] for *ex vivo* bone cores maintenance and mechanical stimulation. Briefly, the bioreactor chamber (Figure 4-1) consists of a MED610™ cylindrical body (body and cap) attached by a M24 x 2.0 mm threaded connection, with the primary function of containing a single bone core with a maximum of 10 mm x 11 mm (diameter x height) dimensions. Both body and cap parts contain a slot to fit an X-ring that help secure sapphire pistons above and below the bone core for chamber enclosure and mechanical stimulation. Additionally, the chamber has inlet and outlet channels for culture medium circulation throughout the bioreactor, and an additional horizontal channel was included in the design to ease support material removal from the inlet channel.

To assemble the bioreactor chamber, a MED610™ tapered plug (for horizonal channel), sapphire pistons, X-rings (silicone rubber), and 19 mm and 11 mm ID silicone rubber O-rings seals (No. 5233T315 and 5233T296, respectively, McMaster-Carr, Elmhurst, IL, USA) are included. A food-grade silicone lubricant (No. 1204K32, McMaster-Carr, Elmhurst, IL, USA) is applied to reduce friction between the pistons and the X-rings.

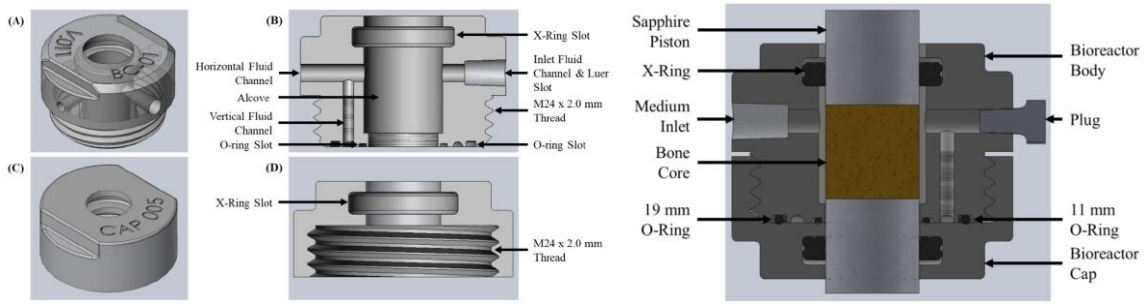

Figure 4-1. On the left side: (A) Isometric and (B) section views of the first version of the 3D printable bioreactor chamber body. (C) Isometric and (D) section views of the first version of the 3D printable bioreactor chamber cap. On the right side, the section view of the assembled bioreactor chamber is shown [30].

4.3.2 Bioreactor System Assembly

The bioreactor and loading system (Figure 4-2) consists of four main components: the bioreactor chamber, culture medium reservoir and its MED610™ culture tube stopper, peristaltic pump (Ismatec™ ISM939D, No. 78000-41, Cole-Parmer Canada) and tubing (18G needles, 0.053" OD PTFE tubing, 1.52 mm ID Tygon® E-Lab tubing, 1.52 mm 2-stop PharMed® BPT pump tubing, polypropylene male luers to 1/16" hose barb adapters, and polyvinylidene fluoride 1/16" barbed male-male adapters), and a mechanical loading system (Biomomentum Mach-1). All components in the system assembly are sterilizable by steam or gas sterilization.

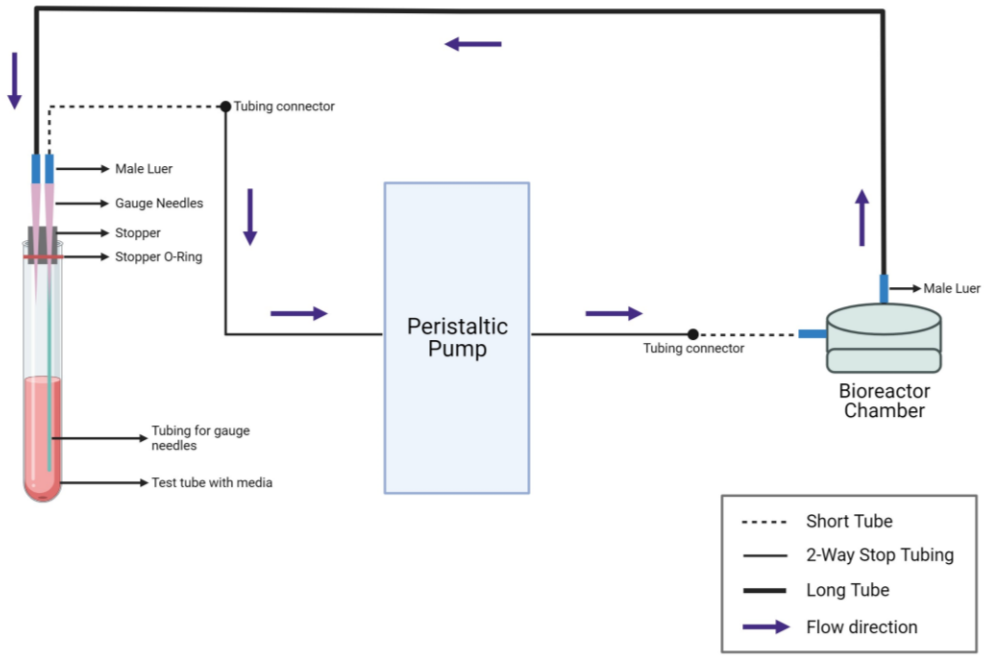

Figure 4-2. Schematics of the bioreactor circuit assembly for culture medium circulation through bioreactor chamber. Both 'short' and 'long' tubes are 1.52 mm ID Tygon® E-Lab tubing. Created with BioRender.com.

4.3.3 Limitations Observed with First Version 3D Printable Bioreactor Chamber Design

Because leakage was observed during the first *ex vivo* trabecular bovine trabecular bone core study with the first version design [30], the leakage source had to be identified for design modifications and improvement. Therefore, four (4) randomly chosen previously-used MED610™ bioreactor chambers from the first study were assembled following the first version system assembly instructions, with no bone cores nor bone surrogates inside (Figure 4-1). A newly printed MED610™ first version bioreactor chamber was used for comparison. The mechanical loading was not applied in this work, to identify the leakage source in the bioreactor circuit.

Once the bioreactor circuit was assembled, colored water was perfused through the empty bioreactor chambers at 0.5 mL/min, with a cloth underneath the chambers to better visualize whether there was leakage or not. After one day of assembly and water circulation, three out of the four previously-used bioreactor chambers showed considerable water leakage (Figure 4-3).

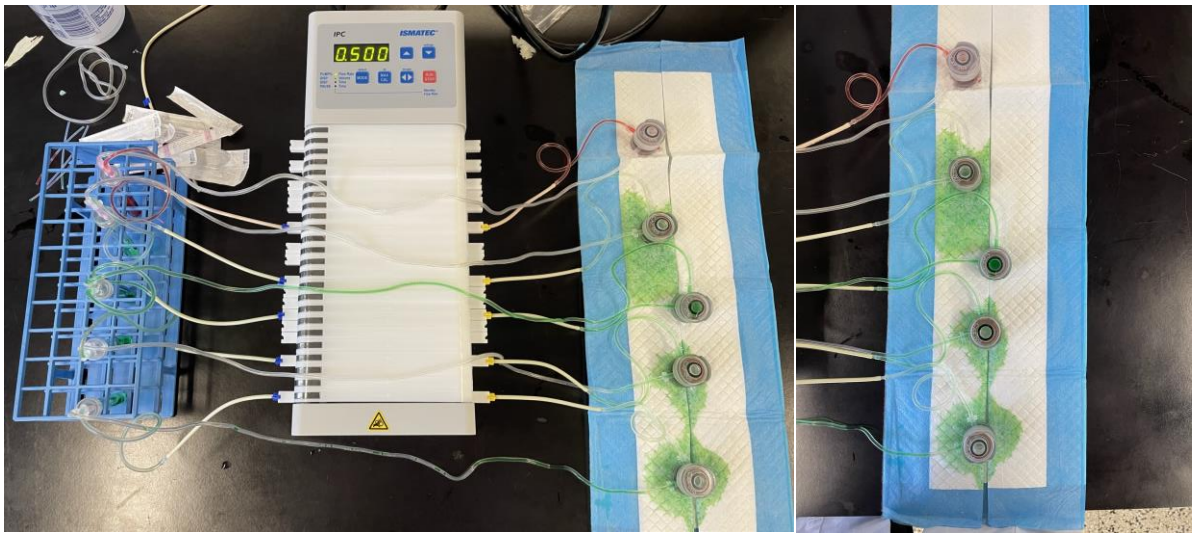

Figure 4-3. Leakage (water with green colorant) observed in three out of the four previously-used empty bioreactor chambers assembled in the bioreactor circuit.

With close inspection of the bioreactor chambers, it was determined that there was one main source of liquid leakage: through the sapphire pistons, potentially due to the X-Ring or O-Ring seals.

Regarding these results, it was noted that the X-Rings used in both the current study and the first MED610™ bioreactor study were dated to the year 2009 (13 years before the moment of the experiment) and no longer available for purchase. These X-rings may have been autoclaved several times (for both PC

and MED610™ bioreactor systems) to ensure sterile conditions in each study. Therefore, the X-rings could have reached their lifespan due to repeated usage and autoclaving, where the bioreactor chambers were constantly under compressive loading for mechanical stimulation of bone cores.

Although unknown, the X-rings from the first bioreactor chamber 3D printable version were potentially made of Buna-N Rubber (McMaster-Carr, Elmhurst, IL, USA), and the temperature range for operation stated is -34 to 107ºC. The Centers for Disease Control (CDC) and Prevention (USA) Sterilization Guidelines in Healthcare Facilities suggest that supplies used should be autoclaved for at least 30 min at 121ºC [114]. Being in a Biosafety Level (BSL) 2 laboratory, this is the routine protocol that is used for sterilization. However, it has been established that for 10 degrees higher than the working temperature (107 to 121ºC in this case), the life expectancy of the product will reduce by 50% [115], and considering the 15 years average shelf life of Buna-N Rubber, the X-Rings used were most likely past their proper functioning period.

4.4 Second Version Bioreactor Chamber Design Requirements and Evaluation

To make sure the bioreactor chamber functions properly, and no leakage occurs, new X-rings had to be purchased, according to the previous inspection. The original X-rings from both the Zetos and the first design version of the 3D printable bioreactor chambers, however, are no longer available for purchase. New X-rings with different dimensions had to be acquired, which implied design changes in the first version of the 3D printable chamber. The X-rings (Buna-N Rubber, dash number 110, No. 90025K222) were obtained from McMaster-Carr (Elmhurst, IL, USA), and the new dimensions were cross-sectional width of 2.62 mm, outer-diameter (OD) of 14.43 mm, and inner-diameter (ID) of 9.19 mm, compared to 2.45 mm, 14.95 mm (OD), and 10.05 mm (ID), respectively, from the old X-rings.

Although the sapphire pistons are of 10 mm diameter, the nearest X-ring ID dimension found in the market was 9.19 mm. Hence, two different X-rings slot cutouts were designed to evaluate the friction between the X-ring and the sapphire pistons. In the first version, there was a 0.55 mm difference between the X-ring slot cut-out and the X-ring cross-sectional width. Thus, two different options were designed and fabricated for the second version (Option 1 and Option 2) with spacing differences between the slot cut-out and the cross-sectional area: 0.55 and 0.45 mm, respectively. Two samples per option were fabricated for a quick evaluation. After printing, the bioreactor chambers were cleaned following the cleaning protocol [30], and the system was assembled following the diagram described above (Figure 4-2).

4.4.1 Evaluation Procedure with Mechanical Testing

In the second version of the system assembly, 10 x 10 mm (height x diameter) Ultem® (polytherimide) polymer bone surrogates (E = 3300 MPa [116]) were assembled with the bioreactor chambers to test for leaking, friction and residual stiffness. For three weeks, the bioreactors were loaded 5 times a week using a Mechanical Testing Machine and a 250 N multiple axis load cell (MA242 and Mach 1, Biomomentum, QC, Canada) to determine if there would be leakage due to frequent cyclic loading. The cyclic loading was set as a sinusoidal waveform with 0.02 mm amplitude and 2 Hz frequency for 150 cycles.

Additionally, the apparent residual stiffness ($K_{app,res}$) was calculated to determine which of the two design options had less effect on the bone surrogate apparent stiffness values. $K_{app,res}$ was considered as the difference between the adjusted apparent stiffness obtained from a bone surrogate between two sapphire pistons system (P+BS), and the apparent stiffness of whole assembled bioreactor and loading system (BR). Therefore, bone surrogate apparent stiffness (K_{app}) was tested within the bioreactor chambers and out of them to obtain $K_{app,res}$. Mechanical testing consisted of a 10 N pre-load, a pre-conditioning loading with 0.0001 mm displacement and 0.5 Hz frequency for 5 cycles, and a 0.11 mm displacement load at 0.1 mm/s. The mechanical stimulation and testing set-up is described in Figure 4-4. A system compliance of 0.000639 mm/N [30] was considered in all calculations.

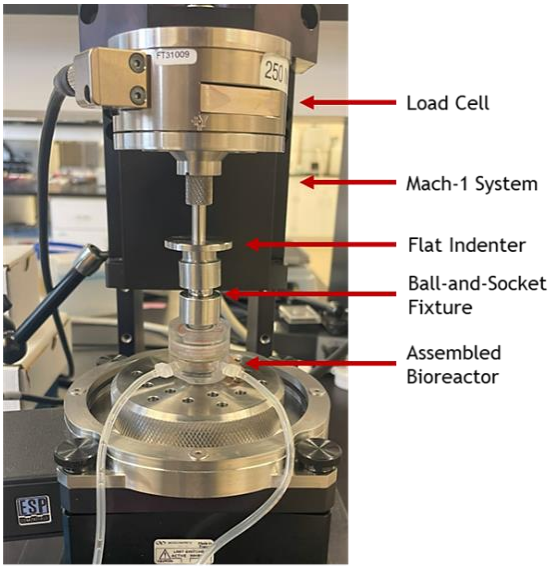

Figure 4-4. Compression testing set-up components using the Mach-1 Micromechanical Testing Machine and a 250 N load cell.

K_{app} results are shown in Figure 4-5. On average, $K_{app,res}$ was 1482 N/mm and 1522 N/mm for Option 1 and 2, respectively (Table 4-1). These results further evaluated the 0.55 mm slot cut-out difference from the first version bioreactor chamber design.

On the other hand, no leakage through the sapphire pistons was observed in either option during the three weeks of mechanical loading on the assembled system. However, a new source of leakage was observed: through the MED610™ horizontal channel tapered plug, which was excluded in the next design version, since its original purpose to facilitate support removal cleaning was not required.

Therefore, because of both design consistency and the $K_{app,res}$ results obtained, Option 1 was chosen as the more appropriate for the second version of the bioreactor chamber design, considering the new X-ring dimensions. It is also important to note that this $K_{app,res}$ method is used as rapid design evaluation, thus why consistency was prioritized.

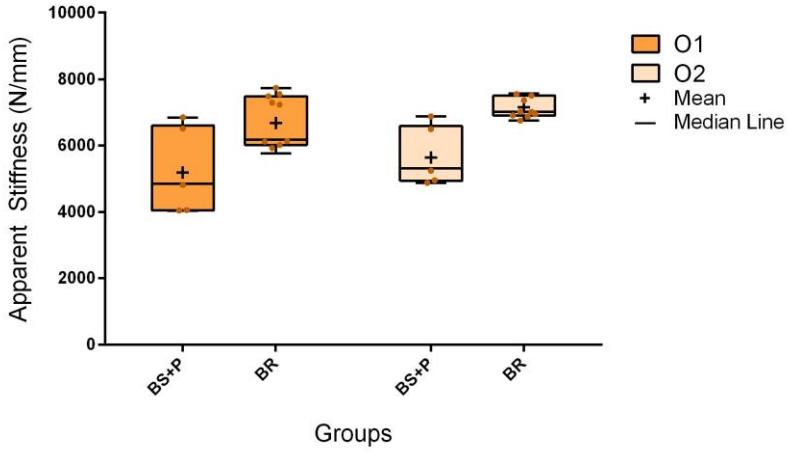

Figure 4-5. Apparent Stiffness (K_{app}) comparison between the corresponding bone surrogate (BS+P) and the bioreactor chamber design option (O1 – Option 1, O2 – Option 2).

Table 4-1. Mean Apparent Stiffness (K_{app}) of bone surrogate obtained for the bioreactor chamber designs, Option 1 and Option 2, as well as the resulting Apparent Residual Stiffness $K_{app,res}$

	Mean Apparent Stiffness (SD) (N/mm)	
	Option 1	**Option 2**
Bone Surrogate	5191 (1214)	5636 (841.4)
Bioreactor	6673 (769.5)	7158 (298.8)
Apparent Residual Stiffness (N/mm)	**1482**	**1522**

4.5 Second Version Bioreactor Chamber Design

Following the establishment of the design modifications and requirements, a second version of the bioreactor chamber was designed (Figure 4-6). In this second version, the main changes were:

- The X-ring cut-outs were adapted according to the new X-ring dimensions. Therefore, the cut-outs in both the body and cap of the bioreactors were set to have a 0.55 mm difference in relation to the new X-ring cross-sectional width, thus having a 3.17 mm height. Additionally, the diameter of the cut-out was set to match that of the new X-ring (14.43 mm).

- The horizontal fluid channel that went through the whole chamber and its plug component were removed due to its leakage potential. However, the connection between the horizontal and vertical fluid channel was maintained, which is why it is now considered the internal fluid channel, similar to the original Zetos design [14], [109].

The design differences between the two 3D printable bioreactor chambers are shown in Figure 4-7. A complete set of the corresponding mechanical drawings and assembly for all the components and parts of the second 3D printable bioreactor chamber designed in the current study are detailed in Appendices C and D.

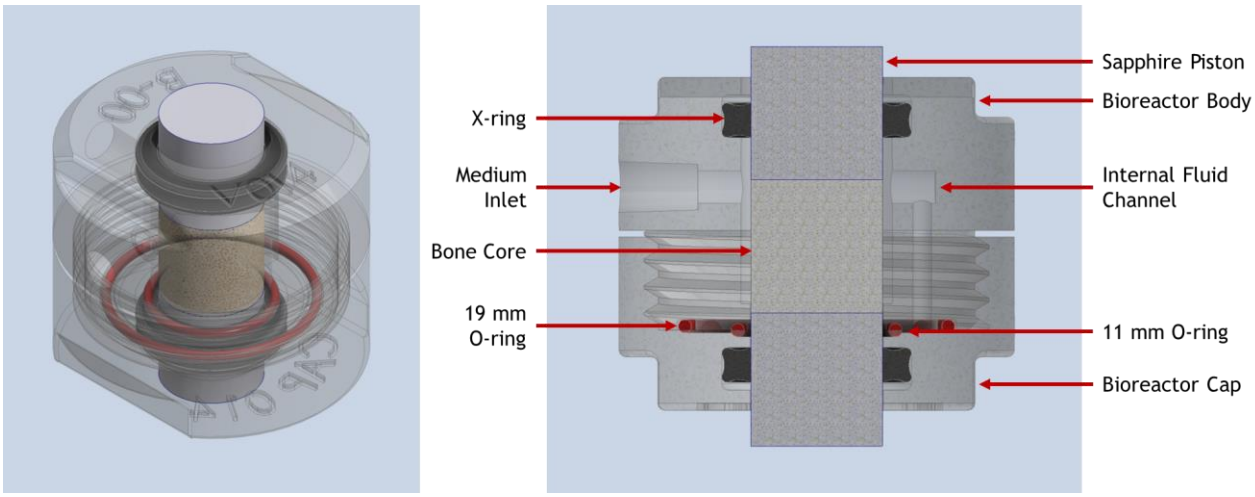

Figure 4-6. Isometric and section views of the second version of the 3D printable bioreactor chamber assembled with the sapphire pistons, X-rings, O-rings and a 10 x 10 mm bone core.

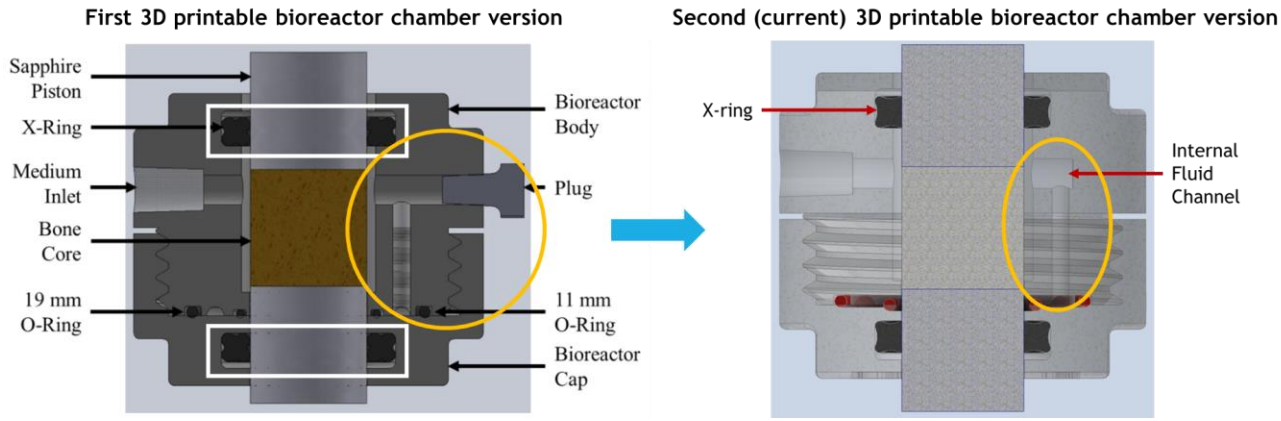

Figure 4-7. Design differences between the first (left) and the second (right) version 3D printable bioreactor chamber designs. The X-ring cut-outs dimensions were adapted to fit the updated X-rings (white rectangles) and the tapered plug was removed, converting the horizontal fluid channel into an internal fluid channel (yellow circumferences).

Chapter 5

CLEANING AND STERILIZATION PROTOCOL AND EVALUATION FOR MED610™ 3D-PRINTED BIOREACTORS

This chapter was written independently for journal submission

PROTOCOL TO DECREASE CYTOTOXICITY OF COMPLEX MED610™ 3D-PRINTED CONSTRUCTS FOR *IN VITRO* OR *EX VIVO* CULTURE STUDIES

Alejandra Correa Belloso (1, 2), Brian A. Kunath (1), Juan F. Vivanco (2), Heidi Ploeg (1), Roshni S. Rainbow (1)

(1) Department of Mechanical and Materials Engineering, Smith Engineering, Queen's University, Kingston ON, Canada
(2) Facultad de Ingeniería y Ciencias, Universidad Adolfo Ibáñez, Viña del Mar, Chile

5.1 Abstract

Polyjet 3D printing enables the manufacturing of complex structures with high resolution and processing accuracy for diverse biomedical applications. In this study, the biological viability of MED610™ for complex constructs was evaluated, with the exemplary application of a 3D printable bioreactor chamber for organ culture. The use of MED610™ for *in vitro* and *in vivo* applications arises contrasting opinions regarding its biocompatibility among the scientific community, however, some evidence suggests that leachates could be negated to decrease their cytotoxicity when appropriate cleaning and sterilization procedures are followed. A sterilization screening initial step using different sterilization protocols was conducted, where the combination of a sonication protocol and autoclaving showed the most promising results in terms of cell viability. Then, a perfusion bioreactor system set-up with MED610™ chambers was used to further validate the proposed sterilization protocol, where increased viability when compared to the control group was observed. The findings of this study support continuing developments of MED610™ 3D printed bioreactors for organ culture and other complex 3D-printed structures for *in vitro* or *ex vivo* studies in biomedical applications.

5.2 Introduction

Within the last two decades, advances achieved with Additive Manufacturing (AM) technologies and materials allow the creation of complex three-dimensional (3D) structures of varying sizes [20],[84], as

well as the possibility to control both the internal and external microarchitectures of fabricated structures [83] for biomedical applications, resulting in high precision and resolution. Along with AM technologies, the study and use of a proper biomaterial is crucial when considering specific biomedical applications. Therefore, different applications must meet different biological, chemical, and mechanical properties to support or promote- cellular or tissue bioactivity and/or the desired performance [117]. Biomaterials used in 3D printing for biomedical applications consist mostly of synthetic or natural-derived polymers; however, their biocompatibility remains a challenge, since changes during the printing process [118] or process conditions (light, heat, and/or chemical exposures) may have adverse effects on the overall construct compatibility [110], [111], [118], [119].

Polyjet 3D printing is based on substrate droplets deposition to produce thin layers that are cured using ultra violet (UV) light to form 3D parts [120]–[122]. Along with the photopolymer material printing, a gel-like soluble substance is also printed as a support structure, and it is commonly referred to as support material. With regards to biomedical applications, there are a number of advantages of polyjet 3D printing as compared to other AM methods, including the ability to print multiple types of materials simultaneously, increased capacity to print thin layers, and high processing accuracy (for example, a 120 µm dimensional deviation in a patient-specific neuro-vascular architecture [123]).

Although the removal of support material post-printing is a relatively simple and damage-free process, the need for this material as part of the printing procedure increases the cost and reduces the surface finish of the product [121]. Moreover, the composition of support materials is thought to be toxic for *in vitro* or *in vivo* applications, particularly if residues come in contact with biological tissues [110], [124], [125]. Additionally, defining optimal printing parameters remains a challenge due to the significant influence of these parameters on the essential characteristics of a printed structure [121].

MED610™ is an acrylic-based polymer used in polyjet 3D printing that has been identified to be biocompatible by the material's manufacturer (Stratasys) as per ISO standard 10993-1:2018 [126]. Specifically, the company lists MED610™ as biocompatible for 24-hour mucosal membrane contact but not for prolonged skin contact. Some researchers have suggested that MED610™ is unsuitable for cell and tissue culture conditions; for example, Schmelzer *et al.* reported that while MED610™ significantly decreased epidermal skin keratinocytes viability via indirect contact, there was no effect on the viability of bone-marrow derived stem cells (BM-MSC) in either direct or indirect contact with the material [125]. An *in vivo* study conducted with OECD zebrafish embryo showed that "as-built" MED610™ was unsafe and

toxic when exposed to the material; increased lethargy of behavioral perturbations (often preceding mortality) was also observed with the exposure due to photopolymer leachates [124].

In contrast with the before-mentioned studies, other researchers contend that MED610™'s biocompatibility is largely influenced by the cleaning technique employed [110], [111], [127]. Ngan *et al.* proposed a sonication protocol using Milli-Q and IPA that significantly decreased cytotoxicity in both *in vitro* and *in vivo* primary mouse myoblast cultures, when compared to the manufacturer's cleaning protocol [110]. Using a custom cleaning protocol and scaffold treatment prior to cell seeding, Egan *et al.* concluded good viability of MED610™ tissue-engineering scaffolds with human osteosarcoma cells (Saos-2) [111]. Another study with cylindrical scaffolds and *Mus musculus* calvaria cells (MC3T3) concluded that MED610™ serves as an excellent bone graft substitute by supporting osteoblast growth, and enhancing bone growth with improved compressive strength; custom study cleaning protocols were also followed [127]. Recently, Schneider *et al.* confirmed low cytotoxicity with a custom protocol, using MTT assay of MED610™ across different cell lines: murine cell line (L929), primary endothelial cells from umbilical cord vein (HUVEC), and primary chondrocytes and synovial fibroblasts [128]. A MED610™ bioreactor design for vascularized engineered soft tissue was also recently evaluated as biocompatible with stem cell-derived cardiomyocytes (iPSC-CM) [129]. Together, these findings support that the impact of MED610™ leachates could be reduced and the fabricated constructs could be used in cell and tissue culture if proper cleaning and sterilization methods are followed.

Therefore, purpose of this study was to establish a cleaning and sterilization protocol for complex MED610™-based 3D printed culture constructs, including a custom-made perfusion bioreactor chamber. The viability resulting from various cleaning and sterilization protocols for printed devices were assessed via a cell viability assay using the ATDC5 murine chondrogenic cell line. As a comparison, polystyrene tissue culture plates were implemented as experimental controls.

5.3 Methods and Materials

5.3.1 Reagents and Chemicals

Unless stated otherwise, all cells, culture reagents, and chemicals were obtained from Millipore Sigma (MA, USA). Unless stated otherwise, all experiments involved cell culture medium utilized DMEM:Ham's F12 (1:1) with 5% fetal bovine serum and 1% antibiotic-antimycotic solution.

5.3.2 MED610™ and SUP705B™ Materials

Two specimens were designed and printed using SolidWorks 2019 (SolidWorks Corp., Dassault Systemes, MA, USA) and a Stratasys Objet30 Prime 3D printer with photopolymer MED610™ and water-soluble SUP706B™ support materials (Stratasys); all parts were printed with a high-quality glossy finish setting (Objet Studio Ver. 9.2.11.6825). Table 5-1 highlights the composition of MED610™ [130] and SUP706B™ [131], as provided by the manufacturer. A significant percentage of the composition list, provided by Stratasys, contains proprietary content, which could include cytotoxic components.

Table 5-1. MED610™ and SUP706B™ compositions and percentage breakdowns.

MED610™ Composition		**SUP706B™ Composition**	
Component	**Weight-%**	**Component**	**Weight-%**
Total Proprietary	95.2-98.4	Total Proprietary	36.3-78.7
Caprolactone Acrylate	1.00-3.00	Propane-1,2-diol	10.0-30.0
1,7,7-Trimethyltricyclo [2.2.1.02,6]heptane	0.10-0.30	Polyethylene Glycol 400	10.0-30.0
2-Propenoic Acid, 1,2-Ethanediyl Ester	0.10-0.30	Acrylic Acid, 2-Hydroxyethyl Ester	1.00-3.00
Acrylic Acid, 2-Hydroxyethyl Ester	0.10-0.30	4-Methoxyphenol/Mequinol	0.10-0.30
Acrylic Acid	0.10-0.30	2,6-Bis(1,1-Dimethylethyl)-4-Methyl-Phenol	0.10-0.30
Camphene	0.10-0.30	Heptane	< 0.10
Glycerol, Propoxylated, Esters with Acrylic Acid	0.10-0.30		

5.3.3 3D Printing and Support Material Removal

To screen sterilization protocols, a simple rectangular specimen (Fig. 5-1 and 5-2) was printed with dimensions of 15 mm x 15 mm x 4 mm (length x width x height). To assess sterilization protocols for more complex cell culture devices, a multi-part specimen was printed using a custom-made bioreactor design (Fig. 5-2), adapted from the polycarbonate (PC) bioreactor used by Vivanco *et al.* [14] and Meyer *et al.* [109]. After printing, all visible exterior and interior support material was manually removed from all parts with a pick tool. Specimens were then individually washed in a high-pressure waterjet and air-dried.

5.3.4 Cell Viability Assay

To assess the effectiveness of sterilization protocols for MED610™ printed specimens, cell viability studies were completed using the ATDC5 murine chondrogenic cell line. Cells were plated in black opaque

96-well plates (Sigma Aldrich, MO, USA) at a seeding density of 10,000 cells/well for the screening protocol studies and 5,000 cells/well for the perfusion studies. After 24 hours of incubation at 37°C and 5% CO_2 to allow for cell attachment, culture medium was removed and replaced with conditioned medium from sterilization experiments (Day 0 and every 2-3 days after). Cell viability was assessed using the Cell-Titer Blue assay kit (Promega, WI, USA) and a Synergy H1 plate reader (BioTek, Winooski, VT, USA) using an excitation and emission filter pair of 560 nm and 590 nm, respectively [132], and a linear cell standard curve ranging from 0 to 50,000 cells (Appendices E and F). Background assay fluorescence was accounted for by measuring the fluorescence of the assay dye in 100 µL of fresh culture medium.

5.3.5 Sterilization Protocol Screening

A screening study was performed using the four rectangular printed specimens to compare four possible sterilization methods (Fig. 16): manufacturer's protocol (MP), sonication protocol (SP), autoclave protocol (AP), and a combined protocol involving both SP and AP (SP+A). Each printed construct was randomly allocated to a specific sterilization protocol test group. After cleaning constructs based on protocols described below, sterilized constructs were placed in individual 60-mm culture dishes containing sterile culture medium. A culture dish containing only medium (no printed specimen) served as a negative control. Dishes were placed at 37°C and 5% CO_2 for 7 days with medium changes occurring on Day 1, 2, 4, and 6. At each of these time points, conditioned medium from dishes was removed completely and replenished with fresh culture medium. Conditioned medium was applied to plated ATDC5 cells and cell viability was assessed on Day 3 and Day 7 (n = 6 wells/group per time point).

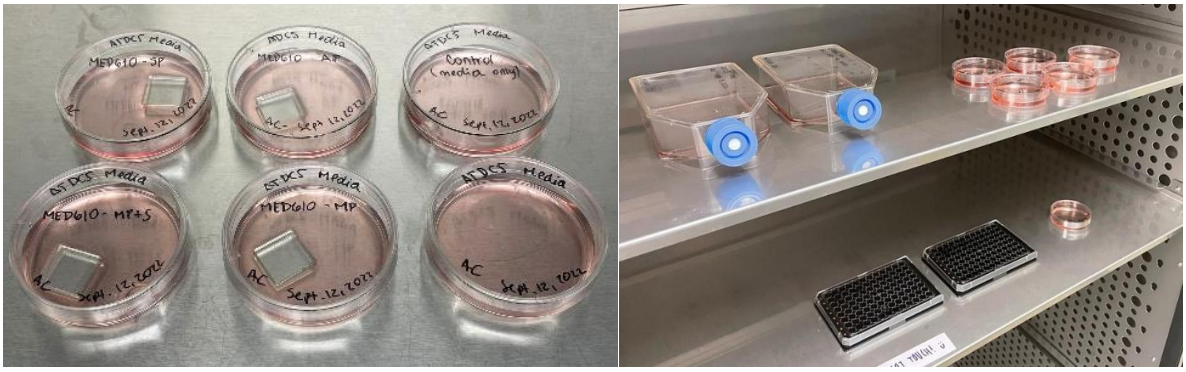

Figure 5-1. Rectangular constructs with the 4 different cleaning and sterilization protocols (MP, AP, SP, and SP+A) used for the sterilization screening protocol study.

5.3.5.1 Manufacturer's Protocol (MP)

The first sterilization protocol assessed was recommended by the manufacturer Stratasys for preparing biocompatible 3D-printed MED610™ [126]. After all visible support material was removed using pick tools and waterjet, printed specimens were further immersed in a solution of 1% w/v sodium metasilicate (Na_2SiO_3) and 2% w/v sodium hydroxide (NaOH) solution for 24 hours; this was followed by additional immersion in 5% v/v acetic acid with stirring for 1 minute to neutralize pH. Specimens were then placed in analytical grade isopropanol (IPA) for 30 minutes, dried at room temperature for 2 hours and then steam sterilized at 132ºC for 4 minutes.

5.3.5.2 Sonication Protocol (SP)

A sonication protocol (SP) was implemented based on a protocol first reported by Ngan *et al.* and who determined that sonication was able to remove MED610™ leachates and minimize adverse effects from MED610™ on cell viability and differentiation [110]. After following the MP and before autoclaved, specimens were rinsed under tap water for 1 minute, specimens were then placed in analytical IPA and exposed to sonication (40 kHz) for 2 hours, followed by additional sonication in Type 1 ultrapure water for 2 hours [110]. During all sonication steps, specimens were fully submerged with a minimum volume ratio of 10:1 for the solvent to specimen in a covered glass beaker. The sonication solvent was replaced with fresh solvent every hour. After sonication, the construct was rinsed in 80% ethanol and sterilized under UV light for 2 hours**.**

5.3.5.3 Autoclaving Protocol (AP)

For the autoclaving protocol (AP), after visible support material was removed with the pick tools and waterjet, specimens underwent steam sterilization at 132ºC for 4 minutes.

5.3.5.4 Combined Protocol (SP+A)

The final sterilization protocol combined SP and AP, as highlighted above. After completing the SP methodology, specimens underwent steam sterilization at 132ºC for 4 minutes.

5.3.6 Perfusion of Conditioned Medium Using MED610™ Sterilized Bioreactors

Using the complex printed bioreactor design, the SP+A protocol was further tested using a perfusion system over 14 days. Here, a printed bioreactor chamber was assembled into a closed-system consisting of the bioreactor, a glass medium reservoir, sterile tubing circuit, and a 24-channel peristaltic pump (Ismatec™ ISM939D, No. 7800041, Cole Parmer Canada, Montreal, QB, Canada); the set up of the system is shown in Figure 5-2. The bioreactor chamber assembly consisted of a MED610™ plug, MED610™ bioreactor, MED610™ bioreactor cap, sapphire pistons, silicone X rings, and silicone O-rings. The tubing circuit consisted of 2-way stop platinum-cured silicon tubing, polytetrafluoroethylene (PTFE) tubing, Tygon® E-Lab tubing, polypropylene luers, and polyvinylidene fluoride 1/16" connectors.

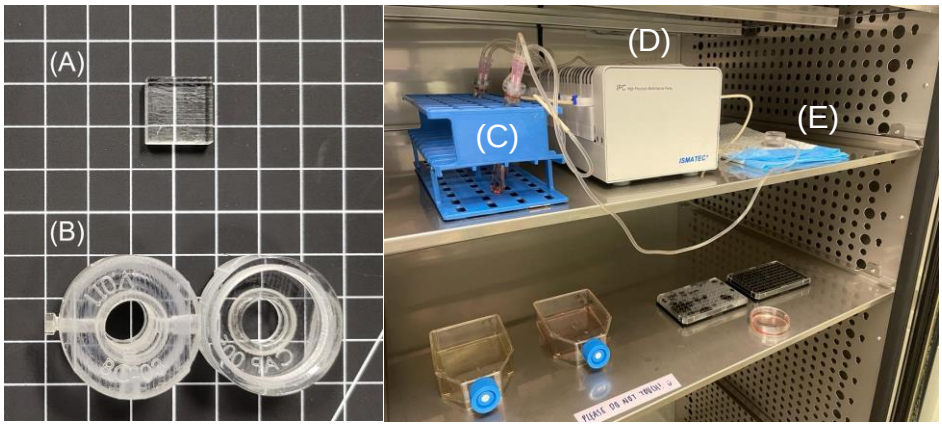

Figure 5-2. Construct differences between the (A) sterilization screening study and the (B) bioreactor perfusion study are shown on the left. On the right, an example of MED610™ bioreactor chambers (E) is shown, assembled with media reservoirs (C), and a peristaltic pump tubing circuit (D) to perfuse culture media through the bioreactors.

Prior to assembly, all non-MED610™ components were autoclaved, while MED610™ parts were cleaned using the SP+A protocol. After assembling the bioreactor system using aseptic techniques, culture medium was perfused through the system with a flow rate of 6.6 mL/hour [14], [109] at 37°C and 5% CO_2. A sterile culture dish containing culture medium alone served as a negative control. On Day 1 and every other day after, culture medium in the system was replaced with fresh medium. Conditioned medium was applied to plated ATDC5 cells on Day 1, 3, 6, 9 and 14. Cell viability was assessed on Days 3, 9, and 14 (n = 6/wells per timepoint).

5.3.7 Statistical Analyses

Statistical analyses of data were performed with SPSS® Statistics 23 (IBM, NY, USA) and GraphPad Prism® 6.1 (Dotmatics, MA, USA). Group normality was assessed with Shapiro-Wilk tests and confirmed lack of normality in the perfusion static bioreactor study. In the sterilization screening study, test group cell

viabilities were compared to the negative controls with a One-way analysis of variance (ANOVA) and Tukey's HSD post hoc multiple comparison test. Test group cell viabilities in the perfusion bioreactor study were compared to the control group with a Mann-Whitney U test. A statistical significance of $\alpha = 0.05$ was assumed in all statistical analyses.

5.4 Results and Discussion

5.4.1 Sterilization Screening Protocol Study

Cell viabilities corresponding to the MP, SP, and AP cell viabilities were not significantly different between each other on Day 3 (Figure 5-3 (A)). Compared to the control group, MP, SP, and AP cell viabilities were significantly lower ($p < 0.001$ for MP; $p < 0.01$ for SP and AP). However, no statistical differences were found between the control group and the SP+A cell viabilities on Day 3. On Day 7, no statistical differences between any of the groups were found (Figure 5-3 (B)). However, the cell count for SP+A was higher than the rest of the groups in both timepoints when compared to the other sterilization protocols.

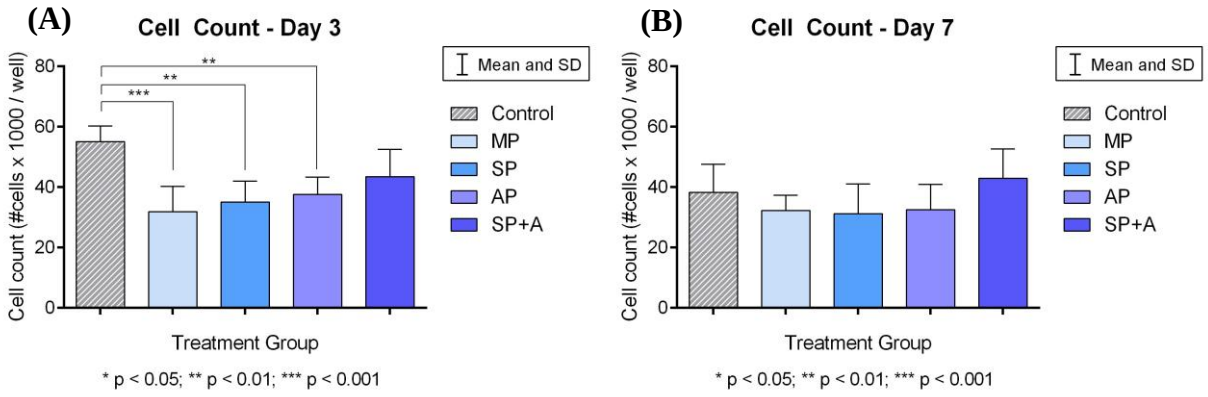

Figure 5-3. (A) Cell count (obtained from the standard curve between RFUS and cell number) data indicating cell viability for the negative control (unconditioned medium) and the different cleaning protocol groups (n = 6) on days (A) 3 and (B) 7. MP: manufacturer's protocol; SP: sonication protocol; AP: autoclave protocol; SP+A: sonication and autoclave protocol (* p-values < 0.05; ** p-values < 0.01; *** p-values < 0.001).

These results are consistent with the literature, showing that the cleaning and sterilization procedure before culture plays an important role in decreasing the cytotoxicity of MED610™ leachates [110], [124]. SP+A was validated and chosen as more suitable than MP, SP, or AP for cell culture, thus, it was chosen as the most appropriate cleaning and sterilization protocol to continue onto the next stage of this study.

5.4.2 Perfusion of Conditioned Medium using MED610™ Sterilized Bioreactor Chambers

The cell viability of the SP+A group was significantly different from the negative control on days 3 and 9 (day 3: $p = 0.026$; day 9: $p = 0.045$) (Figure 5-4). The SP+A cell viability was not statistically different from the negative control on day 14 ($p = 0.052$).

In this second part of the study, the effect of the printed construct complexity did not cause a negative effect on the culture viability. Instead, MED610™ indirect contact showed a greater cell proliferation of ATDC5 cells when compared to the control group in all three timepoints. When qualitatively compared to the results showed in the literature, Ngan *et al.*'s [110] fluorescence units in viability assays of the SP protocol are similar to the control group, however, their results were limited to 48 hours after culture exposure to MED610™, whereas the first timepoint of this study was set to day 3 in both stages (sterilization screening and bioreactor perfusion). Also assessed after 48 hours of incubation, Egan *et al.*'s MED610™ cell count had a mean of 95.6% relative to the control (2.0% standard deviation) [111].

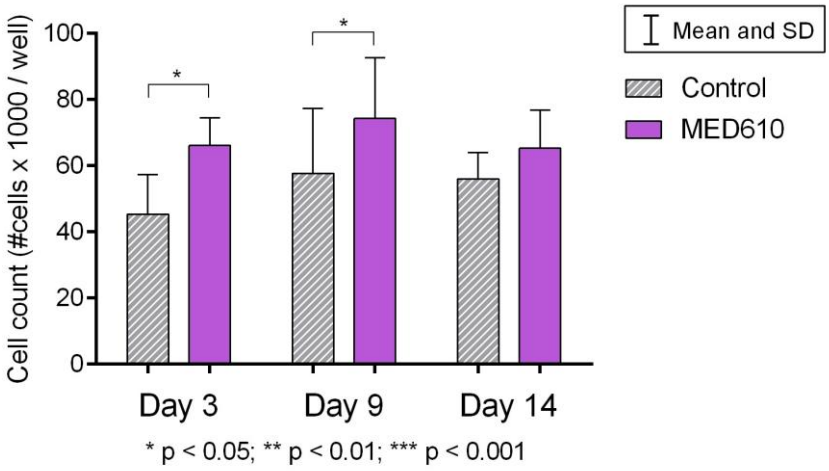

Figure 5-4. Cell count (obtained from the standard curve between RFUS and cell number) data indicating cell viability for the negative control (unconditioned medium) and the perfusion of conditioned medium through bioreactors on days 3, 9, and 14.

The combined results of both studies demonstrate that long-term cultures remain viable with indirect contact to MED610™ when the SP+A protocol is followed. The results obtained were not consistent with Schmelzer *et al.*, who also conducted indirect contact culture of epidermal skin keratinocytes and reported significant loss of viability in the MED610™ groups, as well as an strong up-regulation of CTSD (an early estrogen response gene), that indicates that plasticizers from the material can act as estrogen-like substances, leach out from the material and affect the cells [125]. However, the cleaning protocol used in their study only consisted of briefly rinsing with 100% ethanol, washing 5 times with de-mineralized water, and

sterilizing with ethylene oxide gas. On the other hand, Alifui-Segbaya *et al.* also reported adverse effects on zebrafish embryo when exposed to MED610™, but the material was evaluated "as built". The authors did declare better biocompatibility results after ethanol treatment [124].

It is important to note that, because of the proprietary contents of both MED610™ and SUB706B™, the sterilization protocol provided by the manufacturer should at least be considered the baseline of cleaning and sterilizing, such as Ngan *et al.*'s study. This same experimental design was followed in this work, where the SP+A contemplates both MP (where autoclaving at 132ºC for 4 minutes is suggested) and SP, with promising results observed.

The increased ATDC5 cell viability of the MED610™ group in the perfusion study brings an interesting insight of the material biological performance. While additional parts (such as tubing) in the bioreactor system could contribute to the results obtained in the indirect contact studies, it is unlikely that there is a significant impact on cell viability as all the additional materials used are commonly used in *in vitro* and *ex vivo* cultures and are biologically inert [14], [109]. Although with contrasting results, Schmelzer *et al*.'s study does highlight an important consideration of MED610™ (and any other biomaterial), and that is the cell-type-specific effects of the materials [125]. Schneider *et al.*'s evaluation of cytotoxicity of MED610™ across a murine cell line (L929), primary endothelial cells from umbilical cord vein (HUVEC), and primary chondrocytes and synovial fibroblasts, showed a viability greater than 80% with respect to the negative control (glass, 100% viability) in all cases [128]. It is thought that MED610™ could potentially promote cell viability and other biological properties in some specific cell lines (like ATDC5), however, further and more specific research should confirm this hypothesis. For bone tissue engineering scaffolds, specifically, Egan *et al.* already reported increased osteoblast growth support, and bone growth enhancement with improved compressive strength in Saos-2 cells-seeded MED610™ scaffolds [111].

MED610™ can be considered suitable for long-term culture studies, however its biocompatibility as a material cannot be concluded from the data gathered. Biocompatibility is a broad term with varying material biological performance requirements, depending on the application; which is why biocompatibility should be considered as a property of the entire system, not just the material itself [133]. Because of this, the aim of this work was to propose MED610™ as a promising material for complex construct rapid-prototyping, that can be used as support or specific apparatus needed for on-demand culture studies, such as a 3D printable bioreactor chamber for *in vitro* and *ex vivo* bioreactor system for mechanical stimulation of bone cores or bone grafts substitutes.

The results of the sterilization screening and perfusion bioreactor studies combined indicate that the SP+A cleaning protocol was able to clean and sterilize the MED610™ bioreactors for use in cell culture, reducing the cytotoxicity of leachates. Based on these findings, an updated cleaning and sterilization protocol for complex constructs fabricated with MED610™ is proposed, as listed in Table 5-2. This protocol includes support material removal and the SP+A cleaning and sterilization method, which has been established by integrating a sonication protocol proposed by Ngan *et al.* [110] and additional autoclaving.

Table 5-2. Updated outline to clean and sterilize MED610™ 3D printed parts.

Summary outline of the sonication and autoclave protocol for cleaning and sterilizing MED610™ parts
1. Remove all visible support material from parts. a. Remove visible exterior and interior support material using a pick tool. b. Thoroughly wash parts in a high-pressure water jet to remove remaining visible support material. 2. Follow manufacturer's support removal to remove any remaining support material. a. Soak parts in a distilled water solution with 1% Na_2SiO_3 and 2% NaOH caustic soda for 24 hours. b. Soak parts in 5% acetic acid solution for 1 minute to neutralize caustic soda pH. c. Rinse parts with water for 1 minute and then soak in distilled water for 5 minutes. 3. Sonicate parts in a covered glass beaker with IPA (10x volume of parts) for 2 hours. The solvent should be replaced every hour. 4. Sonicate parts in a covered beaker with Milli-Q water (10x volume of parts) for 2 hours. The solvent should be replaced every hour. 5. Rinse parts in 80% ethanol. 6. Dry parts in a biosafety cabinet under UV light for a minimum of 2 hours. 7. Autoclave parts at 132°C for 4 minutes.

5.5 Conclusions

This study demonstrated that the combination of sonicating and autoclaving 3D printed MED610™ parts can negate the toxicity of MED610™ leachates on ATDC5 cell lines in 2D culture, as well as in the perfusion of conditioned medium through the MED610™ parts. Further research should address the limitations of this study (such as indirect contact culture) to gather better understanding of MED610™ biocompatibility; its high resolution and processing accuracy, as well as promising biological performance results would eventually allow a great and diverse range of different biomedical applications. The findings of this study support continuing developments of 3D printed bioreactor chambers for organ culture and other complex 3D-printed shapes for *in vitro* or *ex vivo* studies that require biological viability.

Chapter 6

MECHANICAL LOADING OF *EX VIVO* BOVINE TRABECULAR BONE CORES IN 3D PRINTED BIOREACTOR CHAMBERS

6.1 Abstract

Existing bioreactor and loading systems, like Zetos, allow the study of trabecular bone explants in a closed system that can be mechanically stimulated, using polycarbonate (PC) bioreactor chambers that have been successful to study trabecular bone tissue mechanics in trabecular bone cores *ex vivo*. However, PC bioreactor chambers are difficult and expensive to fabricate, and the height-diameter ratio (½) for bone cores is below the standard for mechanical compression tests. A new bioreactor and loading system inspired by Zetos was developed using polyjet three-dimensional (3D) printing and MED610™ as printing material for the bioreactor chambers. The first version of the bioreactor chamber showed leakage and concerns regarding the material biological viability remain unresolved; therefore, a second version of the chamber has been designed and tested. An *ex vivo* bovine trabecular bone core study with the second-version bioreactor chambers found the first-version chamber issues were addressed: neither chamber leakage nor loss of samples occurred throughout the study, and bone cores remained visibly viable during the 21-day period. Unexpected response of trabecular bone core to mechanical loading was observed when compared to previous similar studies. Mean apparent elastic modulus (E_{app}) decreased in the loading treatment groups by 14.7% (versus a mean 25.0% E_{app} decrease in the control group). Despite the results obtained, valuable design and functionality insights were found for the *ex vivo* bioreactor and loading system with 3D printed bioreactor chambers, and its continuing validation process.

6.2 Introduction

In 2021, 18.3% of the world's population was diagnosed with osteoporosis [8]. Bone biomechanical behavior studies have shown that better understanding of bone tissue mechanics is key in the development of more effective strategies to prevent bone fracture, regenerate, and repair osteoporotic bone [2]. Bone, as a highly active tissue, has shown to be responsive to mechanical stimulation, where -1000 to -3000 με mechanical stimulation promotes bone remodeling and increased apparent stiffness [48], [49]. To investigate the dynamics and cellular processes of bone tissue during remodeling or healing, trabecular bone core explants have been tested with *ex vivo* bioreactor and loading systems [14], [28], [29], [72], [109], [113]. These *ex vivo* bioreactor and loading systems help maintain bone viability for set periods of time (3-

7 weeks) [91], while also offering the possibility to study cellular interactions, biomechanical cues, extracellular matrices and intercellular communication in the local bone microenvironment in controlled experimental setting [92], where the effect of interest can be isolated. It is possible to maintain the natural diversity of bone cells and their spatial distribution [26], as well as aid in the comprehension of bone mechanisms that otherwise would be too difficult to study under *in vivo* conditions [15].

Existing systems, like the Zetos bioreactor and loading system, allow the study of trabecular bone explants in a closed system that can be mechanically stimulated [28], [29], where polycarbonate (PC) bioreactor chambers have been successful to study trabecular bone tissue mechanics *ex vivo* [14], [30], [109]. However, these bioreactor chambers are difficult and expensive to fabricate, and the height-diameter ratio (½) for bone cores is below the standard for mechanical compression tests [108]. Therefore, a bioreactor and loading system was developed using polyjet 3D printing and MED610™ as material for the bioreactor chambers, aiming for a more cost-effective and adaptable solution. MED610™ is an emerging material for tissue culture constructs, and may also be suitable for long-term culture [110], [111], [129].

The first version MED610™ 3D printable bioreactor chamber had been evaluated in a previous study [30], however, some limitations were observed during the first evaluation *ex vivo* study. Leakage from the bioreactor chambers caused the loss of a considerable amount of bone core specimens (6 out of 23 samples, about 26% of the suitable bone cores retrieved after excision) throughout the course of the 21-day study, and concerns regarding MED610™ for bone explants are still unclear. Thus, after addressing the identified design limitations and confirming MED610™ viability for complex 3D constructs fabrication for culture conditions in previous works, the objective of this study was to run an evaluation iteration of the second version bioreactor chamber in a 3-week *ex vivo* bovine trabecular bone core experiment.

6.3 Methods and Materials

6.3.1 Reagents and Chemicals

Unless stated otherwise, all culture reagents and chemicals were obtained from Millipore Sigma (MA, USA). During trabecular bone core preparation procedure, all bone sections were kept in culture medium containing DMEM:Ham's F12 (1:1) with 10% fetal bovine serum (FBS) and 5% antibiotic-antimycotic (AA) solution. Once assembled, culture medium containing DMEM:Ham's F12 (1:1), 10% FBS, 1% AA solution, and 10 µg/mL ascorbic acid, circulated through the bone cores within the bioreactor circuit.

6.3.2 Bovine Bone Retrieval, Excision Equipment and Tools

A 3-years-old female bovine sternum was retrieved the day of slaughter from a local abattoir in Ontario, Canada, and maintained in a cooler while transporting to ensure viability. No known animal/bone diseases nor pathologies were reported. The bone core excision procedure from the sternum started within the next three hours of retrieval.

For bovine sternum slicing, an Exakt 312 pathology diamond-band saw (Norderstedt, Germany) was used. Two Busy Bee CSA CX605 milling/drilling machines (Vaughan, Canada), and specific system clamp fixtures [30] were used to secure the bone during coring and milling of the bone cores to make them approximately 10 x 10 mm (height x diameter). All surfaces and tools used during the excision procedure were either sterile (new) or previously rinsed with 70% ethanol and/or steam sterilized, depending on the material.

6.3.3 3D Printed Parts

Thirty-five labeled second version bioreactor chambers (Chapter 4) and stoppers for the medium reservoirs were fabricated using a Stratasys Objet30 Prime 3D printer with photopolymer MED610™ and water-soluble SUP706B™ support material (Rehovot, Israel), and sterilized according to the cleaning and sterilization protocol defined in Chapter 5. All parts were printed with a high-quality glossy finish setting (Objet Studio Ver. 9.2.11.6825).

6.3.4 Bovine Bone Core Preparation

Shortly after retrieval, excess soft (fat and cartilage) and bone (ribs) tissues were removed from the sternum using sterile scalpels. Once cleaned, the sternum was cut in half along the median plane. To obtain 10 x 10 mm bovine trabecular bone cores, each half was sliced, cored, and milled (Figure 6-1 and 6-2). During the excision procedure, water or filtered phosphate buffer saline (PBS) solution irrigation was always maintained to prevent the tissue from losing viability due to high-temperature friction during sectioning, slicing, coring, and/or milling.

Trabecular bovine sternum sections were obtained from the most anterior to posterior position by cutting through the cartilage between segments along transverse planes, using the pathology saw. Slices of approximately 12-14 mm thickness, parallel to the median plane, were obtained afterwards, keeping track of the dorsal, ventral, and medial surfaces. Then, bone slices were secured in the filtered PBS-filled bone

coring clamp, with the most medial surface oriented to the bottom of the clamp [30], and cores were cut starting from the most dorsal position, using a 10 mm (diameter) coring bit to carefully cut them out with a low coring speed (~300-400 rpm), to prevent bone exposure to high friction heat and damage. Bone cores were maintained in a 24-well plate filled with filtered PBS until milling. Shortly after, bone cores were secured in the filtered PBS-filled bone milling clamp following the same anatomical orientation. Bone core surfaces were milled to an approximate 10 mm height at low speed (~300-400 rpm). After milling, bone cores dimensions (height and diameter) were measured (digital Vernier caliper, Mastercraft, Canadian Tire) and recorded.

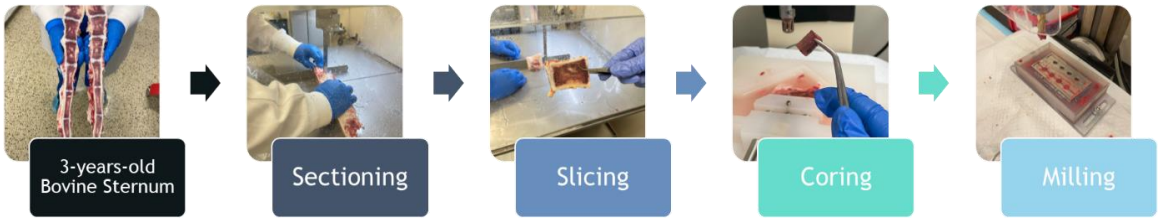

Figure 6-1. Summary of bone cores excision and preparation. Once the bovine sternum was retrieved, a diamond band pathology saw and drilling/milling machines were used to section/slice and core/mill the bone cores, respectively.

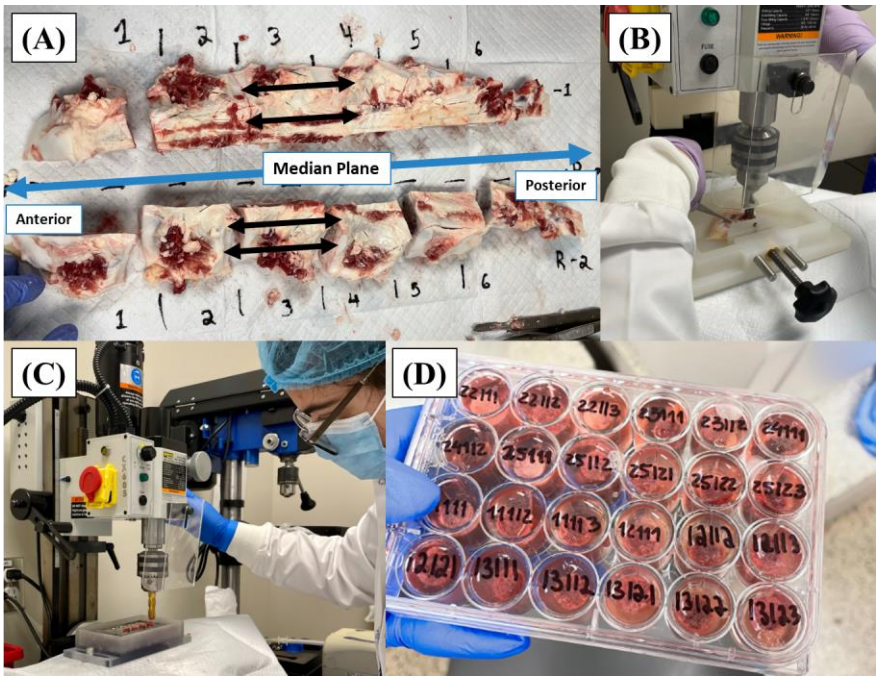

Figure 6-2. Bone core excision and preparation procedure: (A) Sectioning convention of bovine sternum from anterior to posterior position. Sections were sliced with a pathology saw along the cranial-caudal axis. Black arrows show the slicing direction convention used for all segments. (B) Trabecular bone coring procedure to 10 mm diameter using a mill. (C) Bone core milling to ensure 10 mm height. (D) Bone cores in culture medium ready for bioreactor assembly.

At the end of the whole excision and bone core preparation process, thirty-two (32) trabecular bovine bone cores were retrieved. Twenty-four (24) cores were considered suitable for the study (no significant visual damage and no fat observed within the core). They were allowed to rest (in the incubator at 37°C and 5% CO_2) for approximately 18 hours prior to bioreactor assembly in a new 24-well plate filled with culture medium supplemented with 10% FBS and 5% AA.

6.3.5 Bioreactor Chamber and Circuit Assembly

The second version bioreactor chambers and circuits were assembled under sterile conditions the day after bone core excision as follows (Figure 6-3): every assembled bioreactor chamber with one bone core inside, along with two polypropylene male luers to 1/16" hose barb adapters, was connected to a short (inlet) and long (outlet) 1.52 mm ID Tygon® E-Lab tubing (Sigma-Aldrich, USA). The inlet tubing was also connected to a 1.52 mm 2-stop PharMed® BPT pump tubing (Sigma-Aldrich, USA), that went through a 24-channel peristaltic pump (Ismatec™ ISM939D, No. 78000-41, Cole-Parmer, Canada). Both inlet and outlet tubing parts were connected to the medium reservoir filled with culture media, which additionally contained the MED610™ stopper, an 8 mm (ID) O-ring, two 18G needles and one 0.053" (OD) PTFE tubing for medium extraction connected to a needle. All the components from the bioreactor chambers and circuits were either new and sterile or previously steam sterilized.

Once assembled, constant medium flow was set and assessed (6.6 mL/hr) through the whole circuit in each bioreactor [14]. All bioreactor chambers and circuits were kept for 21 days at 37°C and 5% CO_2. Culture medium was changed 3 times a week and pH was controlled on every media change.

Figure 6-3. Assembly of bioreactor chambers and circuits in biological safety cabinet. Bone cores were put into the bioreactor chambers the day after bone core excision and preparation.

6.3.6 Compression Mechanical Testing and Mechanical Stimulation

One day after bioreactor chamber and circuit assembly, bone cores in bioreactors were ranked and sorted based on their apparent elastic modulus (E_{app}) into control and loading groups (n = 11/group). A t-test was done to assess no statistical differences existed between groups. E_{app} was obtained from a quasi-static mechanical loading test (Mach-1 Mechanical Testing Machine, Biomomentum, Canada) with an initial 10 N pre-load, followed by a -3000 με displacement at -50 με/s. Mechanical testing was done at room temperature, with the whole bioreactor closed circuit taken out of the incubator in groups of five per round in random order.

E_{app} (MPa) was calculated on the first and last days of the experiment using MATLAB 2020b (MathWorks, MA, USA), assuming linear elastic behavior (Hooke's Law – Equation 6-1) with the last 50% section of the linear force-displacement curve (Figure 6-4). In equation 6-1, F represents force (N), H corresponds to the sample bone core height (mm), d is the axial displacement due to compression (mm), and A is the sample cross-sectional area (mm²). Force-displacement curves for all bone cores on days 0 and 21 are shown in Appendixes E and F. A system compliance of 0.000639 mm/N [30] was considered in all calculations. E_{app} changes for all specimens over the 21-day period were measured with the E_{app} percent difference (%ΔE_{app}), using equation 6-2.

$$\boldsymbol{E_{app} = \frac{F \cdot H}{d \cdot A}} \qquad \textbf{(6-1)}$$

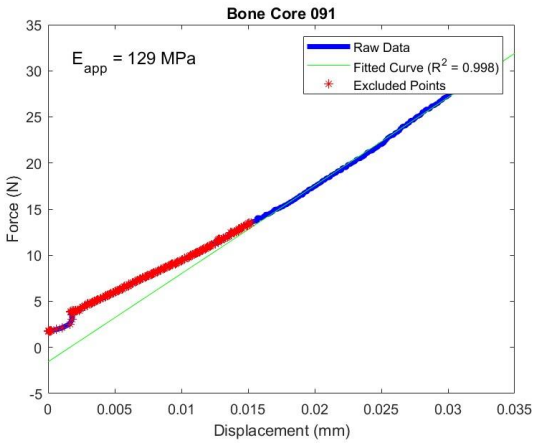

Figure 6-4. Sample representative force-displacement plot from quasi-static loading of bovine trabecular bone cores on day 21 of the study. Linear fit shown (green) was performed with the last 50% of the force-displacement curve and demonstrates the apparent bone core stiffness used to determine the apparent elastic modulus of bone cores. Coefficient of determination (R^2) was used to evaluate goodness of the curve fit. System compliance is considered in the E_{app} shown on the plot.

$$\%\Delta E_{app} = \left(\frac{E_{app,day\ 21} - E_{app,day\ 0}}{E_{app,day\ 0}}\right) \cdot 100\% \qquad \textbf{(6-2)}$$

6.3.7 Cyclic Mechanical Stimulation

The "loading" (treatment) group was stimulated mechanically five times per week (Monday to Friday) with a loading profile that mimicked a physiological low-impact, high strain stimulus, with a Δ3000 με displacement and a strain rate of 3000 με/s for 120 cycles (Figure 6-5). Treatment with mechanical stimulation started five days after bone excision.

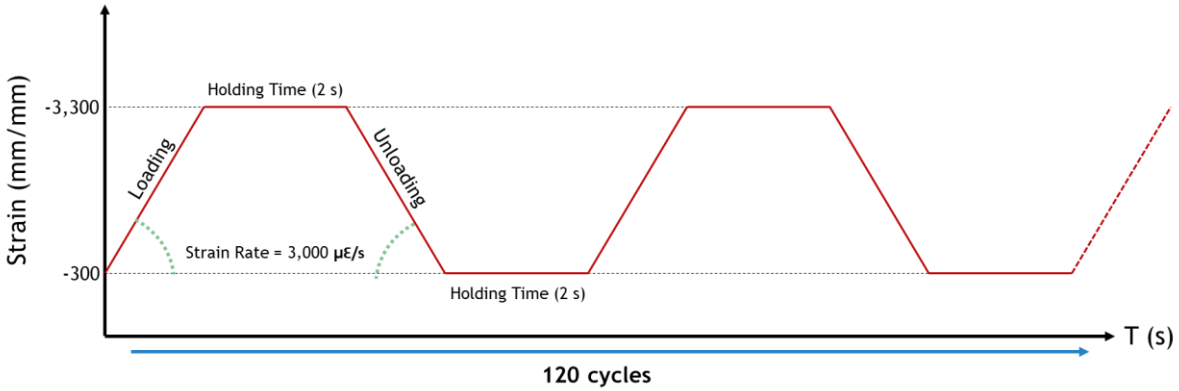

Figure 6-5. Loading waveform for mechanical stimulation of the bioreactor loading group five times per week.

6.3.8 Statistical Analysis

An initial two-tailed t-test between groups was used to confirm lack of significant difference in E_{app} after ranking and groups definition. To compare statistical differences between groups after the 21-day treatment, a two-way analysis of variance (ANOVA) with repeated measures was used with pairwise comparisons for post hoc analyses. Normality and sphericity across groups were confirmed using the Shapiro-Wilk and Mauchly's tests, respectively. A two-tailed t-test was used to compare between groups for percent differences in E_{app} after the 21-days experiment ($\%\Delta E_{app}$). In all cases, a statistical significance of $\alpha = 0.05$ was considered, and adjustments for multiple comparisons were performed with the Bonferroni correction. All statistical analyses were performed in SPSS® Statistics 23 (IBM, NY, USA) and GraphPad Prism® 6.1 (Dotmatics, MA, USA).

6.4 Results and Discussion

Twenty-four bovine trabecular bone cores with average dimensions of 10.8 x 10.1 mm (height x diameter) were retrieved and considered suitable after the bone core excision procedure. Twenty-four second-version bioreactor chambers and circuits were assembled the day after bone core preparation and maintained in culture conditions at 37ºC and 5% CO_2. Neither sample contamination nor system leakage were observed during or after the 21-days experiment, which validated the changes made to the bioreactor

chamber design, thus preventing the loss of samples. Culture medium acidity was highest (pH = 6.2 ± 0.3) on day 2, four days after bone core excision. This result was expected as the bone cores were highly metabolically active and recovering after the excision procedure, producing more CO_2 and increasing acidity to meet the oxygen demand of tissue [134]. During the 21-days period, both the control and loading groups had similar pH readings on average (Appendix J).

The day after bioreactor assembly (day 0), the average and standard deviation (SD) of E_{app} was 90.6 (35.5) MPa. Two of the specimens with the lowest E_{app} were excluded from the loading experiment for the standardization of histological analyses protocols. These specimens were kept together with the rest of the samples within the bioreactor circuit as controls for a calcein dye double labeling. Specimens with the highest E_{app} were chosen for the mechanical loading experiment, since previous studies have found increased growth rate for stiffer samples. Among many factors, osteogenesis, which is related to bone growth due to osteoblasts formation, can be regulated by the matrix stiffness. An enhanced osteogenic differentiation of bone-marrow derived MSC (BM-MSC) has been reported for a stiff matrix, compared to a soft one [135].

The removal of the three samples resulted in a mean (SD) E_{app} of 95.6 (32.7) MPa. After ranking and sorting the control and treatment groups, a t-test confirmed lack of statistically significant differences between both groups (p-value = 0.763), resulting in an initial E_{app} of 97.8 (33.3) MPa and 93.4 (33.6) MPa on average (SD) for the control and loading group, respectively.

Table 6-1. Average E_{app} and % difference between both groups observed on days 0 and 21, and the $\%\Delta E_{app}$ decrease observed in each group after the 21-days. Values are shown as Mean (Standard Deviation – SD).

	$Eapp$ (SD) [MPa] Day 0	$Eapp$ (SD) [MPa] Day 21	$\%\Delta Eapp$ (SD)
Control (n = 11)	97.8 (33.3)	73.4 (32.9)	25.0% (22.3%)
Load (n = 11)	93.4 (33.6)	78.9 (31.6)	14.7% (17.3%)
% Difference	4.6%	7.3%	-

After the 21-days experiment, the average and standard deviation (SD) of E_{app} among all 21 samples decreased to 76.2 (31.7) MPa; the control group, however, tended to show a lower average E_{app} (SD) than the treatment group, 73.4 (32.9) MPa versus 78.9 (31.6) MPa. E_{app} was assessed for both groups only on the first and last days of the study to minimize mechanical stimulation of the control group throughout the

whole course of the study. Table 6-1 shows a summary of the E_{app} results obtained on the first and last days of the study.

The two-way ANOVA showed lack of statistically significant differences in the interaction between treatment and time (p = 0.173, Table 6-2), however, the main effects of time over the course of the 21-days were significant (p = 0.002). The average E_{app} decrease of the control (p = 0.002) and the treatment (p = 0.008) groups were both significant, according to post hoc analyses. Treatment, on the other hand, did not show statistically significant main effects between groups (p = 0.959). Summaries of statistical differences of E_{app} and multiple comparisons are shown on Table 6-2 and Figure 6-6.

Table 6-2. Two-way ANOVA results to evaluate the effects of time and group on E_{app} (F-statistic and p-value). Sphericity is assumed in all reported values. Bonferroni corrections are considered in adjustments for multiple comparisons. P-values legends: *p < 0.05; **p < 0.01.

	F-statistic	p-value
Treatment	0.003	0.959
Time	4128	0.002**
Treatment*Time	270	0.173

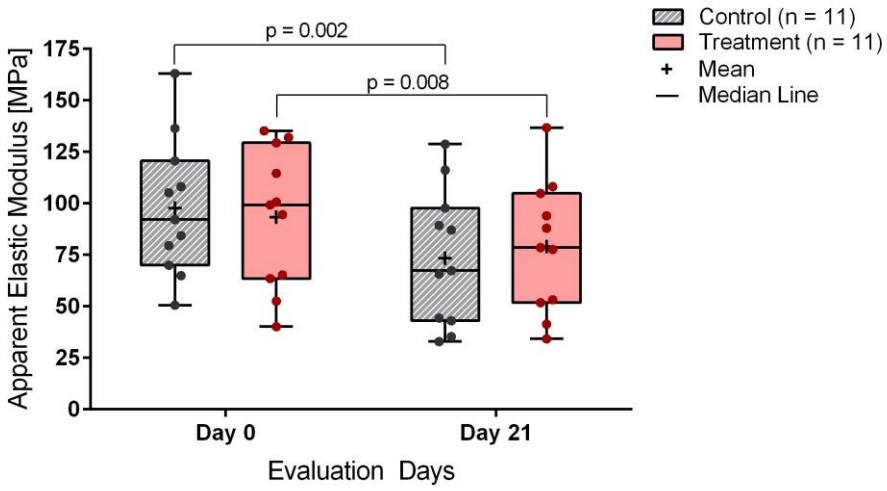

Figure 6-6. Apparent Elastic Modulus (E_{app}) on both days 0 and 21 for both the control and loading (treatment) groups.

On day 0, the percentage difference (% difference) between the means of both groups was 4.6% (Table 6-1). Although the average E_{app} decreased in both groups, the % difference between group means tended to increase to 7.3% after treatment in the loading group (Figure 6-7 (A)). The average percent decrease of E_{app} ($\%\Delta E_{app}$) was higher in the control group than in the treatment group, with a 25.0% (SD 22.3%)

average E_{app} loss versus 14.7% (SD 17.3%), respectively. No statistical differences (p = 0.24) were found for $\%\Delta E_{app}$ between the control and treatment groups.

Different trends regarding E_{app} change over time with mechanical stimulation are observed when comparing the results of the current study with similar *ex vivo* studies with trabecular bone cores from bovine sternums, Vivanco *et al.* (2013), Meyer *et al.* (2016), and Kunath *et al.* (2022). Previous studies found the average E_{app} increased for bone cores within the treatment or loading group [14], [30], [109], as opposed to the overall mean E_{app} decrease of 19.9% observed in this study.

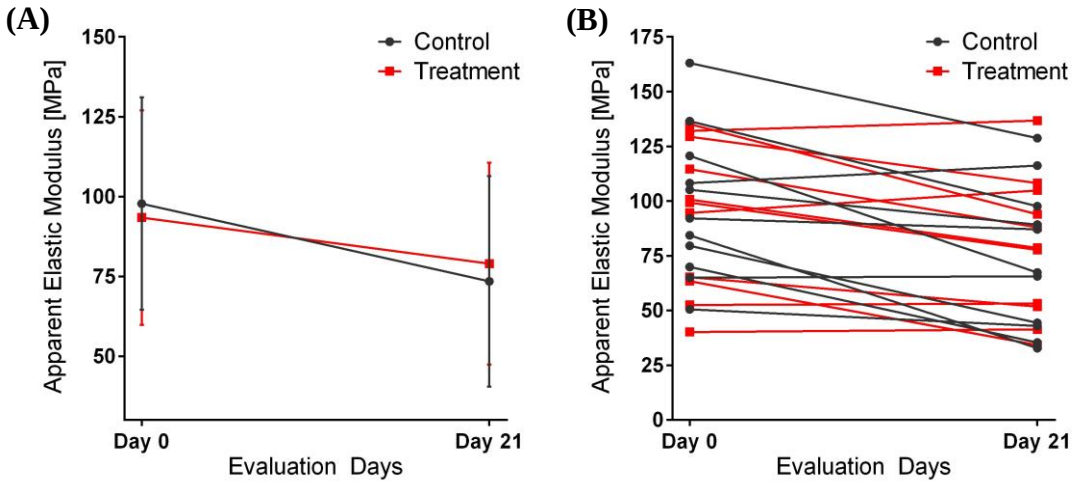

Figure 6-7. (A) Average E_{app} changes over the course of the 21-days study in both the control (black) and treatment (red) groups. The increase in the percentage difference between groups was from 4.6% to 7.3% after the treatment group was loaded 5 times/week for 21-days. Mean E_{app} values for each group and their corresponding standard deviation (SD) are shown. (B) Individual E_{app} changes after the 21-days study for each sample per group.

On day 0, initial E_{app} ranged from 40.2 – 163 MPa across all 22 bone cores, with a mean and standard deviation of 90.6 (35.5) MPa, comparable to previous studies. The initial E_{app} reported by Vivanco *et al.* were 50.7 ± 11.9 MPa for the treatment group, and 30.1 ± 7.70 MPa for the control group. Results are expressed as mean ± standard error of the mean (SEM) two days after bone core excision [14]. The mean (SD) E_{app} reported by Kunath *et al.* was 56.4 (16.4) MPa, were slightly lower; and, Meyer *et al.* initial E_{app} were slightly higher to the ones obtained in this study, with a mean and standard error of 136 ± 12.8 MPa [109]. Different study outcomes could be related to the age and sex of the animal [136], [137] at the time of bone core excision. There is also a natural variation in trabecular E_{app}, with reported coefficient variation from 8% within a single trabecula and up to 22% among samples from five different human

femoral bone specimens [138]. 70-90% of the variances in E_{app} of trabecular bone can be explained by volume fraction or apparent density [139], which could have also influenced the results.

After the 21-days experiment, Vivanco *et al.* reported a 61.2% average E_{app} increase in the treatment group versus a 27.7% increase in the control group, whereas the results obtained in the current study found, on average, 14.7% and 25.0% E_{app} decreases for the treatment and control groups, respectively. Kunath *et al.* also described 56.2% (treatment) and 20.2% (control) average increases.

Meyer *et al.* studied the relation between endothelin-1 (ET1), a signaling molecule that promotes osteogenesis in metastatic disease, and mechanical loading to promote osteogenesis in *ex vivo* trabecular bovine bone cores [109]. Their results found an increase in E_{app}, $\%\Delta E_{app}$ ranged from 3.3% (control group, no load and no ET1 exposure) to 19% (load + ET1), depending on the experimental group, which is considerably less than the E_{app} reported by the other studies.

In the current study, although the mean E_{app} decreased in both the control and treatment groups, it is interesting to observe that six samples increased in E_{app} (Figure 6-7 (B)), where the $\%\Delta E_{app}$ increase ranged from 3.0% to 11%, comparable to Meyer *et al.* (3.3% to 19%) [109]. Four out of the six belonged to the loading group, where mechanical stimulation could have played an important role in bone formation. Increased bone strength, osteogenic stimulation and viability have been reported in early adaptation responses (first five weeks) after mechanical loading treatments [140], [141]. Trabecular bone healing can be a relatively fast process, taking from 1 to 2 weeks in small animals and humans, respectively, mainly due to membranous bone formation being localized and osteoid forming simultaneously across the whole injured tissue [142]. Further analyses are required, however, to draw further conclusions of the results obtained. Mechanical stimulation from quasi-static compression testing was minimized in the control group throughout the 21 days, but E_{app} measurement halfway through the experiment could have provided more insights of the specimens' state and overall system performance. Previous studies (Vivanco *et al.* and Kunath *et al.*), performed additional testing on days 7 and 8, respectively.

It is important to note that between the studies discussed, Vivanco *et al.*, Meyer *et al.*, and Kunath *et al.*, there are experimental differences and similarities in the bioreactor and loading systems used and/or the mechanical loading profiles, compared to the current study, that could explain the differing results. With regards to the bioreactor chamber design and material, in both Vivanco *et al.* and Meyer *et al.* experiments, PC bioreactors (Zetos) and smaller bone core dimensions (5 x 10 mm – height x diameter) were used [14],

[109], whereas 10 x 10 mm bone cores (height x diameter) and MED610™ bioreactor chambers were used in the current study.

With respect to the mechanical stimulation, the mechanical loading profiles were different between all four studies. In the first MED610™ bioreactor chamber study (Kunath *et al.*), a sinusoidal waveform ranging from -1000 to -5000 με (Δ4000 με) was used to mechanically stimulate bone cores in the treatment group 5 days/week with a frequency of 2 Hz and for 120 cycles during 21 days [30]. Kunath *et al.* used a higher applied bulk strain change of Δ4000 με than the current study. Daily mechanical loading for stimulation, however, went beyond the recommended 3000 με threshold for controlled modeling, and could have caused microdamage [48], [49], [143]. Potential dehydration (caused by leakage or poor medium diffusion) over the 21-days could have also caused the overestimation of E_{app}. Lievers *et al.* found that sample dehydration can cause an increase of 26.9% in the estimation of E_{app}, given the natural water constituent of bone [144].

The previous PC bioreactor chamber studies, in contrast, mimicked a physiological high-impact stimulus similar to reaction force from vertical jumps [145], with a maximum strain of -4000 με repeated at 2 Hz for 100 cycles/day for 21 days [14], or a Δ2000 με stimulation every 0.5 seconds for 120 cycles during 23 days [109]. In the current study, a Δ3000 με strain (from -300 to -3300 με) and a strain rate of 3000 με/s for 120 cycles mimicked a physiological low-impact and high-strain stimulus. Loading was applied daily for 5 days per week over 21 days.

Regarding experimental similarities, all four studies compared used trabecular bovine bone cores, and a 6.6 mL/hr medium flow rate is also consistent across all studies to minimize the effect of undesired bone core stimulation [14], [30], [109]. The bioreactor chamber material (MED610™) and bone core dimensions (10 x 10 mm – height x diameter) used in the current study are the same as Kunath *et al.* [30].

In summary, there were several differences between the current and previous studies, such as the lower maximum change in applied bulk strain, the different loading profiles, the 10 x 10 mm bone core dimensions, and the MED610™ bioreactor chambers. For example, similar outcomes are observed between studies: in Meyer *et al.* lower $\%\Delta E_{app}$ increases were observed when compared to Vivanco *et al.*'s work, potentially due to the lower applied strain magnitude (-2000 με versus -4000 με); however, both studies used PC bioreactors, and ET1 could have also played an important role in promoting osteogenesis and mineral apposition [14], [109].

There are several important limitations in the current study. Regarding statistical analyses, the p-values in the within-subject and main effects between groups and timepoints on E_{app} were adjusted for multiple comparisons using the Bonferroni correction, thus reducing the probability of making a Type I error; however, the low sample size (n = 11 per group) might have increased the chances of making a Type II error [146].

Another important limitation of this study was that bone viability was not tested after the excision procedure and should be considered in future iterations of this experiment to provide a Day 0 baseline. For example, Dua *et al.* performed a live-dead assay on bone cores (10 mm height by 15 mm in diameter and a flowrate of 60 mL/hr) using Calcein AM/Ethidium homodimer staining in their own bioreactor system evaluation study [106].

End-side artifacts (unconstrained border damage caused during the excision procedure) could have also caused the underestimation of the true E_{app}. However, the increased bone height (from 5 to 10 mm to meet bone mechanical testing standards [108]) may have reduced culture medium diffusion to the center of the bone core, affecting bone viability over the course of the current study. The dehydration of samples could have caused the overestimation of true E_{app} [144]. The under- and over- estimation of true E_{app}, then, may have cancelled each other out, but such effects were not controlled.

Although minimized with pre-conditioning before testing, bone core stress relaxation was observed during testing and stimulation due to the viscoelastic nature of bone [34], [47], [52], [53], and "toe regions" were evident in some of the force-deflection plots. Bone is a highly anisotropic and heterogeneous material, and E_{app} measurements are highly sensitive to the trabeculae orientation, which varies throughout the whole tissue. However, the heterogeneity of trabecular struts can make accurate determination more complicated [138], [143], [147]. Thus, the trabecular orientation was not consistent across all the samples during testing. Trabecular microstructure orientation could be quantified in future studies from microcomputed tomography (µCT) scans, where the degree of anisotropy can be used as a scalar measure of the preferential trabecular structure orientation [139].

With regards to MED610™ as the bioreactor material, it is unlikely to have caused a negative effect on bone core viability. MED610™ had been evaluated as suitable for complex 3D printed structures (e.g., bioreactor chambers) in previous cell culture studies, and MED610™ bioreactors for chronic electrical stimulation have already been evaluated for soft tissue and induced pluripotent stem cells (iPSC) [129].

Ngan *et al.* also evaluated MED610™ biocompatibility in an *in vivo* study after sonicating the constructs as an additional sterilization step from that of the manufacturer (Stratasys) [110], and Egan *et al.* reported increased osteoblast growth support, as well as bone growth enhancement in MED610™ scaffolds seeded with osteosarcoma Saos-2 cells [111]. Further research is still recommended to evaluate system biocompatibility for bone cells and bone tissue, since cell-specific responses are crucial and can vary within different cell types and lineages [125].

Therefore, despite the unexpected results (decreased change in E_{app}), it was considered a successful progress in the validation process of the MED610™ 3D printable bioreactor and loading system. No chamber or circuit leakages were observed and none of the initial samples showed any signs of visual damage or contamination after the 21-days experiment, thus addressing one of the principal limitations observed during the first version MED610™ 3D printable bioreactor chamber design.

6.5 Conclusions

This work successfully addressed previously identified limitations regarding the first version of the 3D printable MED610™ bioreactor chamber: neither system leakage nor loss of samples occurred throughout the *ex vivo* evaluation study, and bone cores remained visibly viable during the 21-day period. Although contrasting results were found when compared to previous similar *ex vivo* studies with a mean E_{app} decrease in the loading treatment group, these results give new valuable insights for the new 3D printable bioreactor and loading system and its continuing validation process. Since four specimens from the loading group did increase their E_{app}, there is some evidence that the mechanical stimulation might have helped in the overall bone health and formation of the load group. The limitations of this study should be addressed, and further testing with different strain rates (high- and low-strain rates) should be conducted.

Chapter 7
CONCLUSIONS AND FUTURE WORK

7.1 Thesis Summary

The main objective of this thesis was to continue the evaluation and validation process of the MED610™ 3D printable bioreactor chamber designed by Kunath *et al.* (2022). To do so, chamber leakage observed with the design during the first *ex vivo* evaluation study and concerns regarding MED610™ biological viability for the bone core explants culture had to be addressed.

To meet this objective, the specific sub-objectives were followed. As per the first specific sub-objective of this thesis work, the first version 3D printed chambers were re-assembled and carefully evaluated to identify potential sources of leakage. The bioreactor chambers from the first study by Kunath *et al.* (2022) and newly printed bioreactor chambers for comparison were evaluated. After one day of flow circulation (without mechanical loading), 75% of the previously-used bioreactors were leaking through the sapphire pistons. The source of leakage was initially hypothesized to be the loose fit between the X-ring seals and pistons [30], but it was determined that the most probable cause was the use of expired X-rings, which are no longer available for purchase. Available X-rings with the closest dimensions to the original design were acquired and an updated version of the bioreactor chamber design was fabricated using the same 3D printing configurations. Two different design options were tested for leakage and the lowest $K_{app,res}$ between the pistons-bone surrogate subsystem and the assembled bioreactor chamber was calculated. After mechanical stimulation 5 days/week for three weeks, no leakage was observed in either option through the pistons, which then confirmed the effect of the expired X-rings. The updated bioreactor chamber version was adapted to the new X-ring dimensions, but the original dimensioning criteria for the slot cut-outs were maintained. Other small design modifications included the removal of a horizontal tapered plug hole to minimize risks of leakage, creating an internal fluid channel, different from Zetos and the first MED610™ bioreactor chamber design.

Regarding the second specific sub-objective, MED610™ was confirmed as a suitable material to manufacture complex-shaped apparatus for *in vitro* or *ex vivo* culture conditions, when proper cleaning and sterilization protocols are used, and leachates minimized. An initial sterilization screening study confirmed that a protocol combining steam sterilization with the sonication procedure proposed by Ngan *et al.* [110] can effectively remove the support material SUP706B™, increasing the biological viability of the 3D

printed constructs. A second part of this study then evaluated biological suitability of newly 3D printed MED610™ bioreactor chambers in a complex perfusion system consisting of the bioreactor chambers, a medium reservoir with a MED610™ 3D printed stopper, a peristaltic pump, and the tubing circuit. Enough evidence was gathered to consider the material and fabrication procedure suitable and adequate for the proposed application of this project. However, MED610™ should not be considered biocompatible yet, since further research is required, and biocompatibility should be considered as a system property rather than the material itself [133].

The third and last specific sub-objective was met with the evaluation of the updated bioreactor system design in a 21-days experiment of *ex vivo* bovine trabecular bone cores. A low-impact and high-strain stimulation was used to mechanically load the treatment group, different from the loading profiles used in previous similar studies [14], [30], [109]. The treatment group's bone response in E_{app} changes was unexpected and did not follow the same trend as similar studies; average E_{app} decreases were observed in both the control and treatment group, but six out of the twenty-two samples saw increased in E_{app} ranging from 3.0% to 11%. The combination of numerous differences in the methods followed when compared to similar previous studies might have contributed to the results obtained. Despite these results, the experiment is considered successful since no system leakage and no contamination were observed throughout the study, thus meeting the principal requirements of the updated bioreactor chamber.

In summary, the general objective of this thesis is considered complete. Important insights regarding the manufacturing capacity and viability of 3D printable MED610™ bioreactor chambers were obtained, and the results from this work are considered a valuable addition in the ongoing validation process of an open-source 3D printable bioreactor and loading system.

7.2 Limitations and Future Work

The limitations of this thesis project should be considered for results interpretation and addressed in future experiments to gather more detailed insights into the MED610™ 3D printable bioreactor and loading system. Firstly, the data gathered from the MED610™ biological viability study limits the conclusions that can be obtained, since only indirect contact with cells was assessed through the usage of exposed media to the material in the cultures. Additional MED610™ research as a biomaterial is suggested to assess biocompatibility with bone cells and tissue. Different analyses could provide important information regarding MED610™ when direct contact (e.g. cell-seeded scaffolds) is studied: gene expression, adhesion,

morphological changes, and osteogenic differentiation (if MSC are used) [111], [148]. Runx2 and Osterix (OSX) are considered the master regulator genes in bone formation [149], and their expression profiles when bone cells or bone tissue are exposed to MED610™ could provide important information regarding the material effect on bone or stem cells, including osteogenic differentiation. Alizarin Red S staining [135], [150], a method that stains calcium deposition containing osteocytes in bone differentiation of MSC, could be a simpler alternative to test for osteogenic differentiation evaluation.

In the *ex vivo* trabecular bone core culture, it was assumed that bone cores were viable after the excision procedure when no visible signs of damage were observed. To assess bone viability, at least 3-4 random samples at the beginning and end of the study should be destined for corresponding assays. Possible bone tissue specific viability assays include Calcein AM and Ethidium homodimer [97], [106]; an adapted thiazolyl blue tetrazolium bromide (MTT) assay for bone explants; or a lactate dehydrogenase (LDH) assay, an enzyme that has been used to label live osteocytes [151]. In the current study, calcein dye was added for double labeling in all bone cores, following Meyer *et al.* methodology [109], and two unstained bone cores also assembled in the bioreactor circuit were destined for timepoint comparison, hence, future work should be able to standardize histological analysis protocols to observe mineral apposition rate.

Additional interesting biological analyses to perform in future iterations of bioreactor and loading system experiments using bone cores, would be gene expression quantification, depending on the specific research question. For example, cyclooxygenase-2 (COX-2) and interleukin-6 (IL-6) are genes that respond to mechanical loading in bone tissue [39], [152], and could provide a clearer picture of the bone core response to mechanical stimulation.

In the current study, the only bone mechanical behavior response evaluated was E_{app}, however, as a bulk property [153], E_{app} is considered limited to adequately reflect the complex, anisotropic and heterogeneous nature of trabecular bone, thus limiting the ability to conclude and explain what could have happened within the system over the 21-day period. It is also important to consider that the "end-side artifacts" might have caused the underestimation of true E_{app} [154], [155]. Further evaluation and the combination with biological analyses are suggested at the tissue level, by also including micro- or even nano-mechanical testing with numerical models using Finite Element Analysis (FEA) and micro-computed tomography (µCT) scan imaging [147]. µCT imaging could also be used to measure the degree of anisotropy of the trabecular bone specimens for proper trabeculae orientation during mechanical testing and loading [139]. Additional mechanical response information from the bone tissue could be obtained from

the mechanical stimulation data – the loading profile used in the current study could be used for stress-relaxation analyses to study the viscoelastic response of bone to the provided stimuli.

E_{app} was measured only at the start and end of the experiment to avoid mechanical stimulation in the control group halfway through the study with quasi-static loading, limiting the evaluation of the system over the 21-day period. The system could be improved by including sensors and/or indicators that allow fast and simple evaluation of the bone state, while still minimizing undesired mechanical stimulation across all groups. For example, if the bone cores are metabolically active, CO_2 should be released from the specimens [156], which could work as an indicator of the system performance.

3D printing advances in the biomedical field have opened numerous possibilities and applications for different purposes [20], [83]. Although good results regarding resolution and reproducibility in AM technologies have been achieved, the specific manufacturing and sterilization process of the custom-designed 3D printed bioreactor chambers is not automated, and small differences could result from one chamber to the other, despite the best efforts. To account for this potential final product variability, more bioreactor chambers than the intended number of bone specimens should be manufactured when conducting similar experiments using 3D printable chambers, to prevent malfunctions and loss of samples due to apparatus processing irregularities. Bioreactor chambers can be easily exchanged under sterile conditions.

The limitations of this study should be considered in future iterations of a similar experiment, and further testing with different strain rates (high- and low-strain rates) and bulk strain changes should be conducted to find the baseline values that promote healthy bone remodeling and strengthening within this specific mechanical loading system and its compliance. As discussed before, more analyses with the samples used in this study could be performed to better understand the unexpected bone behavior observed. In the future, this system could be applied to study different effects on trabecular bone besides mechanical testing, using a 3D printable bioreactor and loading system as a standardized apparatus rather than the object of study.

In conclusion, an open-source 3D printable bioreactor and loading system is a promising tool for bone tissue mechanics, not only to study bone tissue cellular dynamics, but also to find better and more effective treatment alternatives for bone defects like osteoporosis [65], [92]. Finally, a system like the one proposed in this study can be easily translated to bone tissue engineering applications, where tissue scaffolds could be used as a model of study, and a whole new range of potential applications could be considered using *in vitro* dynamic 3D cell cultures and novel biomaterials for bone healing and regeneration studies [25], [98], [101], [157].

REFERENCES

[1] C. Estrada, A. Paz, and L. López, "Ingeniería de tejido óseo: Consideraciones básicas," *Rev. EIA*, no. 5, pp. 93–100, 2006.

[2] X. Dong, B. Milholland, and J. Vijg, "Evidence for a limit to human lifespan," *Nature*, vol. 538, no. 7624, pp. 257–259, 2016, doi: 10.1038/nature19793.

[3] D. S. Kehler, "Age-related disease burden as a measure of population ageing," *Lancet Public Heal.*, vol. 4, no. 3, pp. e123–e124, 2019, doi: 10.1016/S2468-2667(19)30026-X.

[4] D. NIH Consensus Development Panel on Osteoporosis Prevention and Therapy, "Osteoporosis Prevention, Diagnosis, and Therapy," *JAMA*, vol. 285, no. 6, pp. 785–795, 2001, doi: 10.1001/jama.285.6.785.

[5] C. I. Codrea *et al.*, "Advances in osteoporotic bone tissue engineering," *J. Clin. Med.*, vol. 10, no. 2, pp. 1–27, 2021, doi: 10.3390/jcm10020253.

[6] P. Alejandro and F. Constantinescu, "A Review of Osteoporosis in the Older Adult," *Clin. Geriatr. Med.*, vol. 33, no. 1, pp. 27–40, 2017, doi: 10.1016/j.cger.2016.08.003.

[7] Z. X. Wang *et al.*, "The Treatment Efficacy of Bone Tissue Engineering Strategy for Repairing Segmental Bone Defects under Osteoporotic Conditions," *Tissue Eng. - Part A*, vol. 21, no. 17–18, pp. 2346–2355, 2015, doi: 10.1089/ten.tea.2015.0071.

[8] N. Salari *et al.*, "The global prevalence of osteoporosis in the world: a comprehensive systematic review and meta-analysis," *J. Orthop. Surg. Res.*, vol. 16, no. 1, 2021, doi: 10.1186/s13018-021-02772-0.

[9] R. Aziziyeh *et al.*, "The burden of osteoporosis in four Latin American countries: Brazil, Mexico, Colombia, and Argentina," *J. Med. Econ.*, vol. 22, no. 7, pp. 638–644, 2019, doi: 10.1080/13696998.2019.1590843.

[10] J. Zanchetta *et al.*, "The Latin America Regional Audit: epidemiology, costs & burden of osteoporosis in 2012," Nyon, 2012. doi: 201205-500.

[11] Chinese Orthopaedic Association, "Diagnosis and treatment of osteoporotic fractures.," *Orthop. Surg.*, vol. 1, no. 4, pp. 251–257, 2009, doi: 10.1111/j.1757-7861.2009.00047.x.

[12] M. B. Schaffler and O. D. Kennedy, "Osteocyte signaling in bone," *Curr. Osteoporos. Rep.*, vol. 10, no. 2, pp. 118–125, 2012, doi: 10.1007/s11914-012-0105-4.

[13] W. Cao *et al.*, "Is There a Governing Role of Osteocytes in Bone Tissue Regeneration?," *Curr. Osteoporos. Rep.*, vol. 18, no. 5, pp. 541–550, 2020, doi: 10.1007/s11914-020-00610-6.

[14] J. Vivanco, S. Garcia, H. L. Ploeg, G. Alvarez, D. Cullen, and E. L. Smith, "Apparent elastic

modulus of ex vivo trabecular bovine bone increases with dynamic loading," *Proc. Inst. Mech. Eng. Part H J. Eng. Med.*, vol. 227, no. 8, pp. 904–912, 2013, doi: 10.1177/0954411913486855.

[15] R. Oftadeh, M. Perez-Viloria, J. C. Villa-Camacho, A. Vaziri, and A. Nazarian, "Biomechanics and Mechanobiology of Trabecular Bone: A Review," *J. Biomech. Eng.*, vol. 137, no. 1, pp. 1–15, 2015, doi: 10.1115/1.4029176.

[16] S. Ji and M. Guvendiren, "Recent Advances in Bioink Design for 3D Bioprinting of Tissues and Organs," *Front. Bioeng. Biotechnol.*, vol. 5, no. APR, pp. 1–8, 2017, doi: 10.3389/fbioe.2017.00023.

[17] F. E. Freeman, R. Burdis, and D. J. Kelly, "Printing New Bones: From Print-and-Implant Devices to Bioprinted Bone Organ Precursors," *Trends Mol. Med.*, vol. 27, no. 7, pp. 700–711, 2021, doi: 10.1016/j.molmed.2021.05.001.

[18] A. Kumar *et al.*, "Low temperature additive manufacturing of three dimensional scaffolds for bone-tissue engineering applications: Processing related challenges and property assessment," *Mater. Sci. Eng. R Reports*, vol. 103, pp. 1–39, 2016, doi: 10.1016/j.mser.2016.01.001.

[19] P. Sharma, P. Kumar, R. Sharma, V. D. Bhatt, and P. S. Dhot, "Tissue Engineering ; Current Status & Futuristic Scope," vol. 12, no. 3, pp. 225–229, 2019, doi: 10.25122/jml-2019-0032.

[20] P. Szymczyk-Ziółkowska, M. B. Łabowska, J. Detyna, I. Michalak, and P. Gruber, "A review of fabrication polymer scaffolds for biomedical applications using additive manufacturing techniques," *Biocybern. Biomed. Eng.*, vol. 40, no. 2, pp. 624–638, 2020, doi: 10.1016/j.bbe.2020.01.015.

[21] T. Klüter *et al.*, "An Ex Vivo Bone Defect Model to Evaluate Bone Substitutes and Associated Bone Regeneration Processes," *Tissue Eng. - Part C Methods*, vol. 26, no. 1, pp. 56–65, 2020, doi: 10.1089/ten.tec.2019.0274.

[22] A. Papaioannou *et al.*, "2010 clinical practice guidelines for the diagnosis and management of osteoporosis in Canada: Summary," *Cmaj*, vol. 182, no. 17, pp. 1864–1873, 2010, doi: 10.1503/cmaj.100771.

[23] A. J. El Haj and S. H. Cartmell, "Bioreactors for bone tissue engineering," *Proc. Inst. Mech. Eng. Part H J. Eng. Med.*, vol. 224, no. 12, pp. 1523–1532, 2010, doi: 10.1243/09544119JEIM802.

[24] J. Zhang, E. Wehrle, M. Rubert, and R. Müller, "3d bioprinting of human tissues: Biofabrication, bioinks and bioreactors," *Int. J. Mol. Sci.*, vol. 22, no. 8, 2021, doi: 10.3390/ijms22083971.

[25] A. B. Yeatts and J. P. Fisher, "Bone tissue engineering bioreactors: Dynamic culture and the influence of shear stress," *Bone*, vol. 48, no. 2, pp. 171–181, 2011, doi: 10.1016/j.bone.2010.09.138.

[26] T. Bellido and J. Delgado-Calle, "Ex Vivo Organ Cultures as Models to Study Bone Biology," *JBMR Plus*, vol. 4, no. 3, pp. 1–10, 2020, doi: 10.1002/jbm4.10345.

[27] D. B. Jones, E. Broeckmann, T. Pohl, E. L. Smith, J. Gasser, and P. Prendergast, "Development of

a mechanical testing and loading system for trabecular bonestudies for long term culture," *Eur. Cells Mater.*, vol. 5, pp. 48–60, 2003, doi: 10.22203/eCM.v005a05.

[28] C. M. Davies *et al.*, "Mechanically loaded ex vivo bone culture system 'Zetos': Systems and culture preparation," *Eur. Cells Mater.*, vol. 11, no. 0, pp. 57–75, 2006, doi: 10.22203/eCM.v011a07.

[29] S. Endres, M. Kratz, S. Wunsch, and D. B. Jones, "Zetos: A culture loading system for trabecular bone. Investigation of different loading signal intensities on bovine bone cylinders," *J. Musculoskelet. Neuronal Interact.*, vol. 9, no. 3, pp. 173–183, 2009.

[30] B. A. Kunath, "Design and Validation of an Open-Source 3D printable bioreactor system for ex vivo bone culture," Queen's University, 2022.

[31] D. W. Buck and G. A. Dumanian, "Bone biology and physiology: Part I. the fundamentals," *Plast. Reconstr. Surg.*, vol. 129, no. 6, pp. 1314–1320, 2012, doi: 10.1097/PRS.0b013e31824eca94.

[32] J. G. Betts *et al.*, *Anatomy and Physiology*, vol. 7, no. 2. Rice University, OpenStax, 2013.

[33] K. Grassie and Y. Khan, *Bone Tissue Engineering: Bench to Bedside Using 3D Printing*, 1st ed. Springer Switzerland, 2022.

[34] M. Asgari, J. Abi-Rafeh, G. N. Hendy, and D. Pasini, "Material anisotropy and elasticity of cortical and trabecular bone in the adult mouse femur via AFM indentation," *J. Mech. Behav. Biomed. Mater.*, vol. 93, pp. 81–92, 2019, doi: https://doi.org/10.1016/j.jmbbm.2019.01.024.

[35] T. M. Keaveny, E. F. Morgan, G. L. Niebur, and O. C. Yeh, "Biomechanics of Trabecular Bone," *Annnual Rev. Biomed. Eng.*, vol. 3, no. 1, pp. 307–333, 2001.

[36] E. D. Dyson and W. J. Whitehouse, "Composition of Trabecular Bone in Children and its relation to Radiation Dosimetry," *Nature*, vol. 217, no. 5128, pp. 576–578, 1968, doi: 10.1038/217576a0.

[37] J. S. (Editor) Khurana, *Bone Pathology*, 2nd ed. Springer US, 2009.

[38] K. J. Jepsen, "Systems analysis of bone," *Wiley Interdiscip. Rev. Syst. Biol. Med.*, vol. 1, no. 1, pp. 73–88, 2009, doi: 10.1002/wsbm.15.

[39] M. B. Schaffler, W. Y. Cheung, R. Majeska, and O. Kennedy, "Osteocytes: Master orchestrators of bone," *Calcif. Tissue Int.*, vol. 94, no. 1, pp. 5–24, 2014, doi: 10.1007/s00223-013-9790-y.

[40] J. A. Shibli *et al.*, "Bone Tissue Engineering Using Osteogenic Cells: From the Bench to the Clinical Application," *Tissue Eng. Part C Methods*, vol. 28, no. 5, pp. 179–192, 2022, doi: 10.1089/ten.tec.2022.0021.

[41] A. Mahnama, M. Tafazzoli-Shadpour, F. Geramipanah, and M. Mehdi Dehghan, "Verification of the mechanostat theory in mandible remodeling after tooth extraction: Animal study and numerical modeling," *J. Mech. Behav. Biomed. Mater.*, vol. 20, pp. 354–362, 2013, doi: 10.1016/j.jmbbm.2013.02.013.

[42] E. F. Eriksen, “Cellular mechanisms of bone remodeling,” *Reviews in Endocrine and Metabolic Disorders*, vol. 11, no. 4. pp. 219–227, 2010, doi: 10.1007/s11154-010-9153-1.

[43] L. J. Raggatt and N. C. Partridge, “Cellular and Molecular Mechanisms of Bone Remodeling *,” *J. Biol. Chem.*, vol. 285, no. 33, pp. 25103–25108, 2010, doi: 10.1074/jbc.R109.041087.

[44] L. Oton-Gonzalez *et al.*, “Genetics and Epigenetics of Bone Remodeling and Metabolic Bone Diseases,” *International Journal of Molecular Sciences*, vol. 23, no. 3. 2022, doi: 10.3390/ijms23031500.

[45] A. M. Parfitt, “Osteonal and hemi-osteonal remodeling: the spatial and temporal framework for signal traffic in adult human bone.,” *J. Cell. Biochem.*, vol. 55, no. 3, pp. 273–286, 1994, doi: 10.1002/jcb.240550303.

[46] R. Florencio-Silva, G. Rodrigues, E. Sasso-cerri, M. J. Simões, P. S. Cerri, and B. Cells, “Biology of Bone Tissue: Structure , Function , and Factors That Influence Bone Cells,” *Biomed Res. Int.*, 2015, doi: 10.1155/2015/421746.

[47] K. Manda, R. J. Wallace, S. Xie, F. Levrero-Florencio, and P. Pankaj, “Nonlinear viscoelastic characterization of bovine trabecular bone,” *Environ. Econ. Policy Stud.*, vol. 16, no. 1, pp. 173–189, 2017, doi: 10.1007/s10237-016-0809-y.

[48] H. M. Frost, “Bone’s Mechanostat: A 2003 Update,” *Anat. Rec. - Part A Discov. Mol. Cell. Evol. Biol.*, vol. 275, no. 2, pp. 1081–1101, 2003, doi: 10.1002/ar.a.10119.

[49] N. Rosa, R. Simoes, F. D. Magalhães, and A. T. Marques, “From mechanical stimulus to bone formation: A review,” *Med. Eng. Phys.*, vol. 37, no. 8, pp. 719–728, 2015, doi: 10.1016/j.medengphy.2015.05.015.

[50] X. Ojanen *et al.*, “Relationships between tissue composition and viscoelastic properties in human trabecular bone,” *J. Biomech.*, vol. 48, no. 2, pp. 269–275, 2015, doi: 10.1016/j.jbiomech.2014.11.034.

[51] S. Ehnert, H. Rinderknecht, R. H. Aspera-Werz, V. Häussling, and A. K. Nussler, “Use of in vitro bone models to screen for altered bone metabolism, osteopathies, and fracture healing: challenges of complex models,” *Arch. Toxicol.*, vol. 94, no. 12, pp. 3937–3958, 2020, doi: 10.1007/s00204-020-02906-z.

[52] R. M. Guedes, J. A. Simões, and J. L. Morais, “Viscoelastic behaviour and failure of bovine cancellous bone under constant strain rate,” *J. Biomech.*, vol. 39, no. 1, pp. 49–60, 2006, doi: 10.1016/j.jbiomech.2004.11.005.

[53] V. Quaglini, V. La Russa, and S. Corneo, “Nonlinear stress relaxation of trabecular bone,” *Mech. Res. Commun.*, vol. 36, no. 3, pp. 275–283, 2009, doi: 10.1016/j.mechrescom.2008.10.012.

[54] D. L. Kopperdahl and T. M. Keaveny, “Yield strain behavior of trabecular bone,” *J. Biomech.*, vol. 31, no. 7, pp. 601–608, 1998, doi: 10.1016/s0021-9290(98)00057-8.

[55] C. Sandino, D. D. McErlain, J. Schipilow, and S. K. Boyd, “The poro-viscoelastic properties of trabecular bone: A micro computed tomography-based finite element study,” *J. Mech. Behav. Biomed. Mater.*, vol. 44, pp. 1–9, 2015, doi: 10.1016/j.jmbbm.2014.12.018.

[56] J. H. Hong, M. S. Mun, and T. H. Lim, “Strain rate dependent poroelastic behavior of bovine vertebral trabecular bone,” *KSME Int. J.*, vol. 15, no. 7, pp. 1032–1040, 2001, doi: 10.1007/BF03185281.

[57] P. Manfredini, G. Cocchetti, G. Maier, A. Redaelli, and F. M. Montevecchi, “Poroelastic finite element analysis of a bone specimen under cyclic loading,” *J. Biomech.*, vol. 32, no. 2, pp. 135–144, 1999, doi: 10.1016/S0021-9290(98)00162-6.

[58] C. S. Bahney *et al.*, “Cellular Biology of Fracture Healing,” *J. Orthop. Res.*, 2019, doi: 10.1002/jor.24170.

[59] P. Augat, U. Simon, A. Liedert, and L. Claes, “Mechanics and mechano-biology of fracture healing in normal and osteoporotic bone,” *Osteoporos. Int.*, vol. 16, no. SUPPL. 2, pp. 36–43, 2005, doi: 10.1007/s00198-004-1728-9.

[60] I. H. Kalfas, “Principles of bone healing.,” *Neurosurg. Focus*, vol. 10, no. 4, pp. 6–9, 2001, doi: 10.3171/foc.2001.10.4.2.

[61] H. Schell, G. N. Duda, A. Peters, S. Tsitsilonis, K. A. Johnson, and K. Schmidt-Bleek, “The haematoma and its role in bone healing,” *J. Exp. Orthop.*, vol. 4, no. 1, 2017, doi: 10.1186/s40634-017-0079-3.

[62] C. Li and P. Fennessy, “The periosteum: a simple tissue with many faces, with special reference to the antler-lineage periostea,” *Biol. Direct*, vol. 16, no. 1, p. 17, 2021, doi: 10.1186/s13062-021-00310-w.

[63] F. M. Hannan, P. J. Newey, M. P. Whyte, and R. V. Thakker, “Genetic approaches to metabolic bone diseases,” *Br. J. Clin. Pharmacol.*, vol. 85, no. 6, pp. 1147–1160, 2019, doi: 10.1111/bcp.13803.

[64] N. C. Wright *et al.*, “The recent prevalence of osteoporosis and low bone mass in the United States based on bone mineral density at the femoral neck or lumbar spine,” *J. Bone Miner. Res.*, vol. 29, no. 11, pp. 2520–2526, 2014, doi: 10.1002/jbmr.2269.

[65] K. N. Tu *et al.*, “Osteoporosis: A review of treatment options,” *P T*, vol. 43, no. 2, pp. 92–104, 2018.

[66] F. Marini, L. Cianferotti, and M. L. Brandi, “Epigenetic mechanisms in bone biology and osteoporosis: Can they drive therapeutic choices?,” *Int. J. Mol. Sci.*, vol. 17, no. 8, 2016, doi:

10.3390/ijms17081329.

[67] G. S. Firestein, S. E. Gabriel, I. B. McInnes, and J. R. O'Dell, *Kelley and Firestein's textbook of rheumatology* , Tenth edit. Philadelphia, PA: Elsevier, 2021.

[68] E. F. Kranioti, A. Bonicelli, and J. G. García-donas, "Bone-mineral density : clinical significance, methods of quantification and forensic applications," *Res. Reports Forensic Med. Sci.*, no. 9, pp. 9–21, 2019, doi: 10.2147/RRFMS.S164933.

[69] F. Cosman *et al.*, "Clinician's Guide to Prevention and Treatment of Osteoporosis," *Osteoporos. Int.*, vol. 25, no. 10, pp. 2359–2381, 2014, doi: 10.1007/s00198-014-2794-2.

[70] E. G. Dawson, "Osteoporosis: The Silent Thief," *Health Central*, 2015. https://www.spineuniverse.com/conditions/osteoporosis/osteoporosis-silent-thief (accessed Jul. 06, 2022).

[71] D. A. Hanley, J. D. Adachi, A. Bell, and V. Brown, "Denosumab: mechanism of action and clinical outcomes," *Int. J. Clin. Pract.*, vol. 66, no. 12, pp. 1139–1146, 2012, doi: https://doi.org/10.1111/ijcp.12022.

[72] R. M. Neer *et al.*, "Effect of parathyroid hormone (1-34) on fractures and bone mineral density in postmenopausal women with osteoporosis.," *N. Engl. J. Med.*, vol. 344, no. 19, pp. 1434–1441, 2001, doi: 10.1056/NEJM200105103441904.

[73] L. Bandeira, E. M. Lewiecki, and J. P. Bilezikian, "Romosozumab for the treatment of osteoporosis," *Expert Opin. Biol. Ther.*, vol. 17, no. 2, pp. 255–263, 2017, doi: 10.1080/14712598.2017.1280455.

[74] N. M. Appelman-Dijkstra and S. E. Papapoulos, "Clinical advantages and disadvantages of anabolic bone therapies targeting the WNT pathway," *Nat. Rev. Endocrinol.*, vol. 14, no. 10, pp. 605–623, 2018, doi: 10.1038/s41574-018-0087-0.

[75] O. Johnell and J. A. Kanis, "An estimate of the worldwide prevalence and disability associated with osteoporotic fractures.," *Osteoporos. Int.*, vol. 17, no. 12, pp. 1726–1733, 2006, doi: 10.1007/s00198-006-0172-4.

[76] J. H. Kim, Y.-S. Park, K. J. Oh, and H. S. Choi, "Surgical treatment of severe osteoporosis including new concept of advanced severe osteoporosis," *Osteoporos. Sarcopenia*, vol. 3, no. 4, pp. 164–169, 2017, doi: 10.1016/j.afos.2017.11.006.

[77] C. M. Klotzbuecher, P. D. Ross, P. B. Landsman, T. A. A. Iii, and M. Berger, "Patients with Prior Fractures Have an Increased Risk of Future Fractures : A Summary of the Literature and Statistical Synthesis *," vol. 15, no. 4, 2000.

[78] V. S. Nikolaou, N. Efstathopoulos, G. Kontakis, N. K. Kanakaris, and P. V. Giannoudis, "The

influence of osteoporosis in femoral fracture healing time," *Injury*, vol. 40, no. 6, pp. 663–668, 2009, doi: 10.1016/j.injury.2008.10.035.

[79] M. Marmor *et al.*, "Osteoporotic Fracture Care: Are We Closer to Gold Standards ?," vol. 29, no. 12, pp. 53–56, 2015.

[80] N. M. E. Ayad, S. Kaushik, and V. M. Weaver, "Tissue mechanics, an important regulator of development and disease," *Philos. Trans. R. Soc. B Biol. Sci.*, vol. 374, no. 1779, 2019, doi: 10.1098/rstb.2018.0215.

[81] M. Marques, J. Belinha, A. F. Oliveira, and R. M. Natal Jorge, "Chapter 10 - Determination of the Anisotropic Mechanical Properties of Bone Tissue Using a Homogenization Technique Combined With Meshless Methods," M. H. B. T.-A. in B. and T. R. Doweidar, Ed. Academic Press, 2019, pp. 201–213.

[82] W. Wang and K. W. K. Yeung, "Bioactive Materials Bone grafts and biomaterials substitutes for bone defect repair: A review," *Bioact. Mater.*, vol. 2, no. 4, pp. 224–247, 2017, doi: 10.1016/j.bioactmat.2017.05.007.

[83] A. A. Zadpoor and J. Malda, "Additive Manufacturing of Biomaterials, Tissues, and Organs," *Ann. Biomed. Eng.*, vol. 45, no. 1, pp. 1–11, 2017, doi: 10.1007/s10439-016-1719-y.

[84] P. F. Costa, A. M. Puga, L. Díaz-Gomez, A. Concheiro, D. H. Busch, and C. Alvarez-Lorenzo, "Additive manufacturing of scaffolds with dexamethasone controlled release for enhanced bone regeneration," *Int. J. Pharm.*, vol. 496, no. 2, pp. 541–550, 2015, doi: 10.1016/j.ijpharm.2015.10.055.

[85] A. Eltom, G. Zhong, and A. Muhammad, "Scaffold Techniques and Designs in Tissue Engineering Functions and Purposes: A Review," *Adv. Mater. Sci. Eng.*, vol. 2019, 2019, doi: 10.1155/2019/3429527.

[86] A. P. Moreno Madrid, S. M. Vrech, M. A. Sanchez, and A. P. Rodriguez, "Advances in additive manufacturing for bone tissue engineering scaffolds," *Mater. Sci. Eng. C*, vol. 100, no. March, pp. 631–644, 2019, doi: 10.1016/j.msec.2019.03.037.

[87] B. H. B. Isht, A. S. H. Ope, A. N. M. Ukherjee, and M. A. K. P. Aul, "Advances in the Fabrication of Scaffold and 3D Printing of Biomimetic Bone Graft," *Ann. Biomed. Eng.*, vol. 49, no. 4, pp. 1128–1150, 2021, doi: 10.1007/s10439-021-02752-9.

[88] X. Mai, Z. Kang, N. Wang, X. Qin, W. Xie, and F. Song, "Oxygen Plasma Technology-Assisted Preparation of Three-Dimensional Reduced Graphene Oxide/Polypyrrole/Strontium Composite Scaffold for Repair of Bone Defects Caused by Osteoporosis," *Molecules*, vol. 26, no. 15, 2021, doi: 10.3390/molecules26154451.

[89] R. Dua, H. Jones, and P. C. Noble, “Evaluation of bone formation on orthopedic implant surfaces using an ex-vivo bone bioreactor system,” *Sci. Rep.*, vol. 11, no. 1, pp. 1–10, 2021, doi: 10.1038/s41598-021-02070-z.

[90] I. Martin, D. Wendt, and M. Heberer, “The role of bioreactors in tissue engineering,” *Trends Biotechnol.*, vol. 22, no. 2, pp. 80–86, 2004, doi: 10.1016/j.tibtech.2003.12.001.

[91] M. Peroglio, D. Gaspar, D. I. Zeugolis, and M. Alini, “Relevance of Bioreactors and Whole Tissue Cultures for the Translation of New Therapies to Humans,” *J. Orthop. Res.*, pp. 10–21, 2018, doi: 10.1002/jor.23655.

[92] F. Jakob *et al.*, “Bone tissue engineering in osteoporosis,” *Maturitas*, vol. 75, no. 2, pp. 118–124, 2013, doi: 10.1016/j.maturitas.2013.03.004.

[93] V. I. Sikavitsas, G. N. Bancroft, and A. G. Mikos, “Formation of three-dimensional cell/polymer constructs for bone tissue engineering in a spinner flask and a rotating wall vessel bioreactor,” *J. Biomed. Mater. Res.*, vol. 62, no. 1, pp. 136–148, 2002, doi: https://doi.org/10.1002/jbm.10150.

[94] C. M. Begley and S. J. Kleis, “The fluid dynamic and shear environment in the NASA/JSC rotating-wall perfused-vessel bioreactor.,” *Biotechnol. Bioeng.*, vol. 70, no. 1, pp. 32–40, 2000, doi: 10.1002/1097-0290.

[95] J. Schmid *et al.*, “A perfusion bioreactor system for cell seeding and oxygen-controlled cultivation of three-dimensional cell cultures,” *Tissue Eng. - Part C Methods*, vol. 24, no. 10, pp. 585–595, 2018, doi: 10.1089/ten.tec.2018.0204.

[96] M. A. Koch, E. J. Vrij, E. Engel, J. A. Planell, and D. Lacroix, “Perfusion cell seeding on large porous PLA/calcium phosphate composite scaffolds in a perfusion bioreactor system under varying perfusion parameters,” *J. Biomed. Mater. Res. - Part A*, vol. 95, no. 4, pp. 1011–1018, 2010, doi: 10.1002/jbm.a.32927.

[97] S. Marino, K. A. Staines, G. Brown, R. A. Howard-Jones, and M. Adamczyk, “Models of ex vivo explant cultures: applications in bone research,” *Bonekey Rep.*, vol. 5, no. May, pp. 1–18, 2016, doi: 10.1038/bonekey.2016.49.

[98] D. Mitra, J. Whitehead, O. W. Yasui, and J. K. Leach, “Bioreactor culture duration of engineered constructs influences bone formation by mesenchymal stem cells,” *Biomaterials*, vol. 146, pp. 29–39, 2017, doi: 10.1016/j.biomaterials.2017.08.044.

[99] M. B. Keogh, S. Partap, J. S. Daly, and F. J. O’Brien, “Three hours of perfusion culture prior to 28 days of static culture, enhances osteogenesis by human cells in a collagen GAG scaffold,” *Biotechnol. Bioeng.*, vol. 108, no. 5, pp. 1203–1210, 2011, doi: https://doi.org/10.1002/bit.23032.

[100] B. Bhaskar, R. Owen, H. Bahmaee, P. S. Rao, and G. C. Reilly, “Design and Assessment of a

Dynamic Perfusion Bioreactor for Large Bone Tissue Engineering Scaffolds," *Appl. Biochem. Biotechnol.*, vol. 185, no. 2, pp. 555–563, 2018, doi: 10.1007/s12010-017-2671-5.

[101] A. Campos Marín, M. Brunelli, and D. Lacroix, "Flow perfusion rate modulates cell deposition onto scaffold substrate during cell seeding," *Biomech. Model. Mechanobiol.*, vol. 17, no. 3, pp. 675–687, 2018, doi: 10.1007/s10237-017-0985-4.

[102] I. G. Beşkardeş, G. Aydın, Ş. Bektaş, A. Cengiz, and M. Gümüşderelioğlu, "A systematic study for optimal cell seeding and culture conditions in a perfusion mode bone-tissue bioreactor," *Biochem. Eng. J.*, vol. 132, pp. 100–111, 2018, doi: 10.1016/j.bej.2018.01.006.

[103] I. G. Beşkardeş, R. S. Hayden, D. L. Glettig, D. L. Kaplan, and M. Gümüşderelioğlu, "Bone tissue engineering with scaffold-supported perfusion co-cultures of human stem cell-derived osteoblasts and cell line-derived osteoclasts," *Process Biochem.*, vol. 59, pp. 303–311, 2017, doi: 10.1016/j.procbio.2016.05.008.

[104] V. David *et al.*, "Ex vivo bone formation in bovine trabecular bone cultured in a dynamic 3D bioreactor is enhanced by compressive mechanical strain," *Tissue Eng. - Part A.*, vol. 14, no. 1, pp. 117–126, 2008, doi: 10.1089/ten.a.2007.0051.

[105] E. E. A. Cramer, K. Ito, and S. Hofmann, "Ex vivo Bone Models and Their Potential in Preclinical Evaluation," *Curr. Osteoporos. Rep.*, vol. 19, no. 1, pp. 75–87, 2021, doi: 10.1007/s11914-020-00649-5.

[106] R. Dua, H. Jones, and P. C. Noble, "Designing and validation of an automated ex-vivo bioreactor system for long term culture of bone.," *Bone reports*, vol. 14, p. 101074, 2021, doi: 10.1016/j.bonr.2021.101074.

[107] 3D Biotek, "3D Biotek 3D perfusion bioreactor system with pump." https://www.sigmaaldrich.com/CA/en/product/sigma/z687502 (accessed Jul. 07, 2022).

[108] S. Zhao *et al.*, "Standardizing compression testing for measuring the stiffness of human bone.," *Bone Joint Res.*, vol. 7, no. 8, pp. 524–538, 2018, doi: 10.1302/2046-3758.78.BJR-2018-0025.R1.

[109] L. A. Meyer *et al.*, "Combined exposure to big endothelin-1 and mechanical loading in bovine sternal cores promotes osteogenesis.," *Bone*, vol. 85, pp. 115–122, 2016, doi: 10.1016/j.bone.2016.02.001.

[110] C. G. Y. Ngan *et al.*, "Optimising the biocompatibility of 3D printed photopolymer constructs in vitro and in vivo," *Biomed. Mater.*, vol. 14, no. 3, 2019, doi: 10.1088/1748-605X/ab09c4.

[111] P. Egan, X. Wang, H. Greutert, K. Shea, K. Wuertz-Kozak, and S. Ferguson, "Mechanical and Biological Characterization of 3D Printed Lattices," *3D Print. Addit. Manuf.*, vol. 6, no. 2, pp. 73–81, 2019, doi: 10.1089/3dp.2018.0125.

[112] R. Vallejos Baier *et al.*, "Structure-function assessment of 3D-printed porous scaffolds by a low-cost/open source fused filament fabrication printer," *Mater. Sci. Eng. C*, vol. 123, p. 111945, 2021, doi: 10.1016/J.MSEC.2021.111945.

[113] R. Dua, H. Jones, and P. C. Noble, "Bone Reports Designing and validation of an automated ex-vivo bioreactor system for long term culture of bone," *Bone Reports*, vol. 14, p. 101074, 2021, doi: 10.1016/j.bonr.2021.101074.

[114] C. for D. C. adn Prevention, "Steam Sterilization: Guideline for Disinfection and Sterilization in Healthcare Facilities (2008)," 2016. https://www.cdc.gov/infectioncontrol/guidelines/disinfection/sterilization/steam.html (accessed Jul. 03, 2023).

[115] J.-F. S. R. Sheetings, "Life Expectancy of Silicone Rubbers," 2012. https://www.j-flex.com/life-expectancy-of-silicone-rubbers/ (accessed Jul. 03, 2023).

[116] Ensinger, "Ultem 1000," 2021.

[117] S. Bhat and A. Kumar, "Biomaterials and bioengineering tomorrow's healthcare," *Biomatter*, vol. 3, no. 3, 2013, doi: 10.4161/biom.24717.

[118] J. R. H. Joseph Rey *et al.*, "3D printing of biomedically relevant polymer materials and biocompatibility," *MRS Commun.*, vol. 11, no. 2, pp. 197–212, 2021, doi: 10.1557/s43579-021-00038-8.

[119] A. Valls-Esteve *et al.*, "A state-of-the-art guide about the effects of sterilization processes on 3D-printed materials for surgical planning and medical applications: A comparative study," *Int. J. Bioprinting*, vol. 9, no. 5, 2023, doi: 10.18063/ijb.756.

[120] A. Mishra and V. Srivastava, "Biomaterials and 3D printing techniques used in the medical field," *J. Med. Eng. Technol.*, vol. 45, no. 4, pp. 290–302, 2021, doi: 10.1080/03091902.2021.1893845.

[121] P. Patpatiya, K. Chaudhary, A. Shastri, and S. Sharma, "A review on polyjet 3D printing of polymers and multi-material structures," *Proc. Inst. Mech. Eng. Part C J. Mech. Eng. Sci.*, vol. 236, no. 14, pp. 7899–7926, 2022, doi: 10.1177/09544062221079506.

[122] K. Tappa and U. Jammalamadaka, "Novel biomaterials used in medical 3D printing techniques," *J. Funct. Biomater.*, vol. 9, no. 1, 2018, doi: 10.3390/jfb9010017.

[123] C. N. Ionita *et al.*, "Challenges and limitations of patient-specific vascular phantom fabrication using 3D Polyjet printing.," *Proc. SPIE-the Int. Soc. Opt. Eng.*, vol. 9038, p. 90380M, 2014, doi: 10.1117/12.2042266.

[124] F. Alifui-Segbaya, S. Varma, G. J. Lieschke, and R. George, "Biocompatibility of Photopolymers in 3D Printing," *3D Print. Addit. Manuf.*, vol. 4, no. 4, pp. 185–191, 2017, doi:

10.1089/3dp.2017.0064.

[125] E. Schmelzer, P. Over, B. Gridelli, and J. C. Gerlach, “Response of Primary Human Bone Marrow Mesenchymal Stromal Cells and Dermal Keratinocytes to Thermal Printer Materials In Vitro,” *J. Med. Biol. Eng.*, vol. 36, no. 2, pp. 153–167, 2016, doi: 10.1007/s40846-016-0118-z.

[126] Stratasys, “Printing Biocompatible Parts on PolyJet™ 3D Printers with MED610™, Rigid Clear Biocompatible Material,” 2023.

[127] V. M. Mustahsan, A. Anugu, D. E. Komatsu, I. Kao, and S. Pentyala, “Biocompatible customized 3D bone scaffolds treated with CRFP, an osteogenic peptide,” *Bioengineering*, vol. 8, no. 12, pp. 1–14, 2021, doi: 10.3390/bioengineering8120199.

[128] K. H. Schneider *et al.*, “Medical 3D printing with polyjet technology: effect of material type and printing orientation on printability, surface structure and cytotoxicity,” *3D Print. Med.*, vol. 9, no. 1, pp. 1–12, 2023, doi: 10.1186/s41205-023-00190-y.

[129] D. E. Ibarra, M. E. Jewett, D. K. Jarrell, A. Pinales, M. C. VeDepo, and J. G. Jacot, “Bioreactor Design for Culturing Vascularized Engineered Tissue in Flow Conditions,” *Tissue Eng. Part A*, 2023, doi: 10.1089/ten.TEA.2023.0201.

[130] Stratasys, “Safety Data Sheet: Biocompatible Clear, MED610™,” 2023. [Online]. Available: https://us.vwr.com/assetsvc/asset/en_US/id/16490607/contents.

[131] Stratasys, “Safety Data Sheet: Support, SUP706 B™,” *Mater. Saf. Data Sheet*, vol. 4, no. 2, 2021, [Online]. Available: https://us.vwr.com/assetsvc/asset/en_US/id/16490607/contents.

[132] Promega Cooperation, “CellTiter-Blue Assay Protocol, TB317,” *Tech. Bull.*, p. 16, 2016.

[133] D. F. Williams, “Biocompatibility in clinical practice: Predictable and unpredictable outcomes,” *Prog. Biomed. Eng.*, vol. 1, no. 1, 2019, doi: 10.1088/2516-1091/ab22cc.

[134] A. Benner, A. K. Patel, K. Singh, and A. Dua, “Physiology, Bohr Effect.,” Treasure Island (FL), 2023.

[135] M. Witkowska-Zimny, K. Walenko, E. Wrobel, P. Mrowka, A. Mikulska, and J. Przybylski, “Effect of substrate stiffness on the osteogenic differentiation of bone marrow stem cells and bone-derived cells,” *Cell Biol. Int.*, vol. 37, no. 6, pp. 608–616, 2013, doi: 10.1002/cbin.10078.

[136] M. Aido *et al.*, “Effect of in vivo loading on bone composition varies with animal age.,” *Exp. Gerontol.*, vol. 63, pp. 48–58, 2015, doi: 10.1016/j.exger.2015.01.048.

[137] J. Aerssens, S. Boonen, G. Lowet, and J. Dequeker, “Interspecies Differences in Bone Composition, Density, and Quality: Potential Implications for in Vivo Bone Research*,” *Endocrinology*, vol. 139, no. 2, pp. 663–670, 1998, doi: 10.1210/endo.139.2.5751.

[138] J. Norman, J. G. Shapter, K. Short, L. J. Smith, and N. L. Fazzalari, “Micromechanical properties

of human trabecular bone: A hierarchical investigation using nanoindentation," *J. Biomed. Mater. Res. Part A*, vol. 87A, no. 1, pp. 196–202, 2008, doi: https://doi.org/10.1002/jbm.a.31766.

[139] E. F. Morgan, G. U. Unnikrisnan, and A. I. Hussein, "Bone Mechanical Properties in Healthy and Diseased States," *Annu. Rev. Biomed. Eng.*, vol. 20, pp. 119–143, 2018, doi: 10.1146/annurev-bioeng-062117-121139.

[140] E. Takai, R. L. Mauck, C. T. Hung, and X. E. Guo, "Osteocyte Viability and Regulation of Osteoblast Function in a 3D Trabecular Bone Explant Under Dynamic Hydrostatic Pressure," *J. Bone Miner. Res.*, vol. 19, no. 9, pp. 1403–1410, 2004, doi: https://doi.org/10.1359/JBMR.040516.

[141] F. M. Lambers *et al.*, "Trabecular bone adapts to long-term cyclic loading by increasing stiffness and normalization of dynamic morphometric rates," *Bone*, vol. 55, no. 2, pp. 325–334, 2013, doi: https://doi.org/10.1016/j.bone.2013.04.016.

[142] O. H. Sandberg and P. Aspenberg, "Inter-trabecular bone formation: a specific mechanism for healing of cancellous bone.," *Acta Orthop.*, vol. 87, no. 5, pp. 459–465, 2016, doi: 10.1080/17453674.2016.1205172.

[143] R. Carretta, S. Lorenzetti, and R. Müller, "Towards patient-specific material modeling of trabecular bone post-yield behavior," *Int. j. numer. method. biomed. eng.*, vol. 29, no. 2, pp. 250–272, 2013, doi: https://doi.org/10.1002/cnm.2516.

[144] W. B. Lievers, A. S. Poljsak, S. D. Waldman, and A. K. Pilkey, "Effects of dehydration-induced structural and material changes on the apparent modulus of cancellous bone," *Med. Eng. Phys.*, vol. 32, no. 8, pp. 921–925, 2010, doi: 10.1016/j.medengphy.2010.06.001.

[145] P. J. McNair and H. Prapavessis, "Normative data of vertical ground reaction forces during landing from a jump.," *J. Sci. Med. Sport*, vol. 2, no. 1, pp. 86–88, 1999, doi: 10.1016/s1440-2440(99)80187-x.

[146] K. J. Rothman, "Curbing type I and type II errors," *Eur. J. Epidemiol.*, vol. 25, no. 4, pp. 223–224, 2010, doi: 10.1007/s10654-010-9437-5.

[147] D. Wu, P. Isaksson, S. J. Ferguson, and C. Persson, "Young's modulus of trabecular bone at the tissue level: A review," *Acta Biomater.*, vol. 78, pp. 1–12, 2018, doi: 10.1016/j.actbio.2018.08.001.

[148] I. Benjumeda Wijnhoven, R. Vallejos, J. F. Santibanez, C. Millán, and J. F. Vivanco, "Analysis of cell-biomaterial interaction through cellular bridge formation in the interface between hGMSCs and CaP bioceramics," *Sci. Rep.*, vol. 10, no. 1, pp. 1–14, 2020, doi: 10.1038/s41598-020-73428-y.

[149] P. Garg, M. M. Mazur, A. C. Buck, M. E. Wandtke, J. Liu, and N. A. Ebraheim, "Prospective Review of Mesenchymal Stem Cells Differentiation into Osteoblasts," *Orthop. Surg.*, vol. 9, no. 1, pp. 13–19, 2017, doi: 10.1111/os.12304.

[150] J. W. Haycock, "3D Cell Culture: A Review of Current Approaches and Techniques," *Methods Mol. Biol.*, vol. 695, pp. 1–15, 2011, doi: 10.1007/978-1-60761-984-0.

[151] M. J. Stoddart, P. I. Furlong, A. Simpson, C. M. Davies, and R. G. Richards, "A comparison of non-radioactive methods for assessing viability in ex vivo cultured cancellous bone: Technical note," *Eur. Cells Mater.*, vol. 12, no. 0, pp. 16–25, 2006, doi: 10.22203/eCM.v012a02.

[152] C. Sanchez, O. Gabay, C. Salvat, Y. E. Henrotin, and F. Berenbaum, "Mechanical loading highly increases IL-6 production and decreases OPG expression by osteoblasts," *Osteoarthr. Cartil.*, vol. 17, no. 4, pp. 473–481, 2009, doi: https://doi.org/10.1016/j.joca.2008.09.007.

[153] M. S. Tensor, M. S. Tensor, E. Stiffness, E. Compliance, and E. Waves, "Mechanical properties of solids," *Constr. Mater. Their Nat. Behav. Fourth Ed.*, pp. 16–29, 2010, doi: 10.4324/9780203927571.

[154] W. B. Lievers, A. C. Petryshyn, A. S. Poljsak, S. D. Waldman, and A. K. Pilkey, "Specimen diameter and 'side artifacts' in cancellous bone evaluated using end-constrained elastic tension," *Bone*, vol. 47, no. 2, pp. 371–377, 2010, doi: 10.1016/j.bone.2010.03.024.

[155] T. M. Keaveny, T. P. Pinilla, R. P. Crawford, D. L. Kopperdahl, and A. Lou, "Systematic and random errors in compression testing of trabecular bone," *J. Orthop. Res.*, vol. 15, no. 1, pp. 101–110, 1997, doi: 10.1002/jor.1100150115.

[156] R. J. Rivers and C. J. Meininger, "The Tissue Response to Hypoxia: How Therapeutic Carbon Dioxide Moves the Response toward Homeostasis and Away from Instability," *Int. J. Mol. Sci.*, vol. 24, no. 6, 2023, doi: 10.3390/ijms24065181.

[157] A. Ressler *et al.*, "Osteogenic differentiation of human mesenchymal stem cells on substituted calcium phosphate/chitosan composite scaffold," *Carbohydr. Polym.*, vol. 277, no. August 2021, 2022, doi: 10.1016/j.carbpol.2021.118883.

APPENDIX A: Thesis graphical abstract

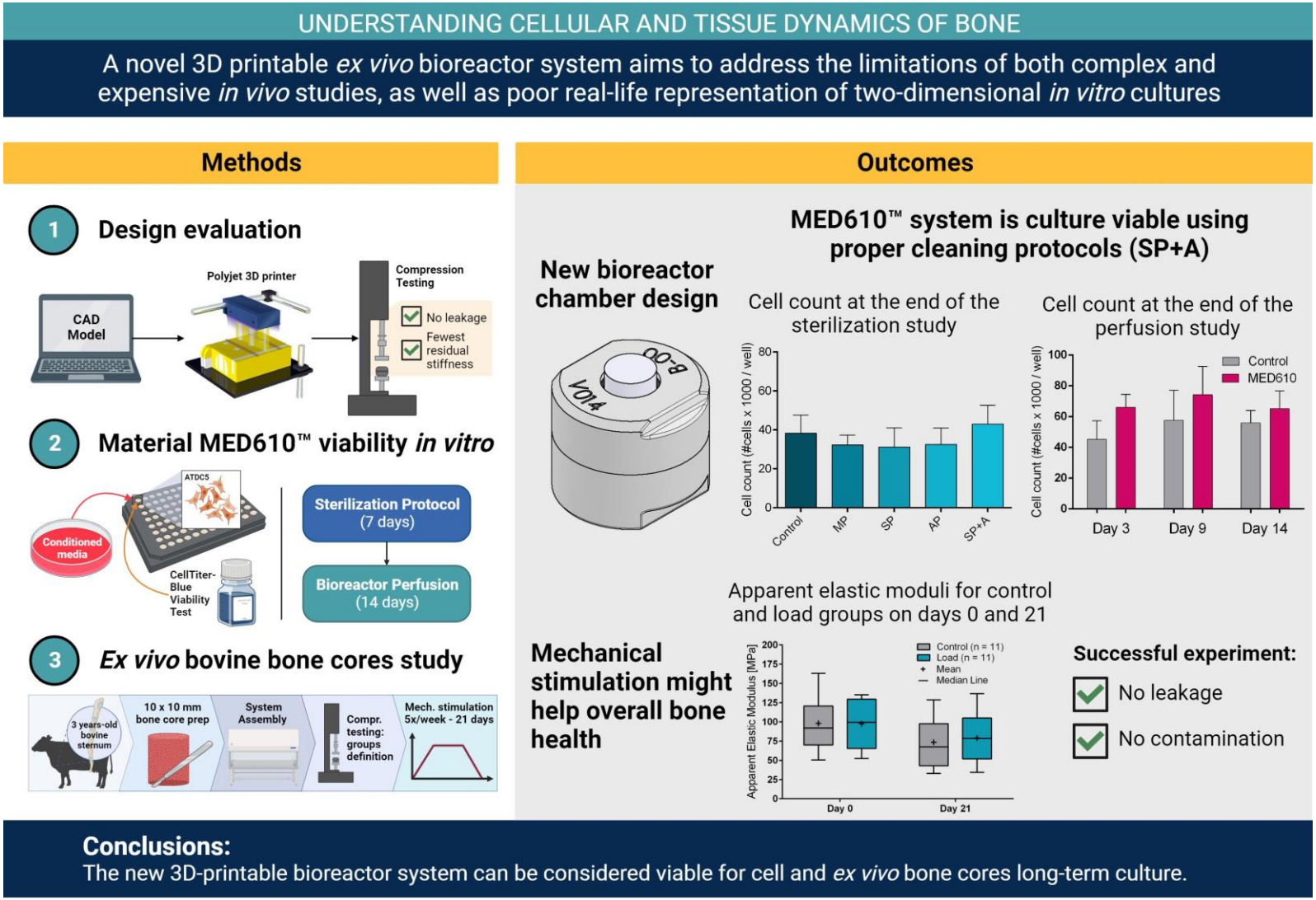

APPENDIX B: Dynamic seeding and culture parameters used in *in vitro* studies

Table B-1. Static and dynamic cell seeding parameters.

Cell line	Scaffold	Cell concentration (cells/mL)	Cells seeded on scaffolds	Sterilization	# Samples	Seeding type	Flow rate (if applicable) *	Ref.
hMSCs line SCP-141	Decellularized cancellous bone matrix, 10 mm³, 450 µm, P-68%	$1 \cdot 10^7$	250 mL from cell suspension $2.5 \cdot 10^6$ cells	Thermostable: autoclave. Thermoplastic: 20% EtOH and 0.1% peroxyacetic acid for 45 min, then rinsed with demineralized water.	3	Static	N/A	[76]
hES-MPs	Polyutethane foam, 30 x 5 mm, coated in gelatin	Not informed	$5 \cdot 10^5$ cells	Scaffolds: by immersion in 0.1% porcine skin gelatin in water and autoclaving. Washed with PBS 3 times before culture	6	Static	N/A	[81]
hMSCs	PCL, 5 mm diameter x 1.5 mm height	$1 \cdot 10^6$	20 µL of cells suspension	Not reported	5 per condition	Static	N/A	[82]
MC3T3-E1 mouse pre-osteoblastic	Chitosan-HA hydrogel, 6 mm diameter x 5 mm height	Not informed	50 µL cell suspension (10^6 cells in growth medium)	Scaffolds: 70% ethanol for 1h, then UV light for 30 min	24	Static	N/A	[84]
MG63 osteoblast-like	PLA and titanium, 6 mm diameter x 12 mm height, P-95.7%	$3.33 \cdot 10^6$	$1 \cdot 10^6$ cells in 300 µL complete medium	Scaffolds: gamma radiation, and 30% ethanol; Bioreactor chambers: autoclave; Plastic parts: ethanol, distilled water and 20 min in UV light	6	Static	N/A	[77]
hMSCs line SCP-141	Decellularized cancellous bone matrix, 10 mm³, 450 µm, P-68%	1.25x10^6 cells/mL	2 mL of cell suspension ($2.5 \cdot 10^6$ cells)	Same as static seeding	3	Dynamic	1000 µL/min	[76]
hMSCs	PCL, 5 mm diameter x 1.5 mm height	Not informed	-	Not reported	5 per condition	Dynamic	600 µL/min for 2h	[82]
MC3T3-E1 mouse pre-osteoblastic	Chitosan-HA hydrogel, 6 mm diameter x 5 mm height	Not informed	10 mL cell suspension ($2 \cdot 10^6$ cells in growth medium)	Scaffolds: 70% ethanol for 1h, then UV light for 30 min	2 in the same bioreactor	Dynamic	1000 µL/min for 1 day (bidirectional)	[84]
MG63 osteoblast-like	PLA and titanium, 6 mm diameter x 12 mm height, P-95.7%	-	10 mL cell suspension ($2 \cdot 10^6$ cells in growth medium)	Scaffolds: gamma radiation, and 30% ethanol; Bioreactor chambers: autoclave; Plastic parts: ethanol, distilled water aand 20 min in UV light	2 per condition	Dynamic	Flow velocity: 5 mm/s, 100 cycles of perfusion	[77]
* The only flow rate used or the one that reported best seeding efficiency								

Table B-2. Dynamic perfusion culture parameters

Bioreactor	Flow rate(s)*	Flow Velocity (m/s)	Direction	Ref.
Fabricated using SLA and FDM	10 and 250 µL/min	$1.6 \cdot 10^{-6}$ and $4 \cdot 10^{-4}$	Not informed	[95]
Polycarbonate	3480 µL/min	Not reported	Bidirectional	[100]
P3D-6 chamber	100 µL/min	Not reported	Bidirectional	[102]
* That were reported to have the best results in terms of metabolic activity within each study				

Table B-3. Analyses and characterization tests done on scaffolds after culture period.

Metabolic activity	Cell number	Morphology and distribution	Gene expression	Ref.
Cell nuclei stained with 4',6-diamidino-2-phenylindole. Analyzed at 475 nm and 461 nm	Not analyzed	Fluorescence microscopy	Not analyzed	[95]
Resazurin reduction (RR), ALP activity and total DNA quantification tests on day 10	Not analyzed	Not analyzed	Not analyzed	[100]
MTT assay	Not analyzed	SEM	RT-PCR: ALP, COL1A1, osteocalcin, osteoponton and runt-related transcription factor 2	[102]
Not analyzed	LDH detection (colorimetric assay)	Acridine Orange and Ethidium Bromide stain observed under fluorescence stereoscope with DSR and GFP filters	Not analyzed	[96]

APPENDIX C: Bioreactor chamber mechanical drawings

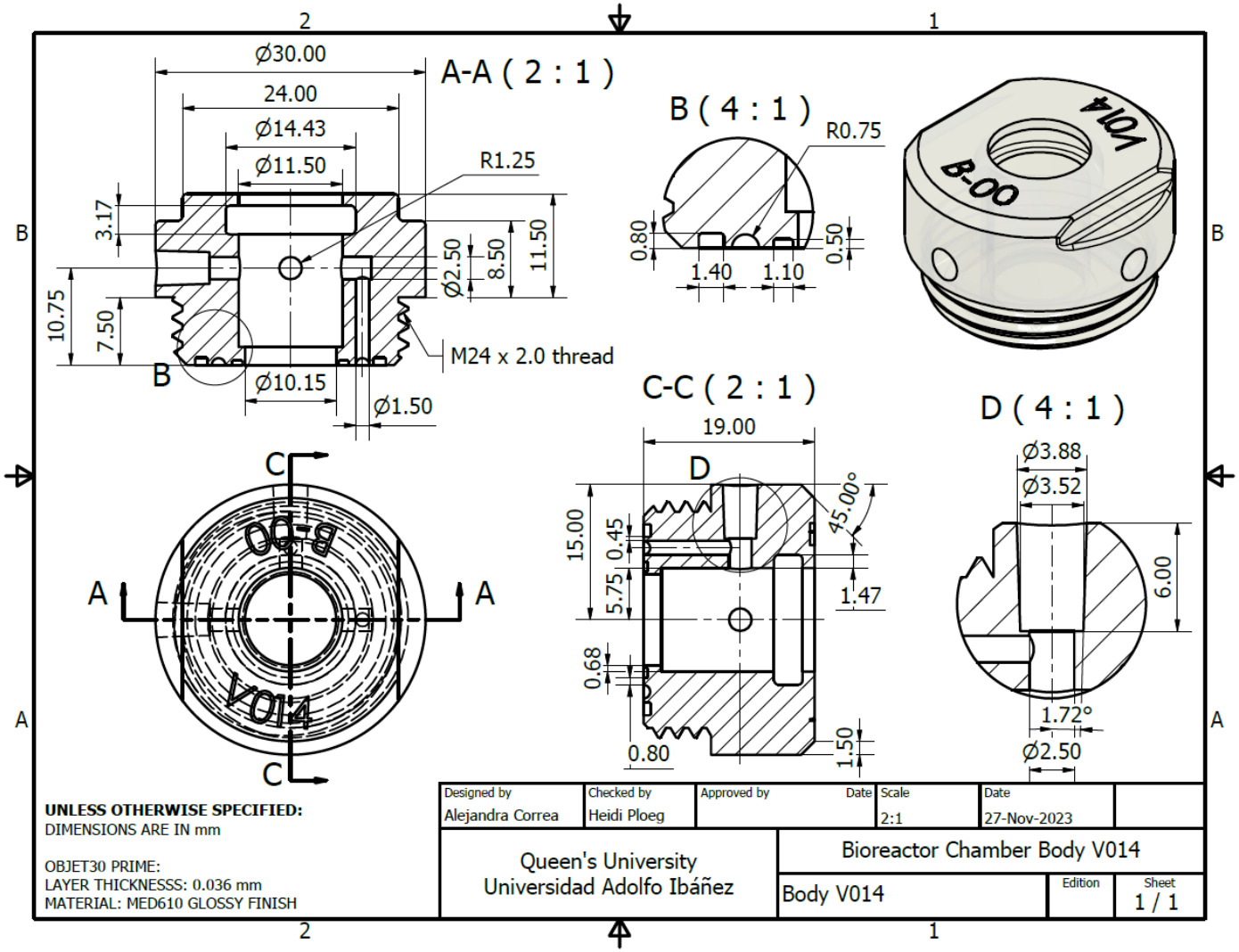

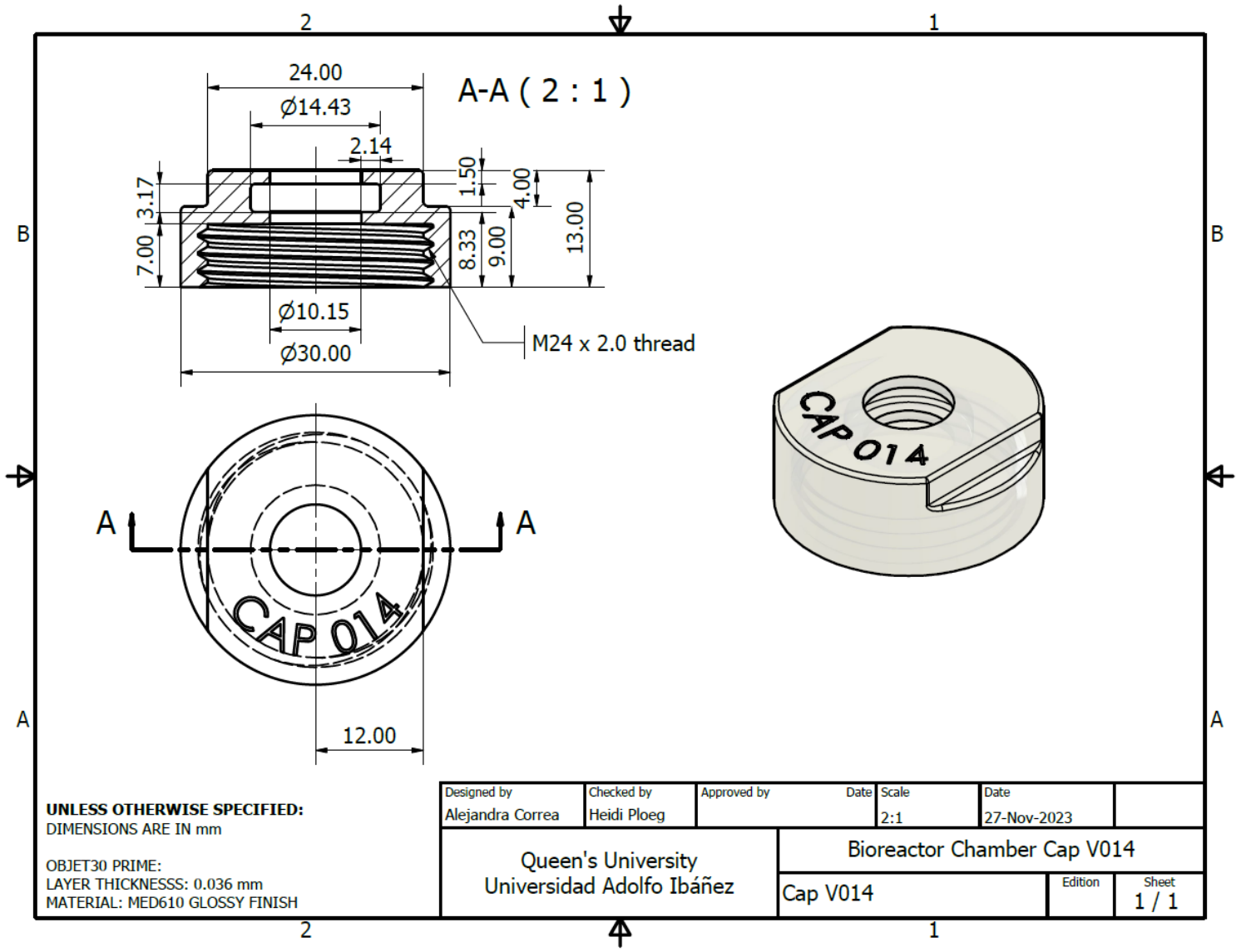
2
1
B
A
24.00
Ø14.43
2.14
A-A (2 : 1)
3.17
7.00
1.50
4.00
8.33
9.00
13.00
Ø10.15
Ø30.00
M24 x 2.0 thread
A
A
CAP 014
12.00
CAP 014
UNLESS OTHERWISE SPECIFIED:
DIMENSIONS ARE IN mm
OBJET30 PRIME:
LAYER THICKNESSS: 0.036 mm
MATERIAL: MED610 GLOSSY FINISH
Designed by
Alejandra Correa
Checked by
Heidi Ploeg
Approved by
Date
Scale
2:1
Date
27-Nov-2023
Queen's University
Universidad Adolfo Ibáñez
Bioreactor Chamber Cap V014
Cap V014
Edition
Sheet
1 / 1

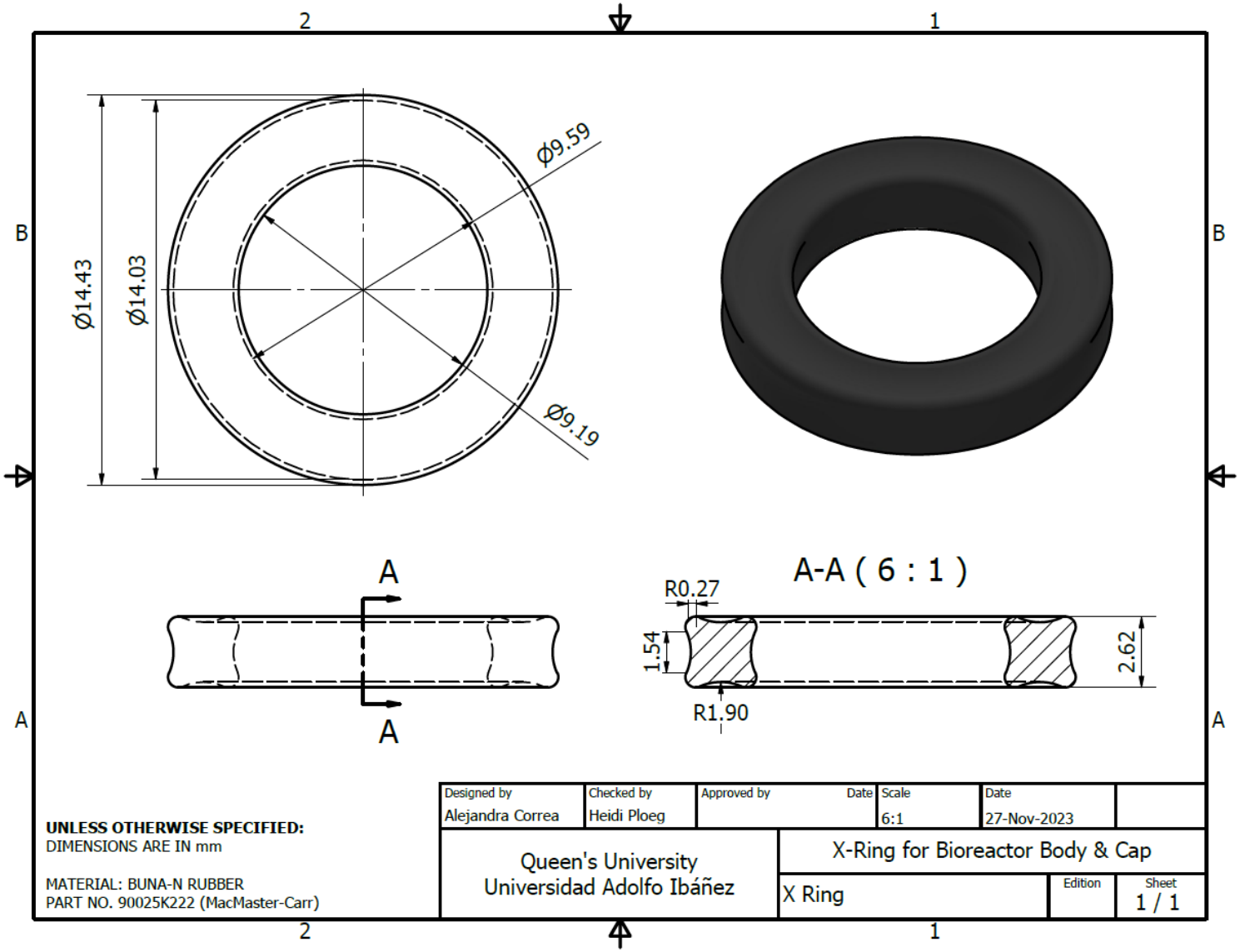
2
1
B
A
Ø14.43
Ø14.03
Ø9.59
Ø9.19
A
A
A-A (6 : 1)
R0.27
1.54
2.62
R1.90
UNLESS OTHERWISE SPECIFIED:
DIMENSIONS ARE IN mm
MATERIAL: BUNA-N RUBBER
PART NO. 90025K222 (MacMaster-Carr)
Designed by
Alejandra Correa
Checked by
Heidi Ploeg
Approved by
Date
Scale
6:1
Date
27-Nov-2023
Queen's University
Universidad Adolfo Ibáñez
X-Ring for Bioreactor Body & Cap
X Ring
Edition
Sheet
1 / 1

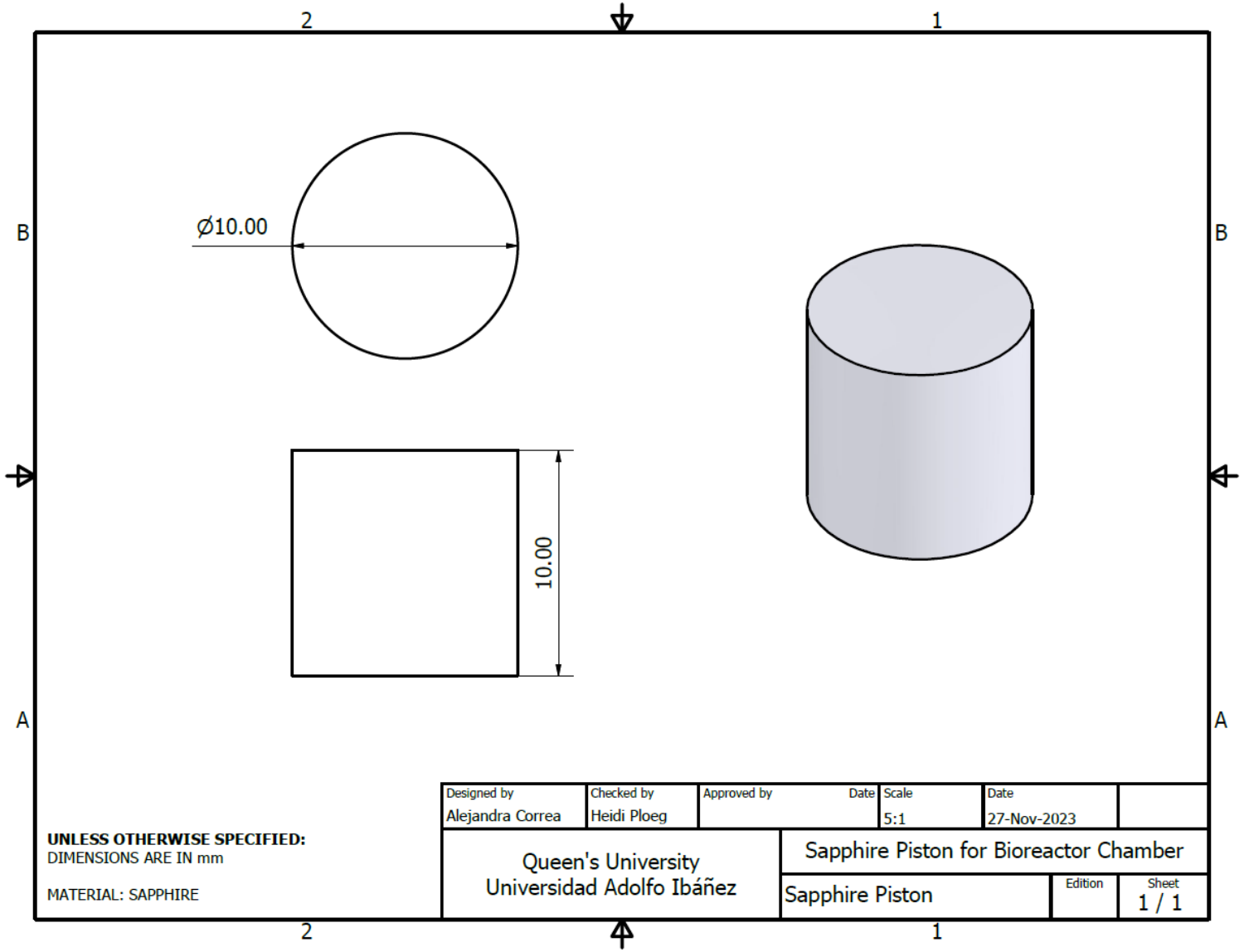
2
1
B
A
Ø10.00
10.00
UNLESS OTHERWISE SPECIFIED:
DIMENSIONS ARE IN mm
MATERIAL: SAPPHIRE
Designed by
Alejandra Correa
Checked by
Heidi Ploeg
Approved by
Date
Scale
5:1
Date
27-Nov-2023
Queen's University
Universidad Adolfo Ibáñez
Sapphire Piston for Bioreactor Chamber
Sapphire Piston
Edition
Sheet
1 / 1

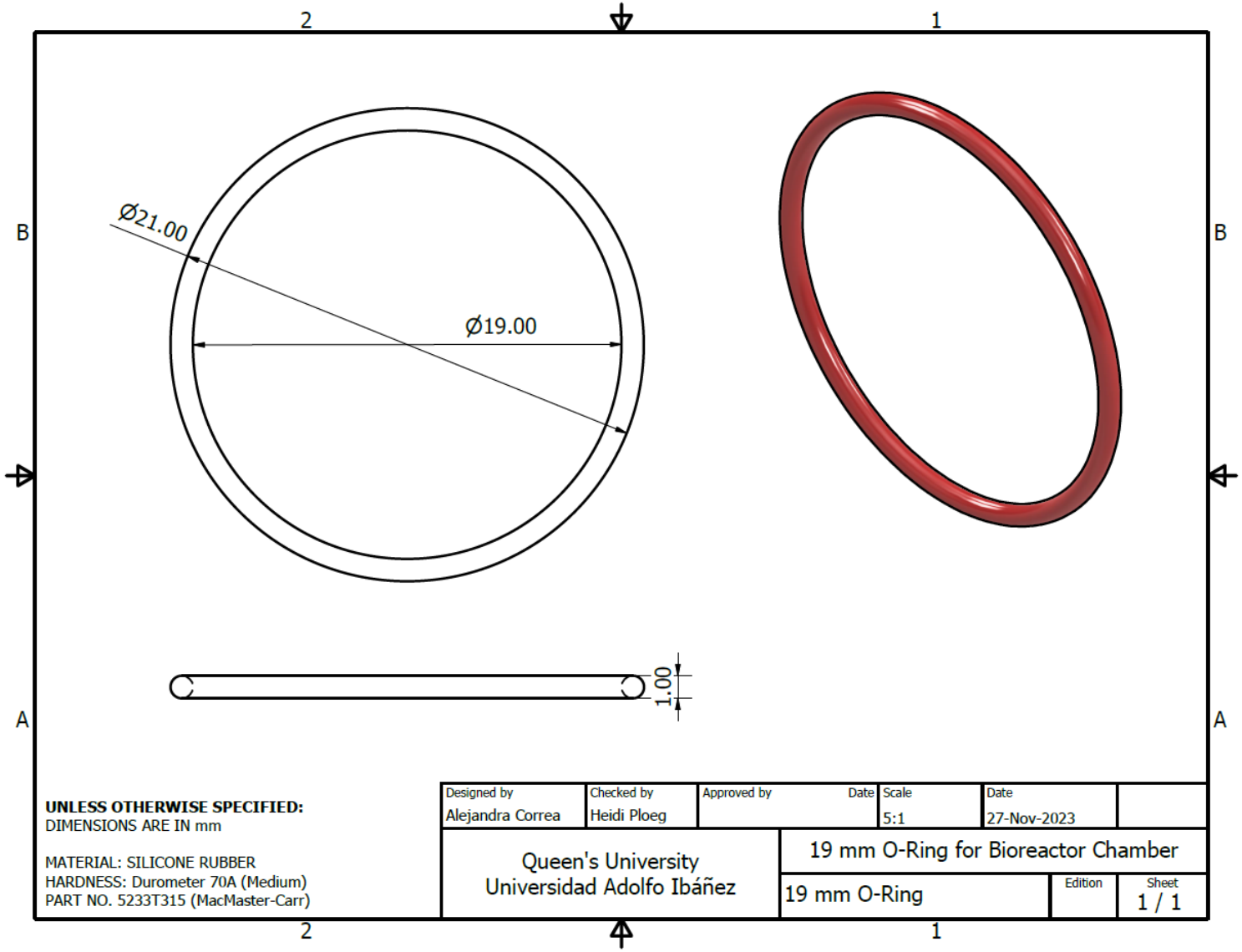
2
1
B
A
Ø21.00
Ø19.00
1.00
UNLESS OTHERWISE SPECIFIED:
DIMENSIONS ARE IN mm
MATERIAL: SILICONE RUBBER
HARDNESS: Durometer 70A (Medium)
PART NO. 5233T315 (MacMaster-Carr)
Designed by
Alejandra Correa
Checked by
Heidi Ploeg
Approved by
Date
Scale
5:1
Date
27-Nov-2023
Queen's University
Universidad Adolfo Ibáñez
19 mm O-Ring for Bioreactor Chamber
19 mm O-Ring
Edition
Sheet
1 / 1

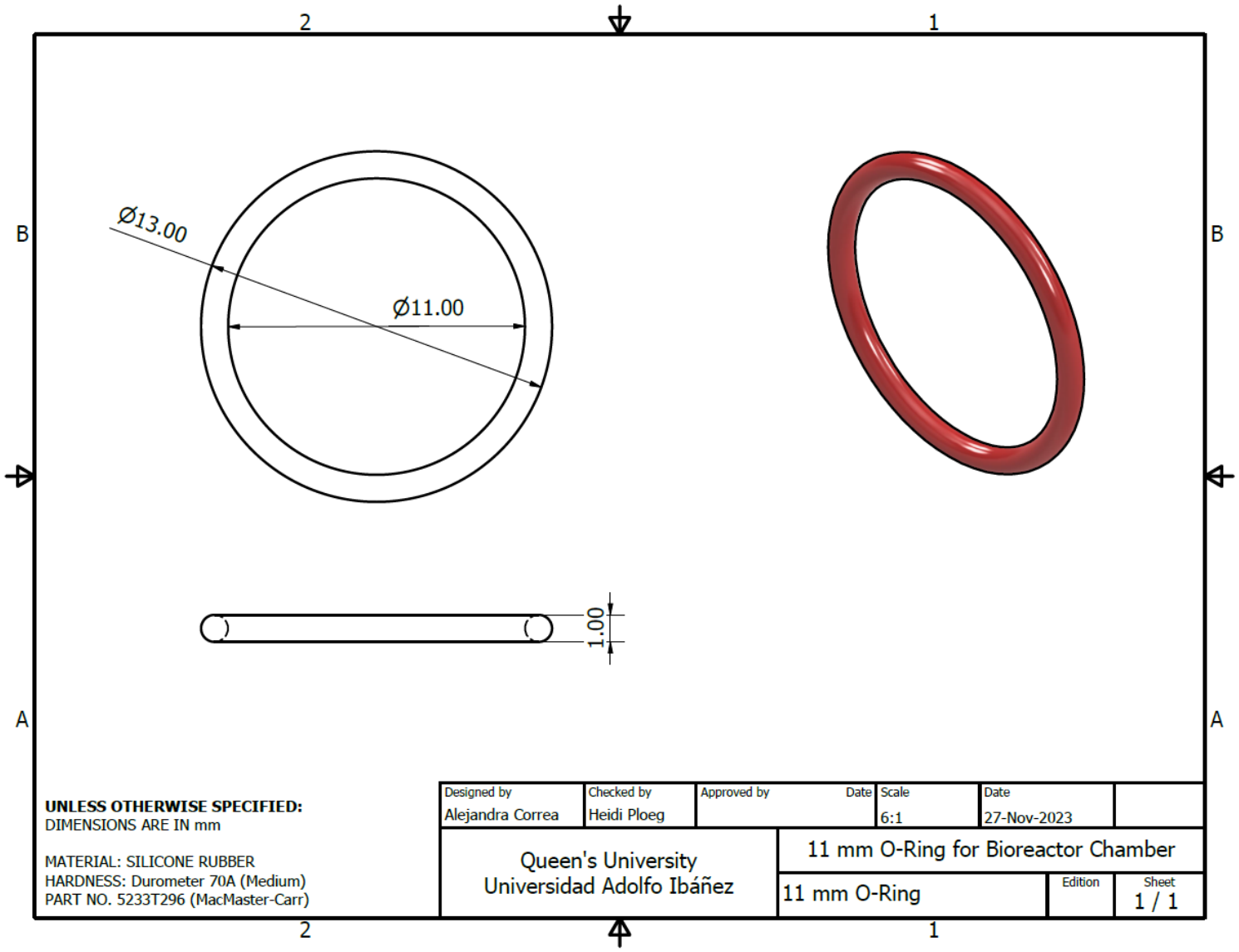
2
1
B
A
Ø13.00
Ø11.00
1.00
UNLESS OTHERWISE SPECIFIED:
DIMENSIONS ARE IN mm
MATERIAL: SILICONE RUBBER
HARDNESS: Durometer 70A (Medium)
PART NO. 5233T296 (MacMaster-Carr)
Designed by
Alejandra Correa
Checked by
Heidi Ploeg
Approved by
Date
Scale
6:1
Date
27-Nov-2023
Queen's University
Universidad Adolfo Ibáñez
11 mm O-Ring for Bioreactor Chamber
11 mm O-Ring
Edition
Sheet
1 / 1

APPENDIX D: Bioreactor chamber assembly

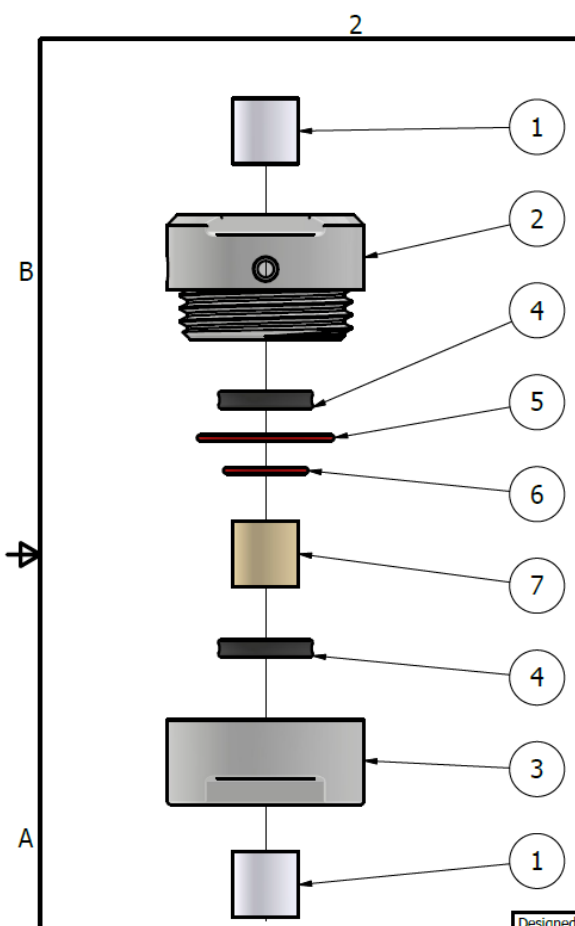

PARTS LIST			
ITEM	QTY	PART NUMBER	MATERIAL
1	2	Piston	Sapphire
2	1	Zetos MK IV_014	MED610
3	1	Zetos MK IV Cap_014	MED610
4	2	X-Ring	Silicone
5	1	19 mm O-Ring	Silicone
6	1	11 mm O-Ring	Silicone
7	1	Bone Core 10 x 10 mm	Bone

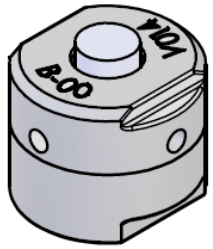

Designed by	Checked by	Approved by	Date	Scale	Date
Alejandra Correa	Heidi Ploeg			1.25:1	27-Nov-2023

Queen's University
Universidad Adolfo Ibáñez

Bioreactor Assembly

Bioreactor 014 Assembly | Edition | Sheet 1 / 2

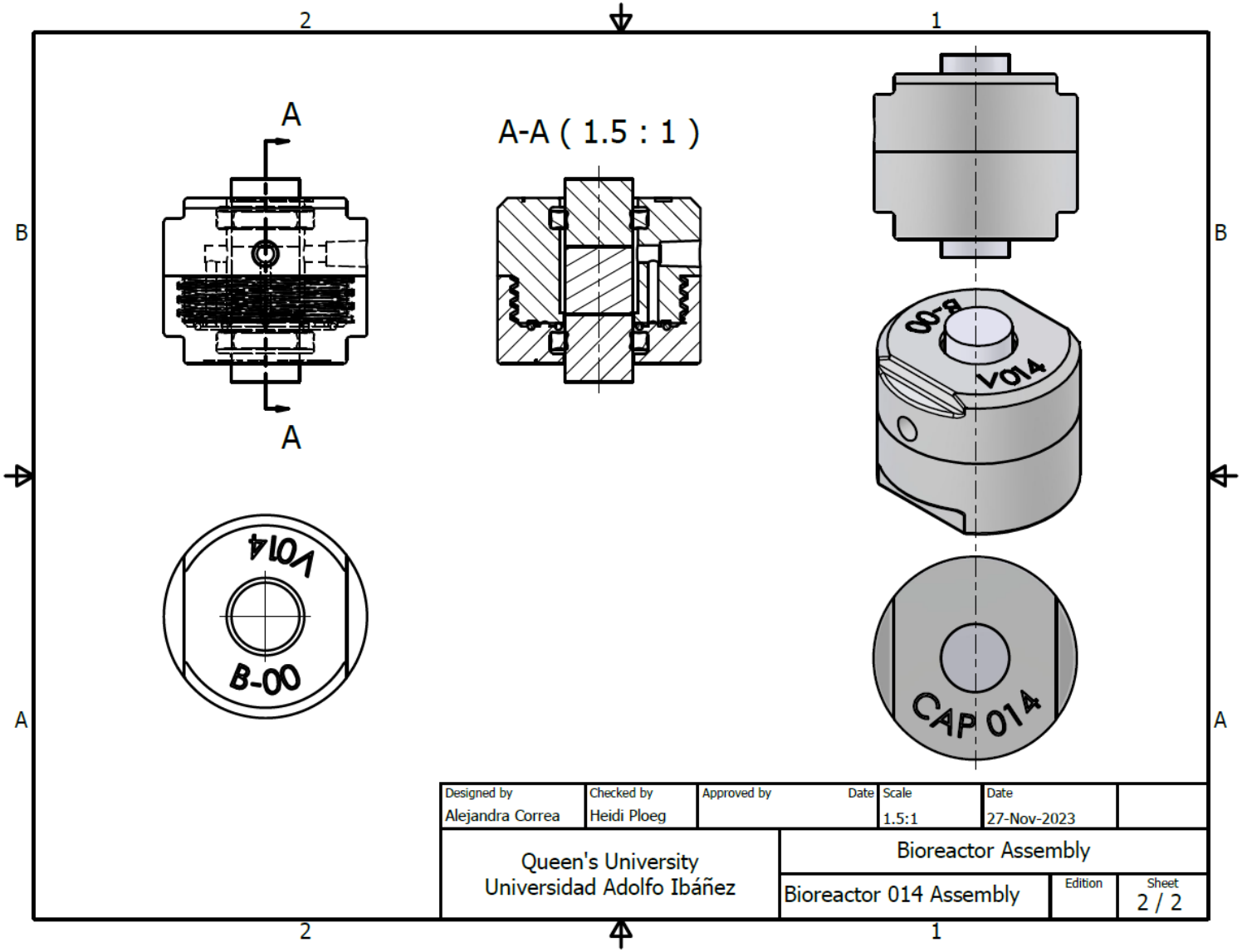
A
A
A-A (1.5 : 1)
B-00
V014
V014
CAP 014
Designed by
Alejandra Correa
Checked by
Heidi Ploeg
Approved by
Date
Scale
1.5:1
Date
27-Nov-2023
Queen's University
Universidad Adolfo Ibáñez
Bioreactor Assembly
Bioreactor 014 Assembly
Edition
Sheet
2 / 2

APPENDIX E: ATDC5 standard curves during MED610™ sterilization protocol screening

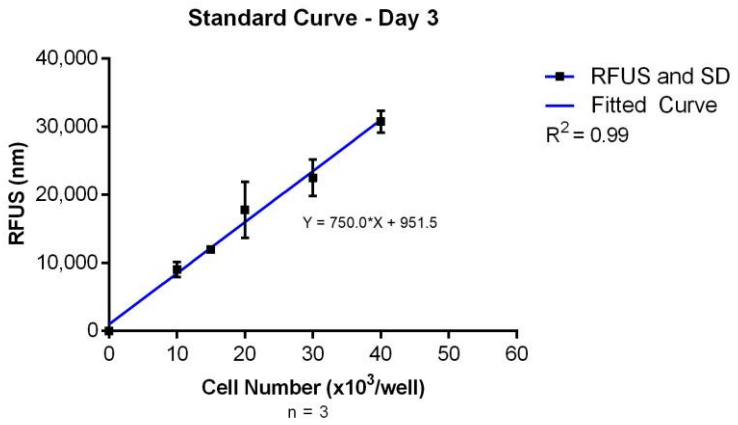

Figure E-1. Linear regression of Day 3 to fit the Relative Fluorescence Units (RFUS) to set values of cell numbers, obtaining a standard curve to obtain measurements in cell numbers. N=3 was used per set cell number value for standardization.

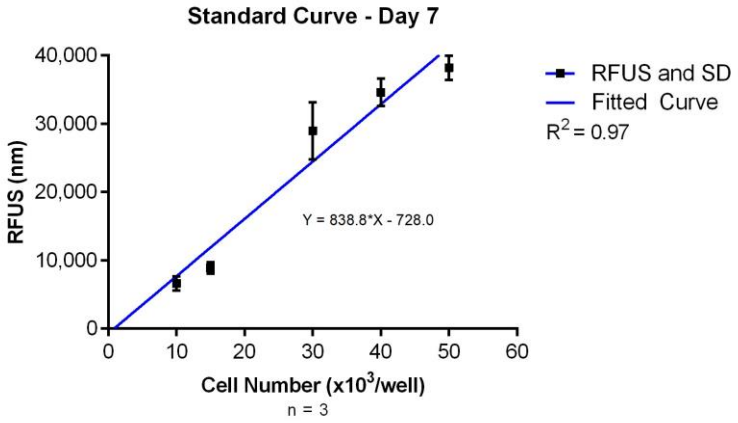

Figure E-2. Linear regression of Day 7 to fit the Relative Fluorescence Units (RFUS) to set values of cell numbers, obtaining a standard curve to obtain measurements in cell numbers. N=3 was used per set cell number value for standardization.

APPENDIX F: ATDC5 standard curves during MED610™ perfusion study

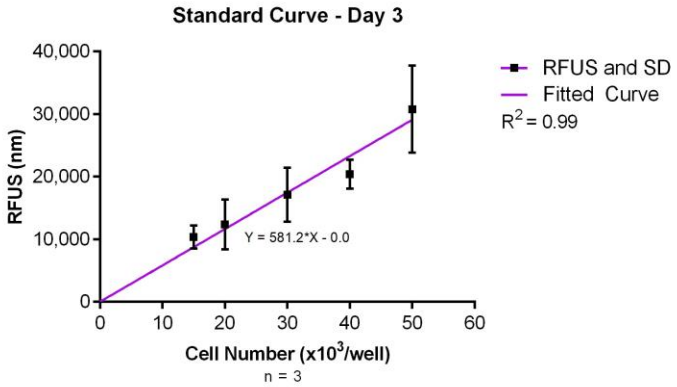

Figure F-1. Linear regression of Day 3 to fit the Relative Fluorescence Units (RFUS) to set values of cell numbers, obtaining a standard curve to obtain measurements in cell numbers. N=3 was used per set cell number value for standardization.

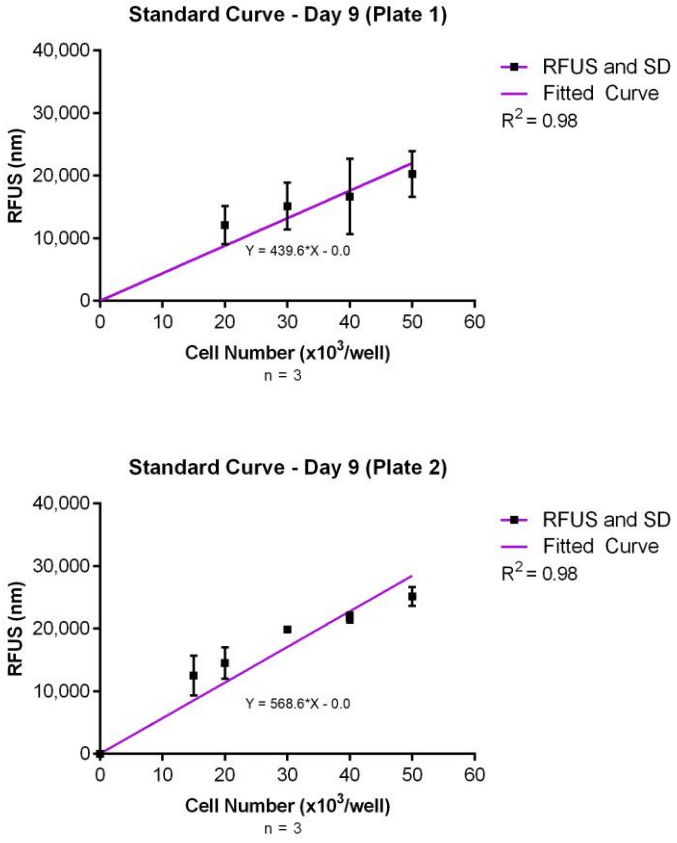

Figure F-2. Linear regressions of Day 9 (two 96-well plates) to fit the Relative Fluorescence Units (RFUS) to set values of cell numbers, obtaining a standard curve to obtain measurements in cell numbers. N=3 was used per set cell number value for standardization.

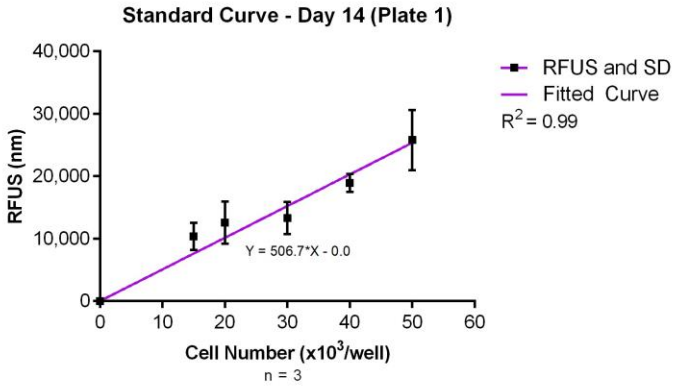

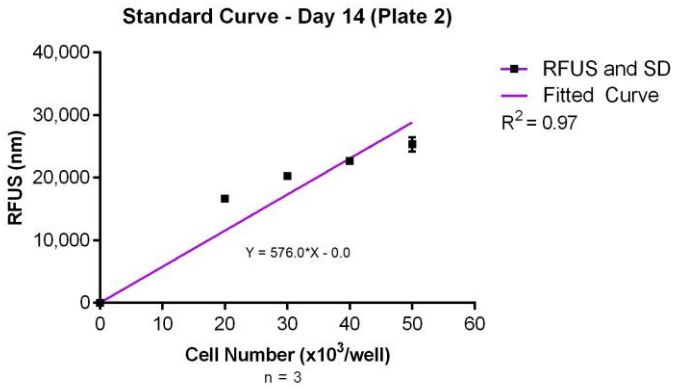

Figure F-3. Linear regressions of Day 14 (two 96-well plates) to fit the Relative Fluorescence Units (RFUS) to set values of cell numbers, obtaining a standard curve to obtain measurements in cell numbers. N=3 was used per set cell number value for standardization.

APPENDIX G: Summary table for timepoints during the *ex vivo* bone core study

Table G-4. Timepoint summary of Chapter 6 ex vivo bovine trabecular bone core study.

Timepoint	Description
Day -2	Bovine sternum retrieval and bone cores excision
Day -2 to Day -1	Recovery period in well-plate with culture medium
Day -1	Bioreactor circuit and bone cores assembly
Day 0	First set of quasi-static compression tests and E_{app} ranking
Day 1 to Day 2	Recovery period within bioreactor chambers (Saturday-Sunday)
Day 5	Calcein label addition
Day 23	Calcein label addition
Day 24	Final set of quasi-static compression tests (after 21-days of treatment)

* Media was changed three times per week, starting from Day 0

**Controlled cyclic load applied to treatment group 5-days a week (Monday-Friday) for 21-days

APPENDIX H: Force-displacement curves for bone cores quasi-static testing on day 0

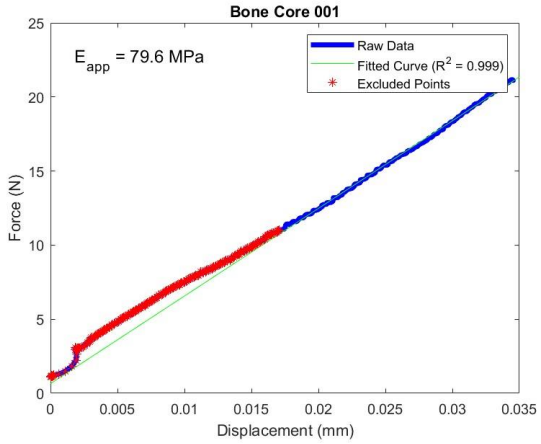

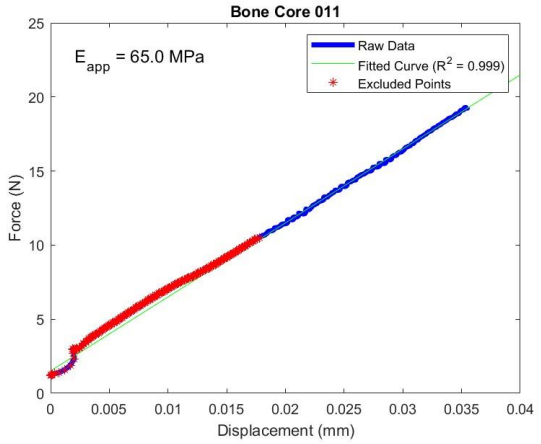

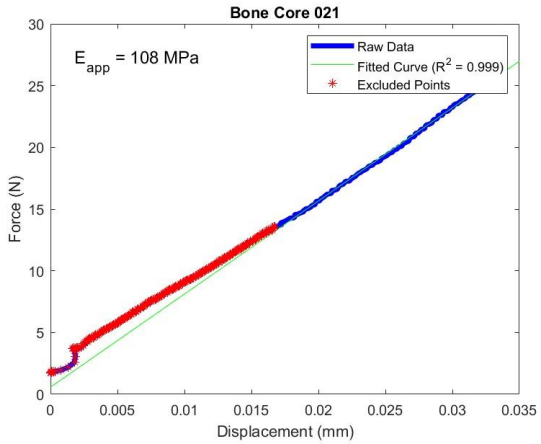

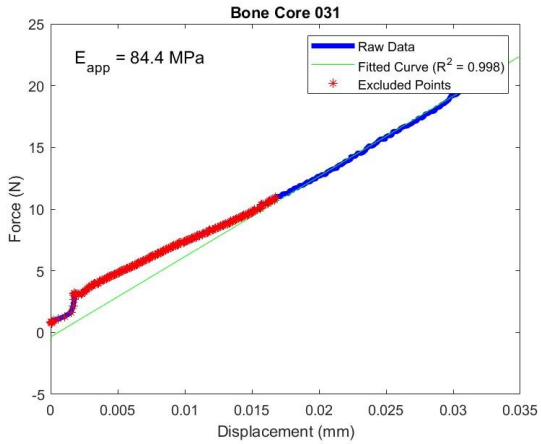

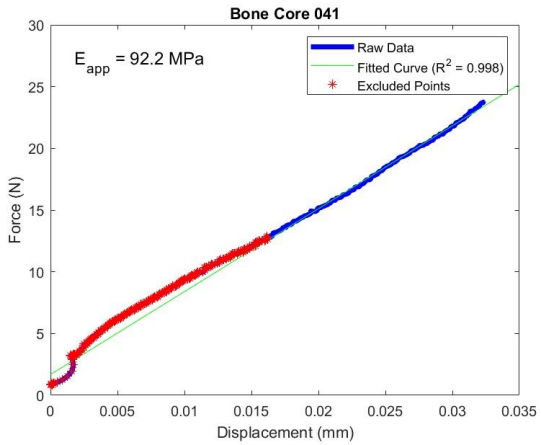

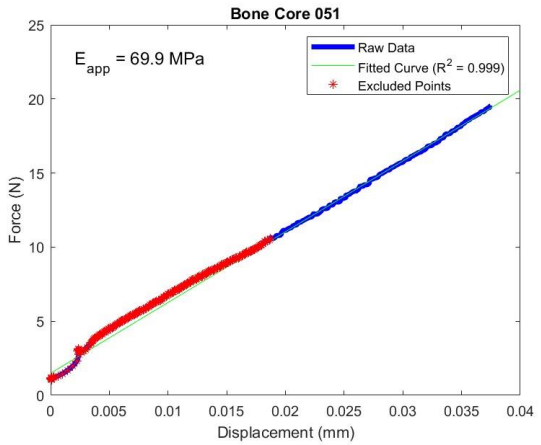

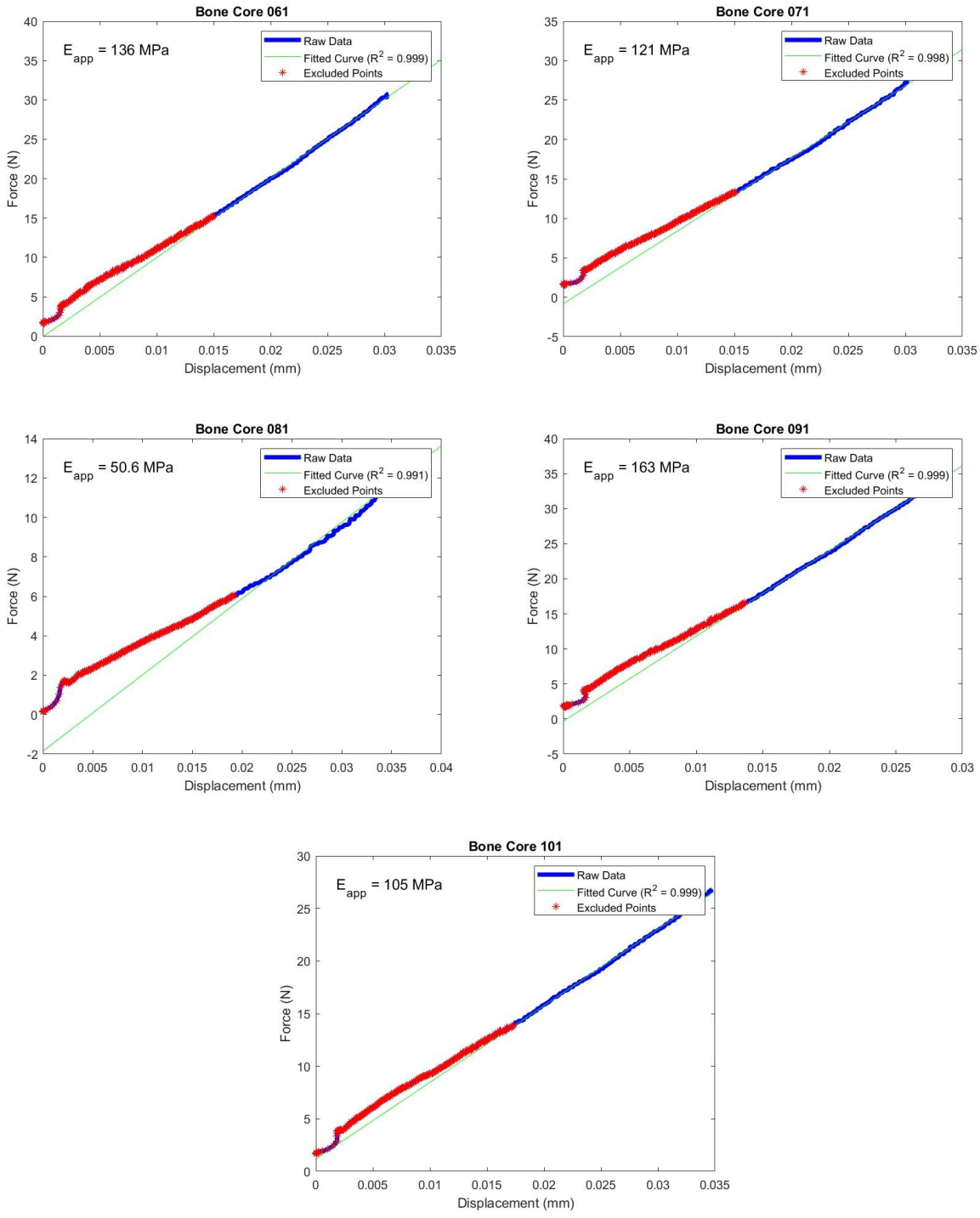

Figure H-1. Force-displacement plots from quasi-static loading of the control group on day 0. Linear fit shown (green) was performed with the last 50% of the force-displacement curve and demonstrates the apparent bone core stiffness used to determine the apparent elastic modulus (E_{app}) of bone cores. System compliance is considered in the specimen E_{app} shown in each plot. Goodness of fit was evaluated with the coefficient of determination (R^2).

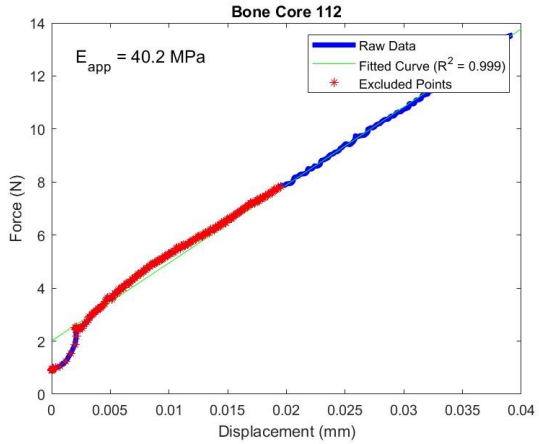
Bone Core 112
E_app = 40.2 MPa
Raw Data
Fitted Curve (R^2 = 0.999)
Excluded Points
Force (N)
Displacement (mm)

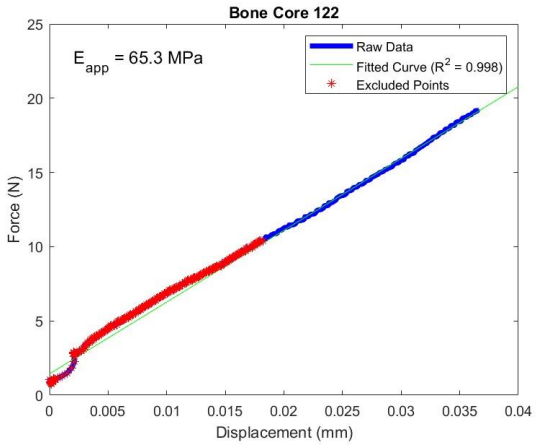
Bone Core 122
E_app = 65.3 MPa
Raw Data
Fitted Curve (R^2 = 0.998)
Excluded Points
Force (N)
Displacement (mm)

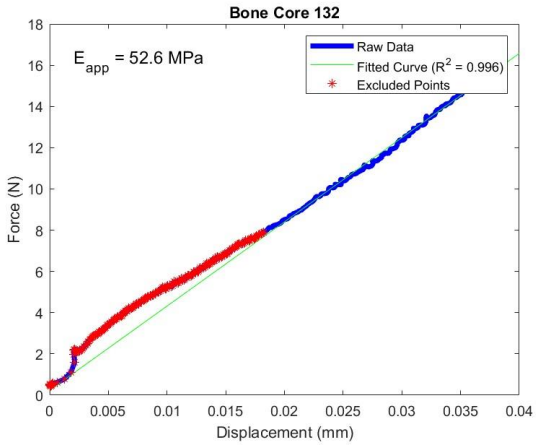
Bone Core 132
E_app = 52.6 MPa
Raw Data
Fitted Curve (R^2 = 0.996)
Excluded Points
Force (N)
Displacement (mm)

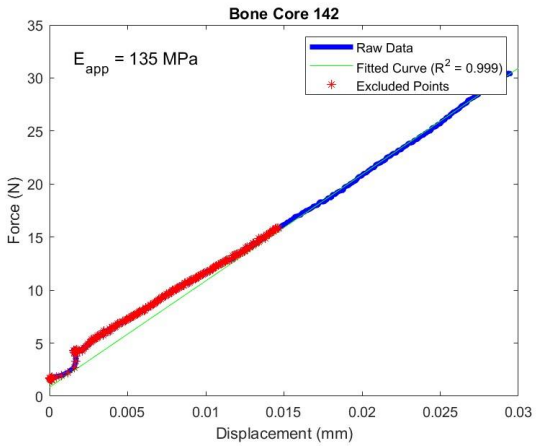
Bone Core 142
E_app = 135 MPa
Raw Data
Fitted Curve (R^2 = 0.999)
Excluded Points
Force (N)
Displacement (mm)

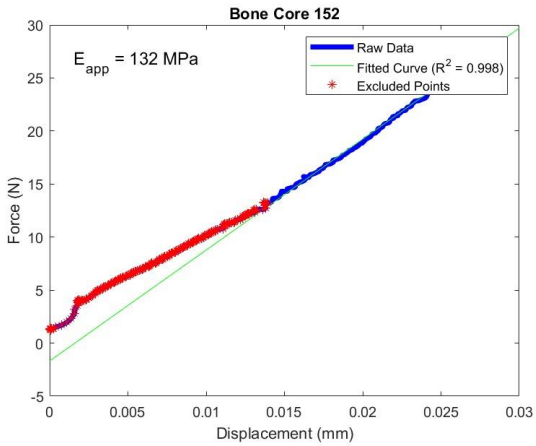
Bone Core 152
E_app = 132 MPa
Raw Data
Fitted Curve (R^2 = 0.998)
Excluded Points
Force (N)
Displacement (mm)

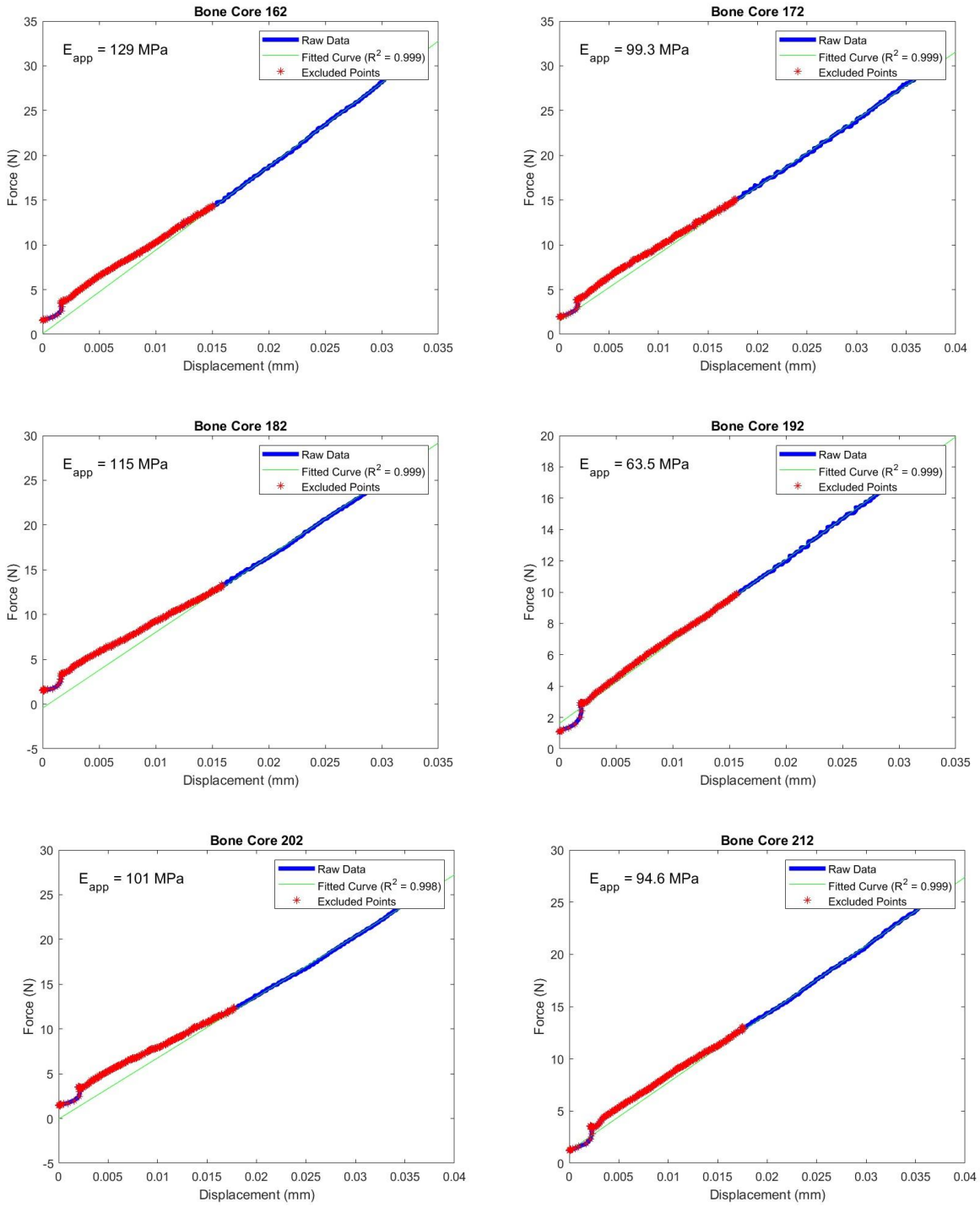

Figure H-2. Force-displacement plots from quasi-static loading of the treatment group on day 0. Linear fit shown (green) was performed with the last 50% of the force-displacement curve and demonstrates the apparent bone core stiffness used to determine the apparent elastic modulus (E_{app}) of bone cores. System compliance is considered in the specimen E_{app} shown in each plot. Goodness of fit was evaluated with the coefficient of determination (R^2).

APPENDIX I: Force-displacement curves for bone cores quasi-static testing on day 21

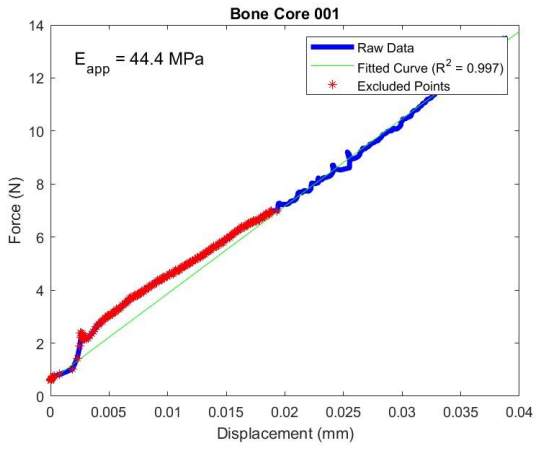

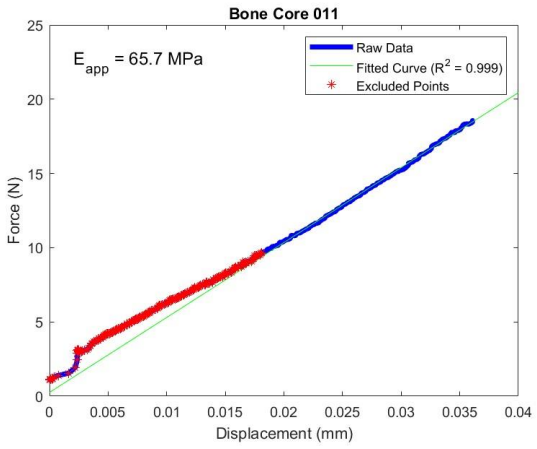

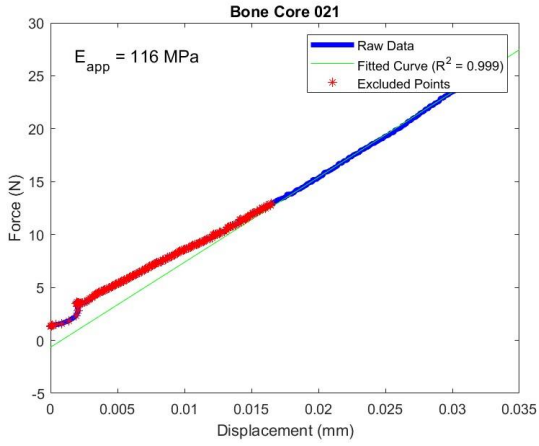

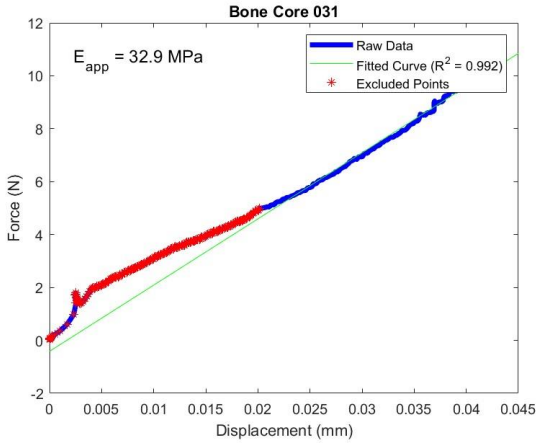

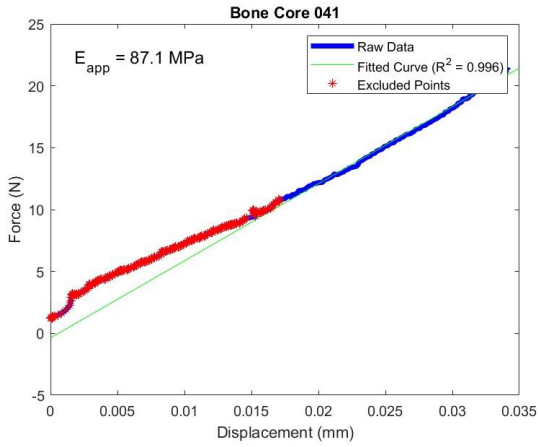

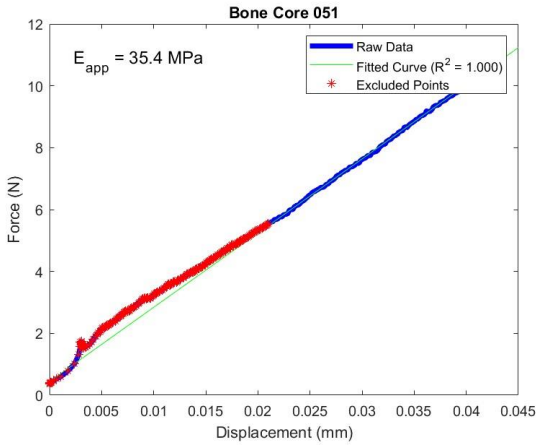

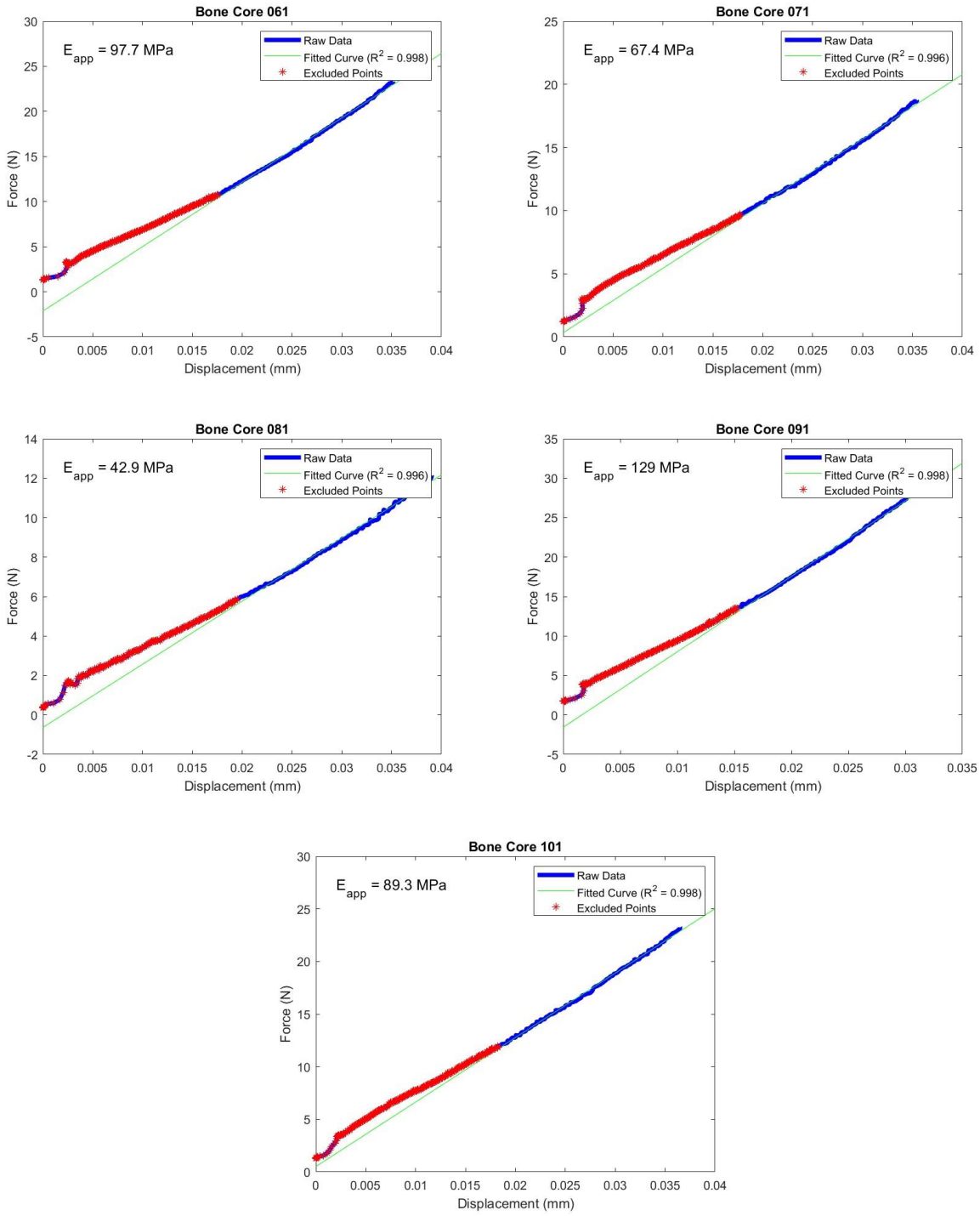

Fig. I-1. Force-displacement plots from quasi-static loading of the control group on day 21. Linear fit shown (green) was performed with the last 50% of the force-displacement curve and demonstrates the apparent bone core stiffness used to determine the apparent elastic modulus (E_{app}) of bone cores. System compliance is considered in the specimen E_{app} shown in each plot. Goodness of fit was evaluated with the coefficient of determination (R^2).

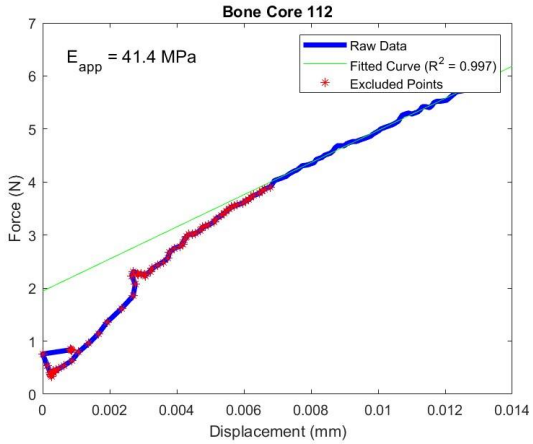
Bone Core 112
E_app = 41.4 MPa
Raw Data
Fitted Curve (R^2 = 0.997)
Excluded Points
Force (N)
Displacement (mm)

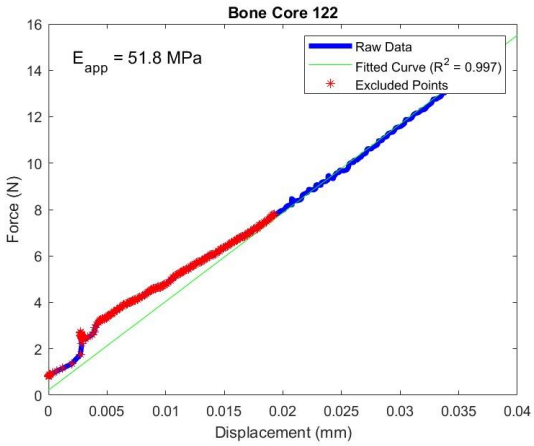
Bone Core 122
E_app = 51.8 MPa
Raw Data
Fitted Curve (R^2 = 0.997)
Excluded Points
Force (N)
Displacement (mm)

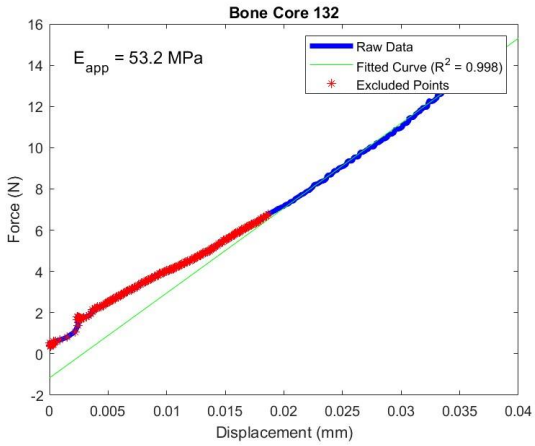
Bone Core 132
E_app = 53.2 MPa
Raw Data
Fitted Curve (R^2 = 0.998)
Excluded Points
Force (N)
Displacement (mm)

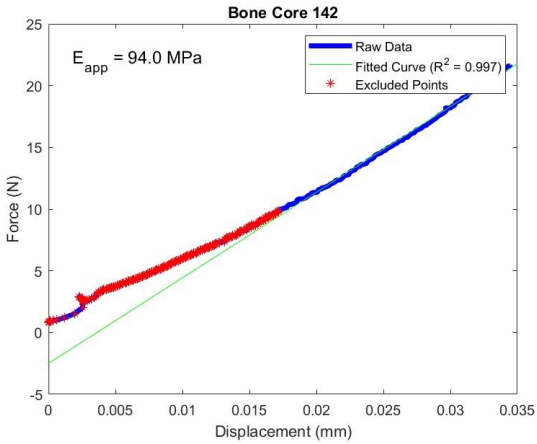
Bone Core 142
E_app = 94.0 MPa
Raw Data
Fitted Curve (R^2 = 0.997)
Excluded Points
Force (N)
Displacement (mm)

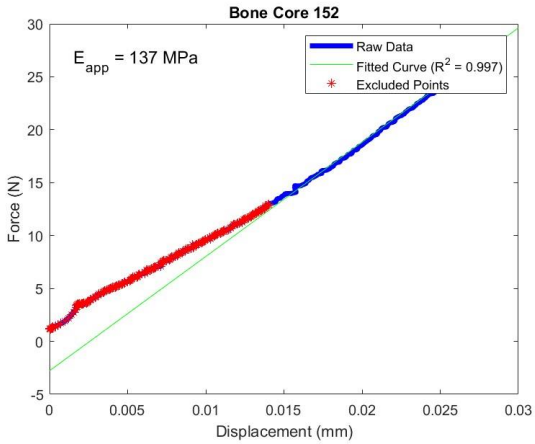
Bone Core 152
E_app = 137 MPa
Raw Data
Fitted Curve (R^2 = 0.997)
Excluded Points
Force (N)
Displacement (mm)

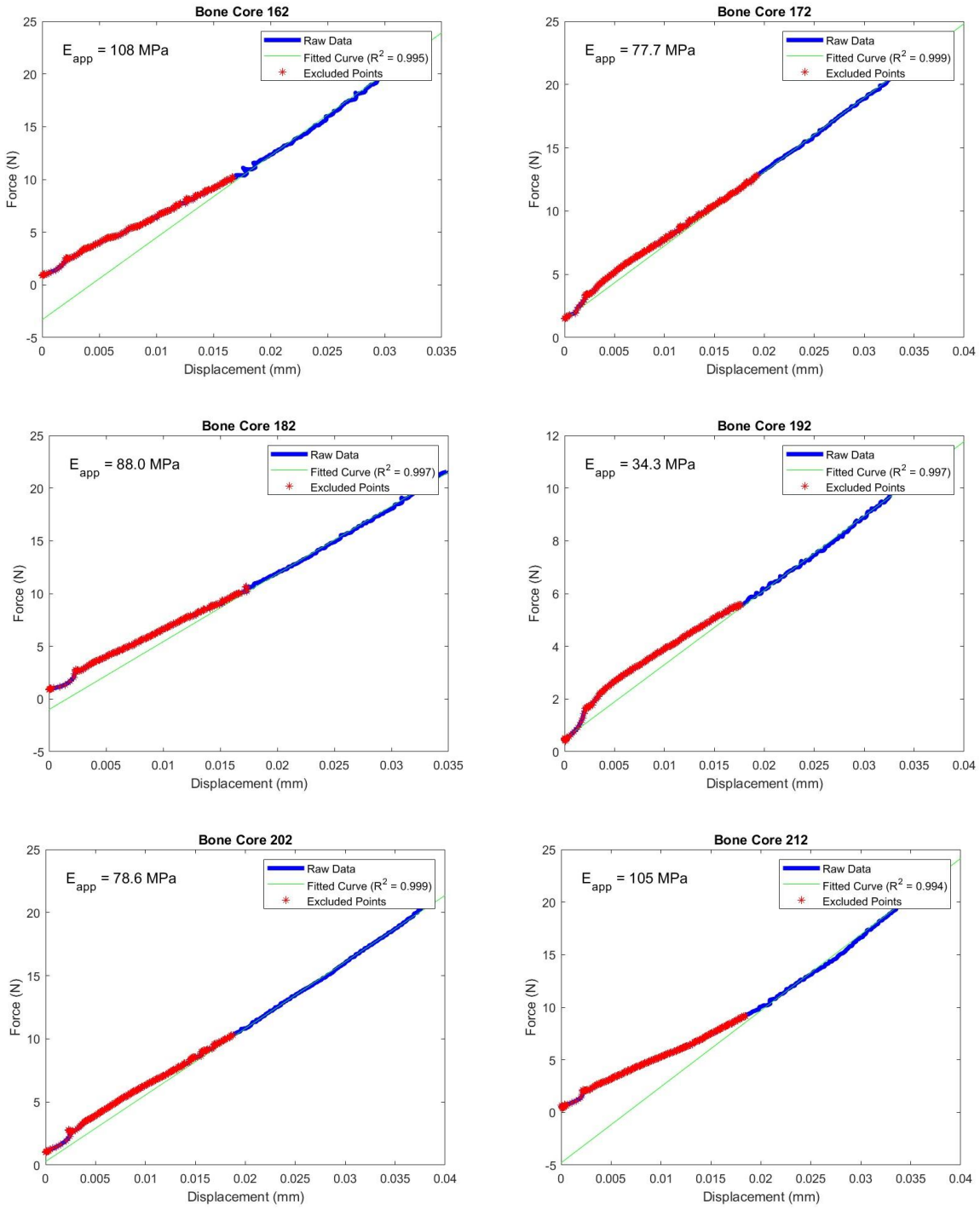

Figure I-2. Force-displacement plots from quasi-static loading of the treatment group on day 21. Linear fit shown (green) was performed with the last 50% of the force-displacement curve and demonstrates the apparent bone core stiffness used to determine the apparent elastic modulus (E_{app}) of bone cores. System compliance is considered in the specimen E_{app} shown in each plot. Goodness of fit was evaluated with the coefficient of determination (R^2).

APPENDIX J: Culture medium pH control during the 21-days study

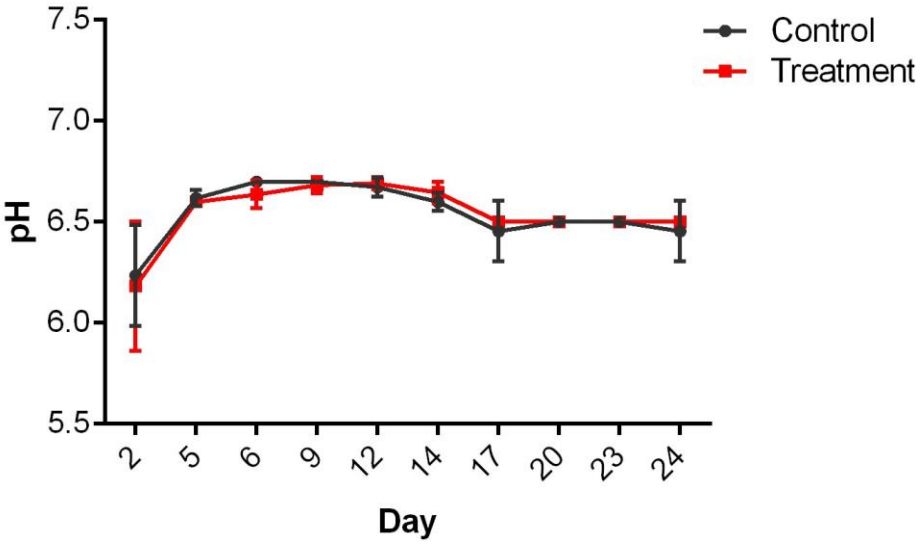

Figure J-1. pH measurements over the ex vivo bovine trabecular bone cores 21-days study. pH was measured for each sample on every media change (three times per week).

APPENDIX K: Conference abstracts

K.1 European Society of Biomechanics 2023

MECHANICAL LOADING OF *EX VIVO* BOVINE TRABECULAR BONE IN 3D-PRINTED BIOREACTORS

Alejandra V. Correa (1, 2), Mahsa Zojaji (2), Andrew Parkhill (2), Brian A. Kunath (2), Juan F. Vivanco (1), Roshni Rainbow (2), Heidi-Lynn Ploeg (2)

1. Facultad de Ingeniería y Ciencias, Universidad Adolfo Ibáñez, Viña del Mar, Chile; 2. Department of Mechanical and Materials Engineering, Queen's University, Kingston ON, Canada

INTRODUCTION

In 2021, 18.3% of the world's population was diagnosed with osteoporosis [8]. Bone biomechanical behavior studies have shown that better understanding of bone tissue mechanics are key in the development of more effective strategies to prevent bone fracture, regenerate, and repair osteoporotic bone defects [2]. Although polycarbonate (PC) bioreactors have been successfully used to study tissue mechanics in bone cores *ex vivo* [14], they are difficult and expensive to fabricate, and the height-diameter ratio for bone cores is below the standard for mechanical compression tests [108]. A bioreactor system was developed using polyjet 3D printing and MED610™, which has been suggested as suitable for long-term culture [5]. This system had been validated in a previous study [6], however, leakage and other experiment limitations were observed. Thus, the objective of this study was to improve and continue the validation of the new bioreactor system in a long-term *ex vivo* bovine trabecular bone core experiment.

METHODS

Twenty-two viable trabecular bone cores (10 mm height, 10 mm diameter) retrieved from a 3-year-old bovine sternum were individually cultured in custom-made 3D printable MED610™ bioreactor chambers at 37°C and 5% CO_2, with constant culture medium perfusion (6.6 mL/hr), for 21-days (Figure 1a). Bone cores in bioreactors were ranked and sorted evenly based on their apparent elastic modulus (E_{app}) into control and loading groups (n = 11/group). The load group was stimulated mechanically (Figure 1b) five times per week with a "trapezoid" waveform that mimicked a physiological high-impact stimulus, with a Δ3000 με displacement and a strain rate of 3000 με/s for 120 cycles. Bone core E_{app} was assessed on days 0 and 21 in random order at room temperature with an initial 10 N pre-load, followed by a quasi-static -3000 με strain at -50 με/s. Data were analyzed in MATLAB 2020b (MathWorks) and E_{app} was calculated

assuming linear elastic behavior with the last 50% of the linear force-displacement curve. A two-way ANOVA and a Tukey post-hoc tests ($\alpha = 0.05$) were used to compare statistical differences between groups on days 0 and 21. A two-tailed t-test was used to compare between groups for percent differences in E_{app} after the 21-days ($\%\Delta E_{app}$). Shapiro-Wilk tests confirmed normality across all groups. All statistical analyses were performed in SPSS® Statistics 23 (IBM) and GraphPad Prism® 6.1 (Dotmatics).

RESULTS

Bone cores tested on day 0 had a mean and a standard deviation E_{app} of 97.7 ± 30.3 MPa, with no significant difference between groups after sorting. After 21-days, the E_{app} decreased in all bone cores by 22.4% (± 20.6% SD) on average (Figure 1c). No significant differences in neither E_{app} nor $\%\Delta E_{app}$ were observed between timepoints nor groups. Though not statistically different, there was a low % difference on day 0 between the E_{app} means of the load and control groups (0.1%), which increased to 7.3% after 21-days. Thus, the load group's E_{app} decreased less, on average, than the control group (19.8% ± 19.6% decrease versus 25.0% ± 22.3%).

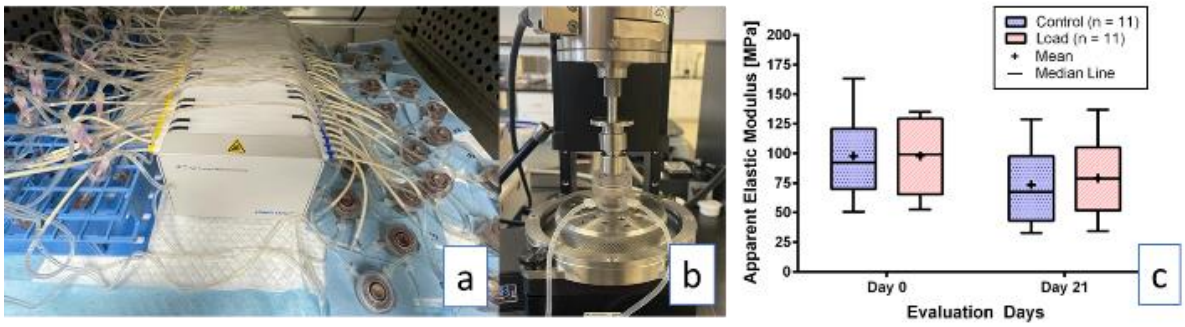

Figure K-1. (a) 3D-printed MED610™ bioreactors containing bone cores setup with peristaltic pump, tubing, and sample specific medium reservoir; (b) Ball-and-socket fixture in Mach-1 System (Biomomentum) for bone cores mechanical compression testing and stimulation; (c) Apparent elastic moduli for both control and load groups in days 0 and 21.

DISCUSSION

The 21-days experiment was successful: no system leakage nor infections were observed. And although data analyses results do not follow the same trends in E_{app} changes as other *ex vivo* trabecular bone core studies using bioreactors [3,6], it is still relevant that the $\%\Delta E_{app}$ decrease was higher in the control group. It is thought, then, that the mechanical stimulation might have helped in the overall bone health of the load group, to some extent. Stress-relaxation, culture medium, and histology analysis are being done for a deeper understanding of the unexpected bone behavior observed. More studies are required to address the small

sample size limitations, as well as other possible sources of error, to confirm if this 3D-printed bioreactor system can be used (or not) for long-term *ex vivo* organ cultures.

REFERENCES

1. N. Salari *et al.*, J. Orthop. Surg. Res., 16 (1), 2021
2. N. Rosa *et al.*, Med. Eng. Phys., 37 (8): 719–728, 2015
3. J. Vivanco *et al.*, Proc. Inst. Mech. Eng., 227 (8): 904–912, 2013
4. S. Zhao *et al.*, Bone Joint Res., 7 (8): 524–538, 2018
5. C. G. Y. Ngan *et al.*, Biomed. Mater., 14 (3), 2019
6. B. A. Kunath, MASc thesis, 2022.

K.2 XXI Congreso Internacional de Metalurgia y Materiales 2023

BIOLOGICAL VIABILITY OF COMPLEX MED610™ 3D-PRINTABLE CONSTRUCTS: PERFUSION BIOREACTOR CHAMBERS

A. Correa Belloso [a,b], B. Kunath [a], J. F. Vivanco [b], H. Ploeg [a], R. Rainbow [a]

[a] *Department of Mechanical and Materials Engineering, Queen's University, Kingston, ON, Canada*
[b] *Facultad de Ingeniería y Ciencias, Universidad Adolfo Ibáñez, Viña del Mar, Chile*
Autor principal: alecorrea@alumnos.uai.cl

INTRODUCTION

Additive Manufacturing (AM) allows the fabrication of complex 3D structures of varying sizes, bringing the possibility to control both internal and external microarchitectures of structures [83] for biomedical applications, resulting in high resolution and precision. For PolyJet 3D-Printing, the material MED610™ is declared to be biocompatible, according to the manufacturer (Stratasys), for 24-hour mucosal membrane contact but not for prolonged skin contact [126]. Though some studies concur with the manufacturer that MED610™ is unsuitable for cell and tissue culture conditions [124], [125], other researchers contend that MED610™'s viability is largely influenced by the cleaning technique employed [110], [111]. In this study, we established a cleaning and sterilization protocol for complex MED610™-based 3D printed culture constructs, including a custom-made perfusion bioreactor chamber.

METHODS

Using the PolyJet Stratasys Objet30 Prime™ 3D printer, MED610™ rectangular constructs were printed and sterilized using four different methods: manufacturer's protocol (MP) [126], sonication protocol (SP)

[110], autoclaving (AP), and SP with autoclaving (SP+A). Post-sterilization, constructs were placed in sterile dishes containing culture media with serum at 37°C and 5% CO_2. Conditioned medium was applied to the ATDC5 murine chondrogenic cell line cultured in 96-well plates (10,000 cells/well, n = 6/group) every 2-3 days. Cell viability was assessed via CellTiter-Blue on days 3 and 7 using a cell standard curve ranging from 0-50,000 cells and compared to a negative (sterile unconditioned media) control. ANOVA and post-hoc Tukey HSD tests ($\alpha = 0.05$) were performed for statistical differences between groups.

Considering a complex 3D-printed bioreactor design, the SP+A protocol was further tested using a perfusion system, assembled with sterile tubing and a peristaltic pump. Medium was circulated (6.6 mL/hr) through the chamber for 14 days; every 2-3 days, medium was changed, and conditioned medium was applied to ATDC5 cells in a 96-well plate (5,000 cells/well, n = 6 for day 3 and 12/group thereafter). Cell viability was assessed on days 3, 9, and 14. To test for statistical differences between the two groups on each timepoint, a Mann-Whitney U test was used ($\alpha = 0.05$), due to lack of normality across groups.

RESULTS

Sterilization Screening: cell viabilities corresponding to the MP, SP, and AP were not significantly different between each other on Day 3 (Figure 1 (A)). Compared to the control group, MP, SP, and AP cell viabilities were significantly different ($p < 0.001$ for MP; $p < 0.01$ for SP and AP). No statistical differences were found between groups on Day 7, although the cell count for SP+A was higher than the rest of the groups. On Day 7, no statistical differences between any of the groups were found. However, the cell count for SP+A was higher than the rest of the groups. **Bioreactor Perfusion:** a higher number of cells was observed for the SP+A group in all timepoints. The cell viability of the SP+A group was significantly different from the negative control on days 3 and 9 (day 3: $p = 0.026$; day 9: $p = 0.045$) (Figure 1 (B)). The SP+A cell viability was not statistically different from the negative control on day 14.

DISCUSSION

The results of the sterilization screening and perfusion bioreactor studies combined indicate that the SP+A cleaning protocol was able to clean and sterilize the MED610™ bioreactor chambers for use in cell culture. This study demonstrated that the toxicity of MED610™ leachates can be negated on ATDC5 cell lines in 2D culture, as well as in the perfusion of conditioned medium through the MED610™ parts. While further studies are required to assess the role of MED610™ in improving cell viability, these findings show the potential of this material in the fabrication of 3D-printed complex constructs in culture conditions for biomedical related research.

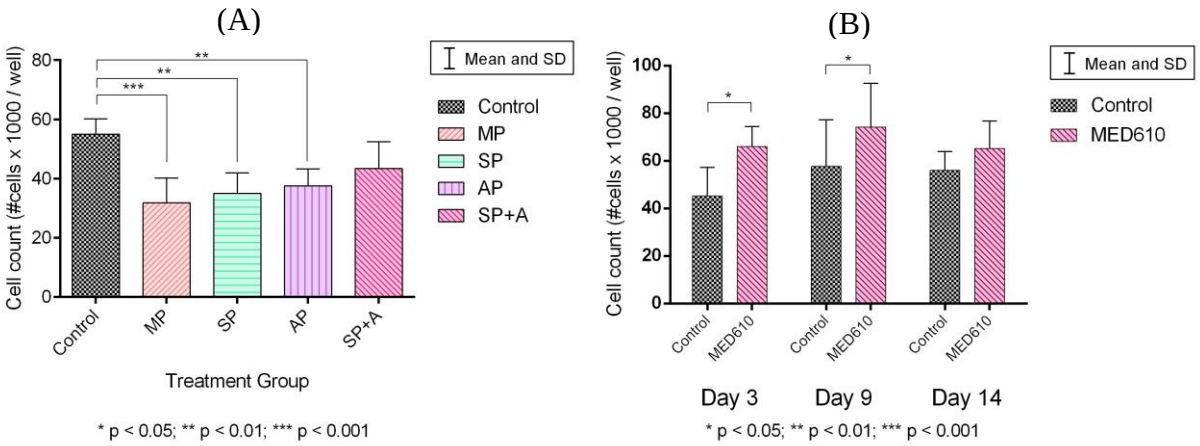

Figure K-2. Cell viability for the negative control (unconditioned medium) and the different testing group(s). Cell counts were obtained from the standard curve between the relative fluorescence units (RFU) and the cell number. (A) Different cleaning protocol groups (n = 6) on day 3 of the sterilization screening study. (B) Perfusion of conditioned medium through bioreactors on days 3 (n = 6), 9, and 14 (n = 12).

Keywords: MED610, Viability, Cleaning Protocol, Additive Manufacturing, PolyJet 3D Printing